

Non-equilibrium dynamics of spin facilitated glass models

Sébastien Léonard¹, Peter Mayer², Peter Sollich³, Ludovic Berthier¹ and Juan P. Garrahan⁴

¹ Laboratoire des Colloïdes, Verres et Nanomatériaux, UMR 5587 Université Montpellier II & CNRS, 34095 Montpellier Cedex 5, France

² Department of Chemistry, Columbia University, 3000 Broadway, New York, NY 10027, USA

³ Department of Mathematics, King's College London, London WC2R 2LS, UK

⁴ School of Physics and Astronomy, University of Nottingham, Nottingham, NG7 2RD, UK

E-mail: leonard@lcvn.univ-montp2.fr, pm2214@columbia.edu,
peter.sollich@kcl.ac.uk, berthier@lcvn.univ-montp2.fr,
juan.garrahan@nottingham.ac.uk

Abstract. We consider the dynamics of spin facilitated models of glasses in the non-equilibrium aging regime following a sudden quench from high to low temperatures. We briefly review known results obtained for the broad class of kinetically constrained models, and then present new results for the behaviour of the one-spin facilitated Fredrickson-Andersen and East models in various spatial dimensions. The time evolution of one-time quantities, such as the energy density, and the detailed properties of two-time correlation and response functions are studied using a combination of theoretical approaches, including exact mappings of master operators and reductions to integrable quantum spin chains, field theory and renormalization group, and independent interval and timescale separation methods. The resulting analytical predictions are confirmed by means of detailed numerical simulations. The models we consider are characterized by trivial static properties, with no finite temperature singularities, but they nevertheless display a surprising variety of dynamic behaviour during aging, which can be directly related to the existence and growth in time of dynamic lengthscales. Well-behaved fluctuation-dissipation ratios can be defined for these models, and we study their properties in detail. We confirm in particular the existence of negative fluctuation-dissipation ratios for a large number of observables. Our results suggest that well-defined violations of fluctuation-dissipation relations, of a purely dynamic origin and unrelated to the thermodynamic concept of effective temperatures, could in general be present in non-equilibrium glassy materials.

PACS numbers: 05.70.Ln, 05.40.-a, 64.70.Pf, 75.40.Gb

1. Why study the aging regime of spin facilitated models?

1.1. A brief survey of kinetically constrained models

This paper is concerned with the dynamics of spin facilitated models of glasses in the non-equilibrium aging regime following a sudden quench from high temperature to the very low temperature glassy regime. Spin facilitated models belong to the broader family of kinetically constrained models (KCMs). These are simple statistical mechanics models which display many of the dynamical features observed in real glassy materials, such as supercooled liquids [1], spin glasses [2], or soft disordered materials [3]. KCMs are generically defined from a simple, usually non-interacting, Hamiltonian. The complexity of glasses is encoded in specific local dynamical rules, or kinetic constraints. For an extensive review of early results on KCMs see [4].

In this paper we focus on spin facilitated models, in particular Fredrickson-Andersen (FA) [5] and East models [6], but we expect that similar behaviour to the one we describe here will also be found in other KCMs such as constrained lattice gases. The main insight of FA [5] was to devise models that are simplistic, as compared to realistic interacting molecular systems, but whose macroscopic behaviour was in agreement with the phenomenology of liquids approaching the glass transition [5, 7], displaying a super-Arrhenius increase of relaxation timescales on decreasing the temperature and non-exponential relaxation functions at equilibrium. Early studies also demonstrated that when suddenly quenched to very low temperatures the subsequent non-equilibrium aging dynamics of the models compares well with experimental observations on aging liquids [8, 9]. Initially it was suggested that FA models would display finite temperature dynamic transitions similar to the one predicted by the mode-coupling theory of supercooled liquids [5], but it was soon realized that most KCMs do not display such singularity, and timescales in fact only diverge in the limit of zero temperature [4, 10, 11]. This implies in particular that after a quench to any non-zero temperature these systems are eventually able to reach thermal equilibrium. The time window of the aging regime, however, becomes large at low temperatures, and the detailed study of this far from equilibrium aging time regime will be the main subject of this paper.

There has been much interest in KCMs recently. This is partly due to the realization [12, 13, 14, 15, 16, 17, 18] that their dynamics is characterized by dynamic heterogeneity, that is, non-trivial spatio-temporal fluctuations of the local relaxation, which is also a hallmark of supercooled liquids [19]. Many of the studies relating to dynamic heterogeneity in KCMs are very recent indeed, having appeared since the review [4] was compiled. These studies characterize in great detail the heterogeneous dynamics of KCMs. They include: papers defining and quantifying relevant dynamic lengthscales in KCMs in equilibrium and their relation to relaxation timescales [10, 11, 20, 21, 22, 23, 24, 25, 26, 27, 28, 29, 30]; studies of more qualitative or phenomenological consequences of kinetic constraints, including dynamic heterogeneity and activated dynamics, for the physics of glassy systems [31, 32, 33, 34, 35, 36]; and the definition and analysis of new KCMs where kinetic rules, or lattice geometry, are

tuned to explore in more detail the range of possible behaviours that can be observed in glass models [37, 38, 39, 40, 41, 42]. These numerous recent studies have in turn been instrumental in encouraging numerical and experimental efforts to measure and characterize in more detail dynamic heterogeneity in supercooled liquids [43, 44, 45, 46, 47, 48, 49, 50], granular materials [51, 52], colloidal systems [50, 53, 54, 55], and soft glassy materials [56, 57, 58, 59].

1.2. Aging dynamics in glassy systems: early studies and open questions

The previous section suggests that dynamic heterogeneity and activated dynamics, which have been well-studied and characterized at thermal equilibrium in various models and systems approaching the glass transition, play central roles in glassy dynamics. However, when moving deeper into the glass phase, glassy materials cannot be equilibrated anymore on experimental or numerical timescales. In this non-equilibrium state, physical properties are not stationary, and the system displays aging behaviour [2]. Experimentally, aging has been well studied at the macroscopic level, in systems as diverse as polymers [60], structural and spin glasses [2], and soft materials [3]. A full understanding of the non-equilibrium glassy state remains a central theoretical challenge [2].

Theoretical studies of mean-field models have provided important insights into the aging dynamics of both structural and spin glasses [2, 61, 62]. In mean-field models, thermal equilibrium is never reached, and aging proceeds by downhill motion in an increasingly flat free energy landscape [63]. Time translational invariance is broken, and two-time correlation and response functions depend on both their arguments. The fluctuation-dissipation theorem (FDT), which relates equilibrium correlation and response functions, does not apply in the aging regime, but a generalized form is shown to hold [64]. This is defined in terms of the two-time connected correlation function for some generic observable $A(t)$,

$$C(t, t_w) = \langle A(t)A(t_w) \rangle - \langle A(t) \rangle \langle A(t_w) \rangle, \quad (1)$$

with $t \geq t_w$, and the corresponding two-time (impulse) response function

$$R(t, t_w) = T \left. \frac{\delta \langle A(t) \rangle}{\delta h(t_w)} \right|_{h=0}. \quad (2)$$

Here h denotes the thermodynamically conjugate field to the observable A so that the perturbation to the Hamiltonian (or energy function) is $\delta E = -hA$, and angled brackets indicate an average over initial conditions and any stochasticity in the dynamics. Note that we have absorbed the temperature T in the definition of the response. The associated generalized FDT is then

$$R(t, t_w) = X(t, t_w) \frac{\partial}{\partial t_w} C(t, t_w), \quad (3)$$

with $X(t, t_w)$ the so-called fluctuation-dissipation ratio (FDR). At equilibrium, correlation and response functions are time translation invariant, depending only on

$\tau = t - t_w$, and equilibrium FDT imposes that $X(t, t_w) = 1$ at all times. A parametric fluctuation-dissipation (FD) plot of the step response or susceptibility

$$\chi(t, t_w) = \int_{t_w}^t dt' R(t, t'), \quad (4)$$

against

$$\Delta C(t, t_w) = C(t, t) - C(t, t_w), \quad (5)$$

is then a straight line with unit slope. These simplifications do not occur in non-equilibrium systems. But the definition of an FDR through Eq. (3) becomes significant for aging systems [61, 62]. In mean-field spin glass models the dependence of the FDR on both time arguments is only through the correlation function $X(t, t_w) \sim X(C(t, t_w))$ at large times. This led to the idea that aging systems might be characterized by an effective temperature [64], defined in terms of the FDR, $T_{\text{eff}} = T/X$. Physically, relaxation in glassy systems occurs in well-separated time sectors [62]; it is then easy to imagine that each sector could be associated with an effective temperature [65]. A thermodynamic interpretation of effective temperatures has also been put forward, relating them to the concept of replica symmetry breaking [66].

Taken together, these results make the mean-field description of aging very appealing, and have set the agenda for a large body of numerical and experimental work, as reviewed in [67]. The broader applicability of the mean-field scenario of aging dynamics remains unclear, however. While some experiments and simulations seem to support the existence of well-behaved effective temperatures [68, 69, 70], other studies also reveal the limits of the mean-field scenario. Experiments have for instance reported anomalously large FDT violations associated with intermittent dynamics [71, 72, 73, 74], while theoretical studies of model systems have also found non-monotonic or even negative response functions [75, 76, 77, 78, 79], and ill-defined or observable-dependent FDRs [80]. In principle, these discrepancies with mean-field predictions are to be expected, since there are many systems of physical interest in which the dynamics are not of mean-field type, displaying both activated processes and spatial heterogeneity. It is thus an important task to understand from the theoretical point of view when the mean-field concept of an FDR-related effective temperature remains viable.

1.3. Aging and dynamic heterogeneity

Studying theoretically the interplay between relevant dynamic lengthscales and thermally activated dynamics in the non-equilibrium regime of disordered materials is clearly a challenging task. This problem has been approached in several different ways, as we briefly summarize in this subsection.

Spin glasses represent a particular class of materials which has been studied in detail by means of experiment, simulation and theory [2]. For these systems mean-field theory provides a set of detailed predictions, in particular for the aging properties [62, 81], without accounting specifically for growing dynamic lengthscales

or thermally activated processes. More phenomenological approaches, on the other hand, directly focus on real space excitations. The resulting predictions [82, 83, 84] differ from those of mean-field, and aging in particular comes to be associated with the logarithmic growth with time of a dynamic correlation lengthscale. This lengthscale is believed to play a crucial role in memory and rejuvenation processes observed experimentally [85, 86, 87, 88], a link that has been confirmed numerically [89, 90]. There exist theoretical attempts to extend the mean-field framework to include spatial fluctuations and dynamic lengthscales [91, 92, 93, 94, 95, 96].

The situation is somewhat similar for structural glasses. While mean-field theories of aging are by now well-established [61], several alternative perspectives insist that dynamic lengthscales and fluctuations should play an important role [18, 31, 97, 98]. This includes the aging regime. Just as in the spin glass case, extensions of the mean-field framework to finite dimensions are feasible in principle [29, 30, 99, 100, 101, 102, 103, 104] but this remains a very difficult task.

A natural approach is to consider directly systems with local, finite ranged interactions. The study of the aging dynamics of KCMs is therefore very promising, as these models combine the necessary features of being defined in terms of (effective) microscopic degrees of freedom, having local dynamical rules, and displaying thermally activated and heterogeneous dynamics.

Early studies on the aging dynamics of KCMs were mainly dedicated to exploring the generic behaviour of FA models after a low temperature quench, or using more complex thermal protocols [8, 9]. The idea was to establish KCMs as reasonable glass models. The Kob-Andersen lattice gas [105] was then studied in some detail, with results that appeared to be in reasonable agreement with mean-field ideas [106, 107]. The same model was also used as a kinetic model to study granular compaction [108, 109, 110, 111]. Both FA and East models were studied numerically in [112, 113], with somewhat unclear results. While two-time correlation functions were shown to exhibit standard scaling properties, non-monotonic response functions were found, leading to apparently ill-defined FDRs. However, these studies considered non-connected correlation functions, making the resulting FDRs of dubious relevance. The one-spin one-dimensional FA model, which we study in detail below, was reconsidered in [114, 115] with a different conclusion, this time indicating that FDT is satisfied for this model at all times. The East model was also reconsidered in [116, 117], with results similar to that found in a family of spin plaquette models [118], which share many similarities with KCMs [26]. Non-monotonic response functions were again found at low temperature, which seemed to prevent the existence of genuine FDRs.

It was later realized that although the non-monotonic response functions were real and physical [114], they did not prevent the possibility of defining FDRs with robust scaling properties. The confusion arose from the use of an incorrect definition of the FDR, whereby the t_w -derivative in Eq. (3) was replaced, for numerical convenience, by a t -derivative. In the graphical representation in terms of an FD plot this corresponds to fixing t_w and letting t vary along the curve, rather than the correct reverse procedure

where the later time t is fixed and the earlier time t_w is varied. As has been emphasized several times [80, 119, 120, 121], this procedure can lead to completely different behaviour or at least incorrect numerical values of the FDR. Unfortunately, the t_w -derivative in its definition makes the numerical measurement of the correct FDR a very demanding task; equivalently, it is normally difficult to obtain the step response $\chi(t, t_w)$ as a function of the earlier time t_w with t fixed. However, novel numerical methods for accessing linear response in simulations have recently become available [121, 122, 123, 124] and have made it possible to systematically study FDRs in KCMs [125, 126, 127]. The results are, perhaps surprisingly, much simpler to interpret physically, as we shall show throughout this paper.

1.4. Summary of main results and plan of paper

The models considered in this paper are characterized by trivial static properties with no finite temperature singularity, yet they display a surprising variety of dynamic behaviour during the aging which can be directly related to the existence and growth with time of a dynamic lengthscale. We find in particular that, as in mean-field models, well-behaved fluctuation-dissipation ratios can often be defined for these models from violations of the FDT. A major difference between mean-field models and KCMs is that FDT violations are only transient in KCMs, and a crossover towards equilibrium is always expected. Therefore, there can be no asymptotic connection between FDT violations and thermodynamic properties. Similarly, it is not obvious how to connect FDRs to effective temperatures in the case of KCMs. In particular the presence of negative fluctuation-dissipation ratios for a large number of observables indicates that the interpretation of FDT violations in terms of some generalized thermodynamics may not be possible. In fact, the aging behaviour of KCMs found in this and related work [125, 126, 127] suggests that well-defined violations of fluctuation-dissipation, of purely dynamic origin and unrelated to the thermodynamic concept of effective temperatures, might generically be present in non-equilibrium glassy materials.

The core material of the paper is divided into the following Secs. 2 and 3 which deal with the FA and East models respectively. For both models we first give a qualitative description of the physical processes governing the aging dynamics. For the FA model we then recall (Sec. 2.1) arguments based on an exact mapping to a diffusion-annihilation process which demonstrate that the upper critical dimension is $d_c = 2$ (rather than $d_c = 4$). Below this dimension, i.e. in $d = 1$, it turns out that exact results can be obtained in an appropriate long-time scaling regime. These are described in Sec. 2.2, first in general terms and then applied to the local, global and Fourier mode correlation and response functions. The latter case (Sec. 2.2.3) includes the other two as opposite limiting behaviours, and simulations confirm the predictions across the entire range. In Sec. 2.3 we turn to dimensions $d > d_c = 2$, where field-theoretic methods can be used to calculate the Fourier mode correlation and response functions. Also these predictions compare well with simulation results. We conclude the section on the FA model with

the derivation of a useful identity for global response functions (Sec. 2.4) that makes the latter much more amenable to numerical simulation. The identity requires only that the dynamics be given by local spin flips that are modified by a kinetic constraint and so should be of general use for numerical studies of KCMs with non-conserved (i.e. Glauber spin-flip rather than Kawasaki spin-exchange) dynamics.

In the analysis of the East model, different techniques come to the fore, in particular master equations based on the independent interval nature of the dynamics. These can be specifically adapted to find correlation and response for local (Sec. 3.1) and global (Sec. 3.2) observables. Fourier modes turn out to be less useful for the East model; instead we consider non-local (distance dependent) quantities (Sec. 3.3) which reveal more clearly the effects of the directedness of the constraint, in particular the very intricate spatial structure of two-time correlations and responses.

We conclude in Sec. 4 with a summary and discussion of our results. Some mathematical background for the FA Fourier mode analysis in $d = 1$, and technical details of the more involved East model calculations, can be found in the appendices.

2. Fredrickson-Andersen model

The FA model [5, 7] describes the dynamics of N binary spin-variables $n_i = 0, 1$ on a hypercubic lattice in d dimensions. An up-spin ($n_i = 1$) represents a highly mobile region or, because of the associated energy cost, a “defect”. Down-spins ($n_i = 0$) model dense, immobile regions and are energetically preferred. The energy function is assumed to be non-interacting, $E = \sum_i n_i$. In a continuous-time Markov dynamics, Glauber rates for flipping spin i are prescribed as

$$w_i(\mathbf{n}) = f_i(\mathbf{n})[(1 - c)n_i + c(1 - n_i)], \quad (6)$$

where $\mathbf{n} = (n_1, \dots, n_N)$ and $c = 1/(1 + e^\beta)$ is the equilibrium up-spin concentration; $\beta = 1/T$ denotes the inverse temperature as usual. Without the factor $f_i(\mathbf{n})$ the model would consist of non-interacting spins, with rates c and $1 - c$ for up- and down-flips, respectively. All the interesting physics is therefore in the facilitation factor $f_i(\mathbf{n})$. It is chosen to be independent of n_i and this ensures that detailed balance with respect to the energy function E is maintained. Physically, f_i represents the assumption that a change of state in region i is possible only if some neighbouring regions are in a mobile state. We will focus exclusively on one-spin facilitated FA models below, which are rather simpler to understand than those imposing facilitation by more than one spin [4]. For simulation purposes it is then simplest to set $f_i(\mathbf{n}) = 0$ if $n_j = 0$ for all nearest neighbours j of site i , and otherwise $f_i(\mathbf{n}) = 1$ [128]. For analytical work it is more convenient to use the form of f_i suggested originally [5, 7],

$$f_i(\mathbf{n}) = \sum_{j=\text{n.n.}(i)} n_j, \quad (7)$$

which is again zero when all n.n. sites are in immobile states, but has nonzero rates increasing in proportion to the number of mobile neighbours. Physically, the key

influence of f_i is to make moves without mobile neighbours impossible; the difference between the two above definitions of f_i for the rates of the *allowed moves* therefore has no qualitative effects on the observed behaviour.

From the point of view of glass modelling the interesting parameter regime of FA models is that of low c , where mobile regions are few and far between. After a quench from high temperature (corresponding to initial defect concentration $c_0 \equiv c(T \rightarrow \infty) = 1/2$) any such defects that are not isolated from each other will quickly flip down, and a state is reached where essentially all defects are isolated from each other. From then on, any further reduction in the defect concentration

$$n(t) = \frac{1}{N} \sum_i \langle n_i(t) \rangle, \quad (8)$$

proceeds via a diffusion-coagulation process. Diffusion of defects can take place when a defect is created next to an existing one, with rate c . Both defects are now mobile and can flip down quickly (rate $1 - c \approx 1$); if the original defect does so first, it leaves the other one behind and has effectively moved by one site. The diffusion constant for this process is $D = c/2$, with the factor $1/2$ accounting for the probability of the newly created defect flipping back down first. When two defects diffusing by this mechanism meet, one of them can flip down, leading to defect coagulation. The reverse process of branching is also possible, by creating two defects next to an existing one which then flips down. However, as two new defects are involved the effective rate is $\sim c^2$ and therefore negligible compared to those for diffusion and coagulation at least in the time window $c^{-1} \ll t \ll c^{-2}$. For larger times branching must of course eventually become important since it is the only process that creates defects and so is able to stabilize the defect density at its equilibrium value, $n(t \rightarrow \infty) = c$.

Conceptually, it is important to note that the effective diffusion-coagulation dynamics has a dynamic critical point at $c \rightarrow 0$, where both timescales and lengthscales diverge [21, 23]. One can define appropriate critical exponents; this is simplest from the equilibrium dynamics at low c . The order parameter exponent $n(t \rightarrow \infty) = c \sim c^\beta$ is fixed to $\beta = 1$ because of detailed balance. The lengthscale ξ and timescale t_{rel} of appropriate relaxation functions define the other exponents as $\xi \sim c^{-\nu}$ and $Dt_{\text{rel}} \sim \xi^z \sim c^{-z\nu}$. We note as an aside that, in the context of dynamic criticality, the asymptotic FDR X^∞ , which is defined as the limit of $X(t, t_w)$ for widely separated times $t \gg t_w$, appears as a universal amplitude ratio that can distinguish different dynamic universality classes [129].

2.1. Mapping to diffusion-annihilation

Initial field-theoretical studies [23] suggested that the FA model was in the dynamic universality class of directed percolation, with an upper critical dimension $d_c = 4$. Closer inspection reveals, however, that there is a hidden symmetry which reduces this value to $d_c = 2$ [24]. This can be deduced from an exact mapping between the FA model and another defect-diffusion model where defects or “particles” annihilate in

pairs ($A + A \rightarrow 0$, where A symbolizes a defect) and are similarly created ($0 \rightarrow A + A$) in pairs.

The mapping is most easily derived in a quantum mechanical representation of the Markov dynamics [130, 131, 132]. One associates to each possible state \mathbf{n} of the system a distinct unit vector $|\mathbf{n}\rangle$ in a vector space, and to the time-dependent probability distribution over states $p_t(\mathbf{n})$ the vector $|p_t\rangle = \sum_{\mathbf{n}} p_t(\mathbf{n})|\mathbf{n}\rangle$. (The basis vectors $|\mathbf{n}\rangle$ have unit length and are mutually orthogonal.) It is then easy to check that the dynamical evolution of this vector takes the form $\partial_t |p_t\rangle = W |p_t\rangle$ with the master operator

$$W = \sum_i (F_i - 1) \hat{f}_i [(1 - c) \hat{n}_i + c(1 - \hat{n}_i)]. \quad (9)$$

Here, $\hat{n}_i = \sum_{\mathbf{n}} n_i |\mathbf{n}\rangle \langle \mathbf{n}|$ is the operator measuring the value of the local spin, $\hat{f}_i = \sum_{j=\text{n.n.}(i)} \hat{n}_j$, and F_i is the operator that flips spin i , $F_i |n_1, \dots, n_i, \dots, n_N\rangle = |n_1, \dots, 1 - n_i, \dots, n_N\rangle$. Averages are obtained by multiplying with the uniform state $\langle \mathbf{e} | = \sum_{\mathbf{n}} \langle \mathbf{n} |$ from the left, e.g. $\langle n_i(t) \rangle = \langle \mathbf{e} | \hat{n}_i |p_t\rangle$.

The key mathematical statement that establishes the mapping mentioned above is that there is an operator V such that the similarity transformation VWV^{-1} of the FA master operator produces the master operator of an annihilation-pair creation process with appropriate rates [24]. One can then verify directly that the equilibrium correlation functions (more precisely those involving only two separate times) of the two models are identical up to trivial factors. As a consequence, also the dynamic exponents and dynamic universality class of the two models must be the same. In particular, one has $d_c = 2$ and the critical exponents are $(z, \nu, \beta) = (2, 1/d, 1)$ in $d < 2$ while they take the mean-field values $(z, \nu, \beta) = (2, 1/2, 1)$ in higher dimensions.

The feature of the annihilation-pair creation process that is responsible for the upper critical dimension being two rather than four is the conservation of parity: if the number of particles is even to start with it remains so for all times, and similarly if it is initially odd. Mathematically, the parity operator,

$$\hat{P} = (-1)^{\sum_i \hat{n}_i}, \quad (10)$$

commutes with the master operator, and maps two different steady states onto each other (which differ only in the sign of the probability amplitude of states with an odd number of particles). The similarity relation between annihilation-pair creation and the FA model implies that the latter also has a symmetry; this is the ‘‘hidden’’ symmetry mentioned above. Its physical nature is somewhat difficult to elucidate since the symmetry operator that commutes with the FA master operator is not diagonal and so does not correspond to a standard observable obeying a conservation law. Mathematically, the symmetry swaps terms in the master operator across n.n. bonds: the term describing a flip of spin i facilitated from a neighbouring site j is mapped to the one encoding flips of spin j facilitated from site i . This insight makes clear that the symmetry also applies to the East model discussed below, except that the mapping here converts the East model into the West model, where the direction of facilitation is reversed. While this does not lead to obvious ways of calculating the correlation and

response functions that we will study below, it does provide some general restrictions. For example, general multi-point two-time equilibrium correlations

$$\left\langle \prod_{\rho=1}^r [n_{i_\rho}(t) - c] \prod_{\sigma=1}^s [n_{j_\sigma}(0) - c] \right\rangle, \quad (11)$$

can be shown to vanish unless the rightmost spins appearing at time 0 and t are identical, i.e. unless $\max_\rho(i_\rho) = \max_\sigma(j_\sigma)$. For two-point correlations ($r = s = 1$) this reduces to the well-known fact that only local correlations are non-vanishing at equilibrium.

The above mapping can be extended in a number of ways, for example to generic coagulation-branching and annihilation-pair creation models, and to “bosonic” processes where each site can be occupied by more than one particle [24]. For the original “fermionic” (hardcore repulsion) versions the mapping also has a very appealing geometric structure, with all operations being effectively rotations on a “spin sphere”.

2.2. Exact results in $d = 1$

In this section we present exact long-time scaling forms for FDT violations in the $1d$ FA model. More precisely, the dynamics following a quench from a random initial state to low temperature $c \ll 1$ is considered, in the nonequilibrium aging regime of times $c^{-1} \ll t \ll c^{-2}$. To probe violations of FDT we introduce the connected correlation and response functions,

$$C_r(t, t_w) = \langle n_{i+r}(t) n_i(t_w) \rangle - n(t) n(t_w), \quad (12)$$

$$R_r(t, t_w) = T \left. \frac{\delta \langle n_{i+r}(t) \rangle}{\delta h_i(t_w)} \right|_{h_i=0}, \quad (13)$$

where temperature is again included in the definition of the response function. The fields h_i are conjugate to the n_i , so that in their presence the energy becomes $E = \sum_i n_i(1-h_i)$. We will also consider the step-response $\chi_r(t, t_w) = \int_{t_w}^t dt' R_r(t, t')$ to a perturbation applied from time t_w onwards.

Our analysis is based on the fact that defects effectively diffuse and coagulate on the $\mathcal{O}(c^{-1})$ timescale. As explained above, the rate for diffusion is $D = c/2$ while coagulations occur with rate $\gamma \sim 1$. We will, from now on and throughout this section, measure time in units of c^{-1} (except when stating simulation parameters) so that $D = \frac{1}{2}$ and $\gamma \sim c^{-1} \gg 1$. The coarsening dynamics of this diffusion-coagulation process at long times $t \gg 1$ becomes independent of γ [133, 134]: defects typically first have to diffuse for a time $\mathcal{O}(t)$ before they occupy adjacent sites where coagulation is possible. The duration of this reaction, which depends on the rate γ , is only $\mathcal{O}(1)$ and therefore negligible in comparison: the process is said to be in the diffusion controlled regime [133]. The irrelevance of the precise value of γ at long times allows us to adjust its value to $\gamma = \frac{1}{2}$, the reason for this choice being that (only) the process with $D = \gamma$ admits an exact solution [131, 132, 135]. Our results will then be exact to leading order at large time $t \gg 1$ for any process with $\gamma > 0$; this includes the FA model. Of course, the diffusion-coagulation picture applies to the FA model only so long as $t \ll c^{-1}$ is still

satisfied. In the FA dynamics, branching events become important on this times scale and initiate a crossover to equilibrium. Therefore, whenever we talk about long time behaviour for $t \rightarrow \infty$ it is understood that the low temperature limit $c \rightarrow 0$ is taken first (in order to remain in the regime $1 \ll t \ll c^{-1}$; recall that our time-unit is now c^{-1}). Throughout this section we will use the symbol “ \sim ” to indicate results which become exact in this long-time limit.

The scaling of the connected two-time correlation $C_r(t, t_w)$ in the effective FA process with $D = \gamma = \frac{1}{2}$ was derived in [127]. The result reads

$$\begin{aligned}
 C_r(t, t_w) &\sim e^{-2t_w} [I_0 + I_1](2t_w) \sum_{i,j=0}^{\infty} G_{(r,r+1),(-i,j+1)}(\tau) H_{i+j+1}(2t_w) \\
 &\quad - \sum_{i,j=0}^{\infty} G_{(+r,+r-1),(i,j)}(\tau) e^{-2t_w} [I_i + I_{i+1}](2t_w) [\delta_{j,0} + H_j(2t_w)] \\
 &\quad - \sum_{i,j=0}^{\infty} G_{(-r,-r-1),(i,j)}(\tau) e^{-2t_w} [I_i + I_{i+1}](2t_w) [\delta_{j,0} + H_j(2t_w)], \tag{14}
 \end{aligned}$$

where $I_n(t)$ denotes modified Bessel functions, Eq. (A.1), and the explicit form of the functions $H_n(t)$ is given in Eq. (A.2). To save space we use the short-hand notation $[\cdot](x)$ to indicate that all functions contained in the square brackets have the same argument x . The $G_{\mathbf{i},\mathbf{j}}(\tau)$ with $\mathbf{i} = (i_1, i_2)$ and $\mathbf{j} = (j_1, j_2)$ are Green’s functions,

$$G_{\mathbf{i},\mathbf{j}}(\tau) = e^{-2\tau} [I_{i_1-j_1} I_{i_2-j_2} - I_{i_1-j_2} I_{i_2-j_1}](\tau). \tag{15}$$

The result Eq. (14) applies to the FA model to leading order in $t_w \gg 1$ but uniformly in $\tau \geq 0$, i.e. including small values of τ .

An expression for the response function $R_r(t, t_w)$ is also given in [127]. Before stating the result we consider the effect of the associated perturbation. It is convenient to express the response function in the operator formalism from above, $R_r(t, t_w) = \langle \mathbf{e} | \hat{n}_{i+r} e^{W\tau} V_i | p_{t_w} \rangle$, where $V_i = T \partial W / \partial h_i |_{h_i=0}$ and W the master operator of the effective FA process. The perturbation operator V_i accounts for the fact that the field h_i reduces the energy barrier for creation of a defect at site i ; recall that $E = \sum_i n_i (1 - h_i)$ in the presence of the perturbation. Consequently the diffusion rates for entering site i are increased. The rates for leaving site i , however, are not affected by h_i because they relate to processes involving the creation of a defect at sites $i - 1$ or $i + 1$. This locally directed perturbation can be represented as the sum of two mechanisms [127]: (i) an *asymmetric* perturbation $V_i^{(a)}$ that increases the rates for entering site i but decreases the ones for leaving it and thus *traps* diffusing defects, and (ii) a *symmetric* perturbation $V_i^{(s)}$ which increases both the rates for entering and leaving site i and thus *accelerates* the local dynamics. In combination $V_i = V_i^{(a)} + V_i^{(s)}$ reproduces the directed perturbation of the local diffusion rates via the field h_i ; the two contributions can be written explicitly as

$$V_i^{(a)} = \frac{1}{4} (F_{i-1} F_i - 1) (\hat{n}_{i-1} - \hat{n}_i) + \frac{1}{4} (F_{i+1} F_i - 1) (\hat{n}_{i+1} - \hat{n}_i), \tag{16}$$

$$V_i^{(s)} = \frac{1}{4} (F_{i-1} F_i - 1) (\hat{n}_{i-1} - \hat{n}_i)^2 + \frac{1}{4} (F_{i+1} F_i - 1) (\hat{n}_{i+1} - \hat{n}_i)^2. \tag{17}$$

Clearly an analogous decomposition then applies to the response function

$$R_r(t, t_w) = R_r^{(a)}(t, t_w) + R_r^{(s)}(t, t_w), \quad (18)$$

with $R_r^{(a/s)}(t, t_w) = \langle \mathbf{e} | \hat{n}_{i+r} e^{W\tau} V_i^{(a/s)} | p_{t_w} \rangle$ the contributions from the asymmetric and symmetric perturbations. We will see below that $R_r^{(a)}(t, t_w)$ and $R_r^{(s)}(t, t_w)$ have very different scaling properties, each being dominant in a different time regime. For now we simply state the relevant expressions [127],

$$R_r^{(a)}(t, t_w) \sim \partial_{t_w} \frac{1}{2} e^{-2t} I_r(t - t_w) [I_{r-1} + 2I_r + I_{r+1}](t + t_w), \quad (19)$$

$$R_r^{(s)}(t, t_w) \sim -\frac{1}{4} e^{-2t} \{ I_r(t - t_w) [-I_{r-2} + 2I_r - I_{r+2}](t + t_w) \\ + [I_{r-1} - I_{r+1}](t - t_w) [I_{r-1} - I_{r+1}](t + t_w) \}. \quad (20)$$

Like Eq. (14), Eq. (19) applies to leading order in $t_w \gg 1$ and uniformly in $\tau \geq 0$. The symmetric contribution $R_r^{(s)}(t, t_w)$, Eq. (20), is sensitive to the value of γ and for this reason only applies when both $\tau, t_w \gg 1$ [127].

2.2.1. Local correlation and response The violation of FDT associated with the local defect observable n_i has been considered in all simulation studies of the FA model [112, 114, 115, 125]. However, as we now explain, this observable is ill suited to the measurement of FDT violations. One can derive the scaling of the relevant autocorrelation $C_0(t, t_w)$ and response $R_0(t, t_w)$ functions from Eqs. (14), (19) and (20) evaluated at $r = 0$. In the quasi-equilibrium regime of small $\tau \geq 0$ and large $t_w \gg 1$ the autocorrelation scales as [127]

$$C_0(t, t_w) \sim \frac{1}{\sqrt{\pi t_w}} e^{-\tau} I_0(\tau) \sim n(t_w) p_r(\tau). \quad (21)$$

Here we have identified the defect concentration $n(t_w) = 1/\sqrt{\pi t_w}$ and the random walk return probability $p_r(\tau) = e^{-\tau} I_0(\tau)$. In the quasi-equilibrium regime defects are typically too far from each other to meet and therefore may be treated as independent random walkers. Correspondingly, the average $\langle n_i(t) n_i(t_w) \rangle$ is given by the probability $n(t_w)$ of having a defect at site i at time t_w multiplied by the probability $p_r(\tau)$ for this defect to return and occupy the same site at time t . This is then also the leading contribution to the local autocorrelation function $C_0(t, t_w)$; the subtraction of $n(t)n(t_w)$ only gives a subleading correction because $n(t) \ll 1$.

In the aging regime of large $t_w \gg 1$ with fixed τ/t_w , an expansion of Eq. (14) yields the scaling behaviour [127]

$$C_0(t, t_w) \sim \frac{4}{\pi^{3/2}} \frac{t_w}{\tau^2} \int_0^\infty dx \int_0^\infty dy (x+y) e^{-(2t_w/\tau)(x^2+y^2)} \Phi(x+y) \\ - \frac{8}{\pi^{3/2}} \frac{t_w}{\tau^2} \int_0^\infty dx \int_0^\infty dy (x-y) e^{-(2t_w/\tau)(x^2+y^2)} e^{-x^2} \Phi(y). \quad (22)$$

Here $\Phi(z) = (2/\sqrt{\pi}) \int_z^\infty du e^{-u^2}$ denotes the complementary error function. The integrals in Eq. (22) can be solved but the result is not particularly simple; we only state

the resulting scaling in the two limiting cases

$$\tau \ll t_w : C_0(t, t_w) \approx \frac{1}{\pi \sqrt{2 \tau t_w}}, \quad (23)$$

$$\tau \gg t_w : C_0(t, t_w) \approx \frac{3\pi - 8 t_w}{3\pi^2 \tau^2}. \quad (24)$$

This completely characterizes the defect autocorrelation $C_0(t, t_w)$: it has the initial value $C_0(t_w, t_w) \sim n(t_w)$ from which it decreases according to Eq. (21). When $1 \ll \tau \ll t_w$ this quasi-equilibrium result matches with the expansion Eq. (23). As τ is further increased beyond t_w the scaling of $C_0(t, t_w)$ finally crosses over from Eq. (23) to Eq. (24).

The scaling of the defect response function $R_0(t, t_w) = R_0^{(a)}(t, t_w) + R_0^{(s)}(t, t_w)$ is unusual in several ways. It is instructive to first discuss the step-response function $\chi_0(t, t_w)$. The latter is always dominated by contributions from the asymmetric perturbation $\chi_0(t, t_w) \sim \chi_0^{(a)}(t, t_w)$ as can be shown [127] from Eqs. (19, 20). An expression for $\chi_0^{(a)}(t, t_w) = \int_{t_w}^t dt' R_0^{(a)}(t, t')$ is straightforwardly obtained from Eq. (19). In the quasi-equilibrium regime of small $\tau \geq 0$ and large $t_w \gg 1$ one finds the scaling

$$\chi_0^{(a)}(t, t_w) \sim n(t_w) [1 - p_r(\tau)], \quad (25)$$

while $\chi_0^{(a)}(t, t_w) \sim n(t)$ in the aging regime $t_w \gg 1$ at fixed τ/t_w . This non-monotonic behaviour of $\chi_0^{(a)}(t, t_w)$ is due to a simple mechanism: when applying the asymmetric perturbation – which traps diffusing defects – at site i and from time t_w onwards, this increases the probability $\langle n_i(t) \rangle$ to find a defect at site i . The step response increases on a $\tau = \mathcal{O}(1)$ timescale, c.f. Eq. (25), from zero to $n(t_w)$. But in the aging regime and for $\tau \gg t_w$, the density of defects $n(t)$ in the system decreases and along with it so does $\chi_0^{(a)}(t, t_w) \sim n(t)$. While this makes perfect sense, one has to be careful when recovering the response $R_0^{(a)}(t, t_w) = -\partial_{t_w} \chi_0^{(a)}(t, t_w)$ from this scaling result: one would incorrectly conclude that $R_0^{(a)}(t, t_w) = -\partial_{t_w} n(t) = 0$. The resolution of the apparent paradox is that $\chi_0^{(a)}(t, t_w)$ is dominated by small τ contributions of $R_0^{(a)}(t, t_w)$, so that the aging behaviour of $R_0^{(a)}(t, t_w)$ only shows up in *subdominant* terms in $\chi_0^{(a)}(t, t_w)$. Summarizing for the step response, $\chi_0(t, t_w) \sim \chi_0^{(a)}(t, t_w)$ is dominated by the trapping effect of the asymmetric perturbation and $\chi_0^{(a)}(t, t_w)$, in turn, is dominated by short time contributions from $R_0^{(a)}(t, t_w)$. This inconvenient insensitivity to aging effects can be avoided by considering directly the response function $R_0(t, t_w)$, rather than the step response $\chi_0(t, t_w)$. From Eqs. (19, 20) its constituent asymmetric and symmetric contributions scale as

$$R_0^{(a)}(t, t_w) \sim \frac{1}{\pi} \frac{t_w}{(t^2 - t_w^2)^{3/2}}, \quad (26)$$

$$R_0^{(s)}(t, t_w) \sim -\frac{1}{2\pi} \frac{t - t_w}{(t^2 - t_w^2)^{3/2}}, \quad (27)$$

in the aging regime $\tau, t_w \gg 1$ and $\tau/t_w = \mathcal{O}(1)$. Note the negative sign of $R_0^{(s)}(t, t_w)$. To understand this, recall that applying the symmetric perturbation at site i increases the local diffusion rates. This in itself does not affect the defect concentration $\langle n_i(t) \rangle$ at site i . However, the locally accelerated dynamics increase the likelihood for coagulation

with neighbouring defects and thus reduce the local concentration $\langle n_i(t) \rangle$. Consequently $R_0^{(s)}(t, t_w)$ is negative. Considering more quantitatively the asymmetric and symmetric response functions, Eqs. (26, 27), we see that they are of the *same* order $\mathcal{O}(t_w^{-2})$ when $\tau/t_w = \mathcal{O}(1)$. For much smaller $\tau \ll t_w$, the trapping effect encoded in $R_0^{(a)}(t, t_w) = \mathcal{O}(\tau^{-3/2}t_w^{-1/2})$ dominates over $R_0^{(s)}(t, t_w) \sim \mathcal{O}(\tau^{-1/2}t_w^{-3/2})$, and this is at the origin of the analogous dominance that we found in the step response. In the opposite regime $\tau \gg t_w$ the situation is reversed, with effects from locally accelerated dynamics described by $R_0^{(s)}(t, t_w) = \mathcal{O}(\tau^{-2})$ dominating over $R_0^{(a)}(t, t_w) = \mathcal{O}(\tau^{-3}t_w)$.

Based on the above insights regarding the scaling of $C_0(t, t_w)$ and $R_0(t, t_w)$ we are now in a position to discuss the resulting violations of the FDT and the usefulness of FD plots in revealing them. In the quasi-equilibrium regime of small $\tau \geq 0$ and large $t_w \gg 1$ we have that $C_0(t, t_w) \sim n(t_w)p_r(\tau)$, Eq. (21), and $\chi_0(t, t_w) \sim \chi_0^{(a)}(t, t_w) \sim n(t_w)[1 - p_r(\tau)]$, Eq. (25). This satisfies the equilibrium FDT $\chi_0(t, t_w) \sim C_0(t, t) - C_0(t, t_w)$ to leading order in $t_w \gg 1$. Furthermore, the autocorrelation $C_0(t, t_w)$ decreases like $p_r(\tau) = \mathcal{O}(\tau^{-1/2})$ with increasing τ and thus drops to a fraction $\mathcal{O}(t_w^{-1/2})$ of its equal time value $C_0(t_w, t_w)$ by the time we reach the aging regime where τ and t_w are of the same order; the susceptibility $\chi_0(t, t_w)$ approaches $n(t)$ up to a small deviation of the same order. Consequently FD plots for the local defect observable show effectively only the quasi-equilibrium behaviour of $C_0(t, t_w)$ and $\chi_0(t, t_w)$, with the nontrivial aging regime essentially invisible at long times [114, 115, 125]. This type of scaling makes the local defect observable a poor choice for probing FDT violations, especially using FD plots. Regardless of these caveats, however, there is a well defined FDR $X_0(t, t_w) = R_0(t, t_w)/\partial_{t_w} C_0(t, t_w)$. It scales as $X_0 \sim X_0(t/t_w)$ in the aging limit [127, 125], crossing over from quasi-equilibrium $X_0 \sim 1$ for $\tau \ll t_w$ to the asymptotic FDR $X_0 \sim X_0^\infty$ for $\tau \gg t_w$. From the expansions Eq. (24) and Eq. (27) one obtains the *negative* value

$$X_0^\infty = -\frac{3\pi}{6\pi - 16} \approx -3.307. \quad (28)$$

We show simulation results in Fig. 1 for various times t . These confirm the findings of this section. In particular, the FD plot closely follows the equilibrium FDT except in the regime of large time differences, and the non-equilibrium part shrinks into the top right corner as t increases. Very detailed measurements in this region, as shown in the inset, are consistent with the predicted asymptotic value of the FDR from Eq. (28).

2.2.2. Global correlation and response A much clearer picture of the violation of the FDT emerges when considering a global observable like the energy [125, 127, 136, 137]. We introduce the corresponding normalized connected correlation and response functions

$$C_E(t, t_w) = \frac{1}{N} (\langle E(t)E(t_w) \rangle - \langle E(t) \rangle \langle E(t_w) \rangle), \quad (29)$$

$$R_E(t, t_w) = \frac{T}{N} \left. \frac{\delta \langle E(t) \rangle}{\delta h_E(t_w)} \right|_{h_E=0}. \quad (30)$$

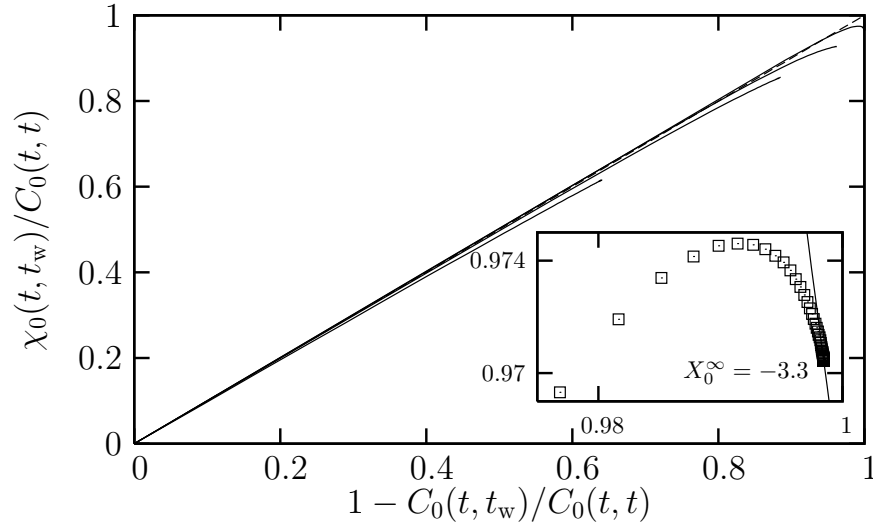


Figure 1. Normalized FD plots for the local observable in the $d = 1$ FA model at temperature $T = 0.1$ and for times $t = 2 \times 10^4$, 5×10^4 , 10^5 , and 10^6 (from bottom to top). The dashed diagonal line indicates the equilibrium FDT. Inset: final part of the $t = 10^6$ data, enlarged to show the nonmonotonic response and the asymptotic FDR, $X_0^\infty = -3.307$ (solid line). From Ref. [125]. Copyright American Physical Society.

The field h_E uniformly shifts the energy according to $E = (1 - h_E) \sum_i n_i$. When substituting $E = \sum_i n_i$ in Eq. (29) and using translational invariance one readily shows that in fact $C_E(t, t_w) = \sum_r C_r(t, t_w)$ and similarly $R_E(t, t_w) = \sum_r R_r(t, t_w)$ from Eq. (30). The scalings of energy correlation and response functions can thus be derived by summing Eqs. (14), (19) and (20) over r .

It can be shown [127] from Eq. (14) that the scaling of energy correlations in the aging regime $t_w \gg 1$ with fixed τ/t_w is given by

$$C_E(t, t_w) \sim \frac{4}{\pi} \frac{t_w}{\tau^{3/2}} \int_0^\infty dx \int_0^\infty dy (x+y) e^{-(t_w/\tau)(x+y)^2} \Phi(x+y) - \frac{8}{\pi} \frac{t_w}{\tau^{3/2}} \int_0^\infty dx \int_0^\infty dy (x-y) e^{-(t_w/\tau)(x-y)^2} e^{-x^2} \Phi(y). \quad (31)$$

Again these integrals can be solved exactly. The result is bulky but would be required in full only if we wanted to inquire into the precise form of the crossover between the simple limit behaviours

$$\tau \ll t_w : C_E(t, t_w) \approx \frac{3 - 2\sqrt{2}}{\sqrt{\pi} t_w}, \quad (32)$$

$$\tau \gg t_w : C_E(t, t_w) \approx \frac{3\pi - 8}{3\pi^{3/2}} \frac{t_w}{\tau^{3/2}}. \quad (33)$$

Energy correlations have the plateau value Eq. (32) for $0 \leq \tau \ll t_w$. This is because defects typically do not meet when $\tau \ll t_w$ and therefore $C_E(t, t_w) \approx C_E(t_w, t_w)$. Only once τ increases to become comparable to t_w do coagulation events start to decorrelate $E(t)$ from $E(t_w)$, leading to the crossover from Eq. (32) to (33).

The scaling of the energy response function $R_E(t, t_w) = R_E^{(a)}(t, t_w) + R_E^{(s)}(t, t_w)$ can

also be understood in very simple terms. The response $R_E^{(a)}(t, t_w) = 0$ vanishes exactly because, when applied to all sites, the asymmetric perturbations of the diffusion rates cancel. Therefore $R_E(t, t_w) = R_E^{(s)}(t, t_w) = \sum_r R_r^{(s)}(t, t_w)$. From Eq. (20) this gives

$$R_E(t, t_w) \sim -\frac{1}{2\sqrt{\pi}t^{3/2}} \sim \partial_t n(t), \quad (34)$$

in the aging regime $t_w \gg 1$ with fixed τ/t_w . Due to the normalisation by $1/N$, $R_E(t, t_w)$ measures changes in the defect concentration $n(t) = (1/N)\langle E(t) \rangle$. Now, in the presence of the perturbation all diffusion rates are increased. This is equivalent to giving the system some additional time δt to evolve. The energy response function is therefore $R_E(t, t_w) \sim [n(t + \delta t) - n(t)]/\delta t \sim \partial_t n(t)$. To understand the sign of this, note that the field h_E decreases the energy barriers for defect creation. While in equilibrium this would increase the density of defects, in the nonequilibrium coarsening dynamics this speeds up the relaxation of the system – it decreases $n(t)$ and hence $R_E(t, t_w) < 0$ is *negative* throughout.

From the scalings Eq. (31) and Eq. (34) one obtains the FD plot for the energy. Contrary to the case of the local defect observable n_i the energy produces a nontrivial FD plot (contained in Fig. 2 below). This can be measured rather easily in simulations as discussed in Sec. 2.4 and makes the energy a good observable for probing violations of FDT in the FA model. From the scalings in Eqs. (33, 34) one shows that the asymptotic FDR for the energy is

$$X_E^\infty = -\frac{3\pi}{6\pi - 16}. \quad (35)$$

It matches exactly the value X_0^∞ , Eq. (28), obtained from the local defect observable but is much more accessible to measurement [125, 136]. We will discuss this and related points further in the following section.

2.2.3. Fourier mode correlation and response The above results describe the two extreme cases of spatially local and global observables. We will now consider observables with a finite intrinsic lengthscale in order to reveal in more detail the physics underlying the violation of FDT in the 1d FA model. Specifically, we consider the Fourier modes of the arrangement of defects, $n_q = \sum_j n_j e^{-iqj}$. The associated connected correlation and response functions are

$$C_q(t, t_w) = \frac{1}{N} [\langle n_q(t)n_{-q}(t_w) \rangle - \langle n_q(t) \rangle \langle n_{-q}(t_w) \rangle], \quad (36)$$

$$R_q(t, t_w) = \frac{T}{N} \left. \frac{\delta \langle n_q(t) \rangle}{\delta h_{-q}(t_w)} \right|_{h_{-q}=0}. \quad (37)$$

The fields h_q are conjugate to n_q , resulting in a perturbation $\delta E = -h_q n_q$. Clearly, $C_q(t, t_w)$ is the dynamic structure factor and $R_q(t, t_w)$ the conjugate response function. Using translational invariance one readily verifies that $C_q(t, t_w) = \sum_r e^{-iqr} C_r(t, t_w)$ is the Fourier transform of the spatial correlations, Eq. (12), and likewise for $R_q(t, t_w)$. The general results Eqs. (14), (19) and (20) are therefore once again the key for analysing the functions $C_q(t, t_w)$ and $R_q(t, t_w)$.

In order to derive $C_q(t, t_w)$ from Eq. (14) the Fourier transforms of the Green's functions are needed; these contain all r dependence in $C_r(t, t_w)$. Using the identity Eq. (A.7) one immediately has

$$G_q^{(+)}(\tau; i, j) = \sum_r e^{-iqr} G_{(r, r+1), (-i, j+1)}(\tau) = e^{i\frac{1}{2}(i-j)q} e^{-2\tau} [I_{i+j} - I_{i+j+2}] \left(2\tau \cos \frac{q}{2} \right),$$

$$G_q^{(-)}(\tau; i, j) = \sum_r e^{-iqr} G_{(r, r-1), (i, j)}(\tau) = e^{-i\frac{1}{2}(i+j+1)q} e^{-2\tau} [I_{i-j-1} - I_{i-j+1}] \left(2\tau \cos \frac{q}{2} \right),$$

and in terms of these functions

$$C_q(t, t_w) \sim e^{-2t_w} [I_0 + I_1] (2t_w) \sum_{i, j=0}^{\infty} \text{Re} [G_q^{(+)}(\tau; i, j)] H_{i+j+1}(2t_w)$$

$$- \sum_{i, j=0}^{\infty} 2 \text{Re} [G_q^{(-)}(\tau; i, j)] e^{-2t_w} [I_i + I_{i+1}] (2t_w) [\delta_{j,0} + H_j(2t_w)]. \quad (38)$$

In the first line of Eq. (38) the imaginary part of $G_q^{(+)}(\tau; i, j)$ drops out since it is odd in $i - j$. The second line, on the other hand, is a sum of two contributions $G_q^{(-)}(\tau; i, j) + G_{-q}^{(-)}(\tau; i, j)$ from Eq. (14), which is again real. The scaling behaviour of Eq. (38) in the aging limit $t_w \rightarrow \infty$ at fixed τ/t_w and $t_w q^2$ follows from the asymptotic expansions Eqs. (A.3, A.4) of the functions $I_n(t)$ and $H_n(t)$, and is given by

$$C_q \sim \frac{4}{\pi} \frac{t_w}{\tau^{3/2}} e^{-\frac{1}{4}\tau q^2} \left[\int_0^{\infty} dx \int_0^{\infty} dy (x+y) \cos(\sqrt{t_w} q (x-y)) e^{-(t_w/\tau)(x+y)^2} \Phi(x+y) \right. \\ \left. - 2 \int_0^{\infty} dx \int_0^{\infty} dy (x-y) \cos(\sqrt{t_w} q (x+y)) e^{-(t_w/\tau)(x-y)^2} e^{-x^2} \Phi(y) \right]. \quad (39)$$

Time arguments $C_q = C_q(t, t_w)$ were omitted to save space. Energy correlations are obtained as the special case $C_E(t, t_w) = C_{q=0}(t, t_w)$ as is clear from the definition of $C_q(t, t_w)$, Eq. (36), and indeed Eq. (39) with $q = 0$ reduces to Eq. (31). Moreover, the inverse Fourier transform $C_{r=0}(t, t_w) = \int (dq/2\pi) C_q(t, t_w)$ yields the autocorrelation. The resulting scaling of $C_{r=0}(t, t_w)$, Eq. (22), is then also a special case of Eq. (39).

Equation (39) can be rearranged into a more useful form. We rotate the integration coordinates $u = y+x$ and $v = y-x$, whereby the integration domain becomes $u \in [0, \infty]$ and $v \in [-u, u]$. In the first line of Eq. (39) the integration over v can then be carried out. In the second line, we integrate by parts in u . This leads to some simplifications and produces, after combining the $v \in [-u, 0]$ and $v \in [0, u]$ integration ranges,

$$C_q \sim \frac{1}{\sqrt{\pi}} \frac{t_w}{t^{3/2}} e^{-\frac{1}{4}(1-t_w^2/t^2)tq^2} - \frac{4}{\pi} \frac{t_w}{\tau^{3/2}} e^{-\frac{1}{4}\tau q^2} \int_0^{\infty} du \frac{\sin(\sqrt{t_w} qu)}{\sqrt{t_w} q} \int_0^u dv v e^{-(t_w/\tau)v^2} f(u, v),$$

where

$$f(u, v) = \frac{u+v}{2} e^{-\frac{1}{4}(u+v)^2} \Phi\left(\frac{u-v}{2}\right) - \frac{u-v}{2} e^{-\frac{1}{4}(u-v)^2} \Phi\left(\frac{u+v}{2}\right). \quad (41)$$

This is our general scaling result for the dynamic structure factor. Let us now consider some limit cases of Eq. (40). We first study the regime $\tau \ll t_w$. In this case the exponential $e^{-(t_w/\tau)v^2}$ peaks sharply at $v = 0$. To leading order in τ/t_w we may replace

the upper integration limit u of the v -integration with ∞ and approximate $f(u, v)$ by its expansion at $v = 0$. Since $f(u, 0) = 0$ we use $f(u, v) \approx v \partial_v f(u, v)|_{v=0}$. Also noting that $f(u, v)$ satisfies the identity $\partial_v f(u, v)|_{v=0} = \partial_u [u e^{-u^2/4} \Phi(u/2) - (2/\sqrt{\pi}) e^{-u^2/2}]$ and using integration by parts in u then gives

$$C_q \approx \frac{1}{\sqrt{\pi t_w}} e^{-\frac{1}{4}\tau q^2} \left[e^{-\frac{1}{4}\tau q^2} - \sqrt{2} e^{-\frac{1}{2}t_w q^2} + \int_0^\infty du \cos(\sqrt{t_w} q u) u e^{-\frac{1}{4}u^2} \Phi\left(\frac{u}{2}\right) \right], \quad (42)$$

in the regime $\tau \ll t_w$ and to leading order in τ/t_w . It turns out that Eq. (42) reduces correctly to the static structure factor for $\tau \rightarrow 0$; this can be verified rigorously by setting $\tau = 0$ in the full expression Eq. (38) and then expanding for large t_w and fixed $t_w q^2$. Either way one ends up with the result

$$C_q(t_w, t_w) \sim \frac{1}{\sqrt{\pi t_w}} \left[1 - \sqrt{2} e^{-\frac{1}{2}t_w q^2} + \int_0^\infty du \cos(\sqrt{t_w} q u) u e^{-\frac{1}{4}u^2} \Phi\left(\frac{u}{2}\right) \right]. \quad (43)$$

The static structure factor has a local minimum at $q = 0$, where it measures energy fluctuations $C_E(t_w, t_w) = C_{q=0}(t_w, t_w)$. We find the value $C_{q=0}(t_w, t_w) = (3 - 2\sqrt{2})/\sqrt{\pi t_w}$ from Eq. (43). This is, of course, consistent with the expansion Eq. (32) of $C_E(t, t_w)$ from above. For $t_w q^2 \gg 1$, $C_q(t_w, t_w)$ quickly approaches $n(t_w) = 1/\sqrt{\pi t_w}$. This large q behaviour originates from the scaling of $C_{r=0}(t_w, t_w) = n(t_w) - n(t_w)^2 \sim n(t_w)$. The local minimum in the static structure factor is caused by an ‘‘effective repulsion’’ of defects in the diffusion-coagulation dynamics: defects that have survived up to time t_w are likely to be far from each other, i.e. at a distance $\mathcal{O}(\sqrt{t_w})$. A similar effect was seen in the aging regime of plaquette models [126].

To understand the scaling of $C_q(t, t_w)$ for $1 \ll \tau \ll t_w$ we return to Eq. (42). The profile of $C_q(t, t_w)$ is as follows: on the scale $t_w q^2 = \mathcal{O}(1)$, where $\tau q^2 \ll 1$ since $\tau \ll t_w$, Eq. (42) is still essentially equal to the static structure factor Eq. (43). However, on the larger scale in q where $\tau q^2 = \mathcal{O}(1)$, and hence $t_w q^2 \gg 1$, one has from Eq. (42),

$$C_q(t, t_w) \approx \frac{1}{\sqrt{\pi t_w}} e^{-\frac{1}{2}\tau q^2}. \quad (44)$$

This makes sense intuitively. The wavevector scale $\tau q^2 = \mathcal{O}(1)$ corresponds to a length scale $\ell(\tau) = \mathcal{O}(\sqrt{\tau})$. Here, since $\tau \ll t_w$, we may treat defects as independent random walkers. Correlations in $C_r(t, t_w)$ on the lengthscale $\ell(\tau)$ are diffusive, and this is consistent with Eq. (44). On the lengthscale $\ell(t_w) = \mathcal{O}(\sqrt{t_w})$, corresponding to $t_w q^2 = \mathcal{O}(1)$, on the other hand, spatial correlations $C_r(t, t_w)$ are still essentially static and this translates into $C_q(t, t_w) \approx C_q(t_w, t_w)$, c.f. Eq. (42) and Eq. (43).

We now turn to the scaling of $C_q(t, t_w)$ in the opposite regime $\tau \gg t_w$. Here an expansion of Eq. (40) follows rather straightforwardly. The exponential $e^{-(t_w/\tau)v^2}$ becomes flat and may be replaced by unity to leading order in t_w/τ ; this is justified since $f(u, v)$ vanishes sufficiently fast in v . Moreover, the only relevant wavevector scale is $\tau q^2 = \mathcal{O}(1)$ so that $\sin(\sqrt{t_w} q u) \approx \sqrt{t_w} q u$. Here we have used $\sqrt{t_w} q \ll 1$ since $t_w \ll \tau$ and the fact that again only small u contribute to the integral. Thus altogether,

$$C_q(t, t_w) \approx \frac{t_w}{\tau^{3/2}} e^{-\frac{1}{4}\tau q^2} \left[\frac{1}{\sqrt{\pi}} - \frac{4}{\pi} \int_0^\infty du u \int_0^u dv v f(u, v) \right], \quad (45)$$

The expression in the square brackets only produces an overall coefficient. To evaluate it one has to change the integration variables back to x, y . Then the integrals can be factorized and one readily obtains

$$C_q(t, t_w) \approx \frac{3\pi - 8}{3\pi^{3/2}} \frac{t_w}{\tau^{3/2}} e^{-\frac{1}{4}\tau q^2}, \quad (46)$$

in the regime $\tau \gg t_w$ and to leading order in t_w/τ . This result contrasts with Eq. (44) in several ways. First, the scaling of the amplitude of correlations $C_q(t, t_w)$ changes from $\mathcal{O}(t_w^{-1/2})$ in the regime $\tau \ll t_w$ to $\mathcal{O}(t_w/\tau^{3/2})$ when $\tau \gg t_w$. Second, the shape of $C_q(t, t_w)$ on the wavevector scale $\tau q^2 = \mathcal{O}(1)$ is always Gaussian, however, the exponents in Eq. (44) and Eq. (46) differ by a factor of $\frac{1}{2}$. Third, the overall coefficient in Eq. (46) is *not* related to the static structure factor at $q = 0$. These differences between Eq. (44) and Eq. (46) arise from the fact that for $\tau \gg t_w$ many-body effects play an important role; defects meet and coagulate. This regime is fluctuation-dominated with all loop diagrams contributing in a field theoretic framework, see Sec. 2.3.4 below.

Having discussed the dynamic structure factor $C_q(t, t_w)$ in detail we now turn to the analysis of response functions. Let us first consider the asymmetric part $R_r^{(a)}(t, t_w)$ of the response function. The Fourier transform of Eq. (19) follows immediately from the identity Eq. (A.8) and is given by

$$R_q^{(a)}(t, t_w) \sim \partial_{t_w} e^{-2t} \left[I_0(2A) + \frac{t \cos(q/2)^2 + t_w \sin(q/2)^2}{A} I_1(2A) \right], \quad (47)$$

where $A = \sqrt{t^2 \cos(q/2)^2 + t_w^2 \sin(q/2)^2}$. The scaling of this expression in the aging limit $t_w \rightarrow \infty$ with τ/t_w and $t_w q^2$ fixed follows using Eq. (A.3) as

$$R_q^{(a)}(t, t_w) \sim \partial_{t_w} \frac{1}{\sqrt{\pi t}} e^{-\frac{1}{4}(1-t_w^2/t^2)tq^2}. \quad (48)$$

At $q = 0$ this reduces to the asymmetric part of the energy response $R_E^{(a)}(t, t_w) = R_{q=0}^{(a)}(t, t_w)$ and vanishes, c.f. Eq. (48), since – as discussed above – the asymmetric perturbations cancel when applied uniformly. Integration over q , on the other hand, yields the scaling Eq. (26) for the auto-response $R_{r=0}^{(a)}(t, t_w) = \int (dq/2\pi) R_q^{(a)}(t, t_w)$. The small and large τ scaling forms of Eq. (48) are

$$\tau \ll t_w : R_q^{(a)}(t, t_w) \approx \frac{1}{2} t_w q^2 \frac{1}{\sqrt{\pi} t_w^{3/2}} e^{-\frac{1}{2}\tau q^2}, \quad (49)$$

$$\tau \gg t_w : R_q^{(a)}(t, t_w) \approx \frac{1}{2} t_w q^2 \frac{1}{\sqrt{\pi} \tau^{3/2}} e^{-\frac{1}{4}\tau q^2}. \quad (50)$$

In analogy with the results for correlations, the exponents in the Gaussians differs by a factor of $\frac{1}{2}$ between Eq. (49) and Eq. (50). For the construction of FD plots we need the step response function associated with $R_q^{(a)}(t, t_w)$. This is obtained straightforwardly from Eq. (48),

$$\chi_q^{(a)}(t, t_w) = \int_{t_w}^t dt' R_q^{(a)}(t, t') \sim \frac{1}{\sqrt{\pi t}} \left[1 - e^{-\frac{1}{4}(1-t_w^2/t^2)tq^2} \right]. \quad (51)$$

It remains to work out the scaling of the symmetric part $R_q^{(s)}(t, t_w)$ of the response function. To calculate the Fourier transform of Eq. (20) we use the identities Eq. (A.8) and Eq. (A.9), which produce

$$R_q^{(s)}(t, t_w) \sim -e^{-2t} \cos\left(\frac{q}{2}\right)^2 \left[I_0(2A) - \frac{t^2 - (t - t_w)^2 \sin^2(q/2)}{A^2} I_2(2A) \right], \quad (52)$$

again with $A = \sqrt{t^2 \cos^2(q/2) + t_w^2 \sin^2(q/2)}$. We now perform the usual aging expansion $t_w \rightarrow \infty$ with τ/t_w and $t_w q^2$ fixed. But for Eq. (52) some care is needed: the leading terms in the expansion cancel. Therefore the first subdominant terms in the modified Bessel functions have to be retained. In this way one obtains the scaling

$$R_q^{(s)}(t, t_w) \sim -\frac{1}{2\sqrt{\pi}t^{3/2}} \left(1 - \frac{1}{2}t_w q^2 \frac{t - t_w}{t} \right) e^{-\frac{1}{4}(1-t_w^2/t^2)tq^2}. \quad (53)$$

The small and large τ scaling forms of Eq. (53) are

$$\tau \ll t_w : R_q^{(s)}(t, t_w) \approx -\frac{1}{2\sqrt{\pi}t_w^{3/2}} \left(1 - \frac{1}{2}\tau q^2 \right) e^{-\frac{1}{2}\tau q^2}, \quad (54)$$

$$\tau \gg t_w : R_q^{(s)}(t, t_w) \approx -\frac{1}{2\sqrt{\pi}\tau^{3/2}} e^{-\frac{1}{4}\tau q^2}. \quad (55)$$

Once again the coefficient in the exponents of the Gaussians crosses over from $\frac{1}{2}$ to $\frac{1}{4}$ as we go from the regime $\tau \ll t_w$ to $\tau \gg t_w$.

Integration of the expression Eq. (53) yields a simple result for the step response function associated with $R_q^{(s)}(t, t_w)$,

$$\chi_q^{(s)}(t, t_w) = \int_{t_w}^t dt' R_q^{(s)}(t, t') \sim -\frac{t - t_w}{2\sqrt{\pi}t^{3/2}} e^{-\frac{1}{4}(1-t_w^2/t^2)tq^2}. \quad (56)$$

Putting together the results from above yields the FD plots for the observables n_q in the FA model. In contrast to the case of the local observable n_i non-trivial limit plots do exist as long as we keep tq^2 or equivalently $\sqrt{t}q$ constant as we increase t . We use normalized plots showing $\tilde{\chi}_q$ versus $\Delta\tilde{C}_q = 1 - \tilde{C}_q$ where

$$\tilde{\chi}_q(t, t_w) = \frac{\chi_q(t, t_w)}{C_q(t, t)} \quad \text{and} \quad \tilde{C}_q(t, t_w) = \frac{C_q(t, t_w)}{C_q(t, t)}. \quad (57)$$

If parameterized with t_w , the slope in the plots directly gives the FDR X_q . For our wavevector observables we use $C_q(t, t)$, Eq. (43), to normalize the plots. The scaling expression for $C_q(t, t_w)$ is stated in Eq. (40) and $\chi_q(t, t_w) = \chi_q^{(a)}(t, t_w) + \chi_q^{(s)}(t, t_w)$ is given by Eq. (51) and Eq. (56), respectively. Numerical evaluation of these quantities produces the FD plots shown in Fig. 2.

We first note that observables n_q with $\sqrt{t}q \gg 1$ produce FD plots close to the equilibrium line $\tilde{\chi}_q = 1 - \tilde{C}_q$, similarly as is the case for the local defect observable n_i . Very small values of q , $\sqrt{t}q \ll 1$, on the other hand, yield essentially the same FD plot as the energy ($q = 0$ curve in Fig. 2). For intermediate wavevectors q the FD plots interpolate between these two extremes. The wavevectors q have an associated intrinsic lengthscale $\ell = 1/q$. Thus the observables n_q allow one to probe violations of FDT on any given lengthscale. While the coarsening dynamics equilibrate short length scales

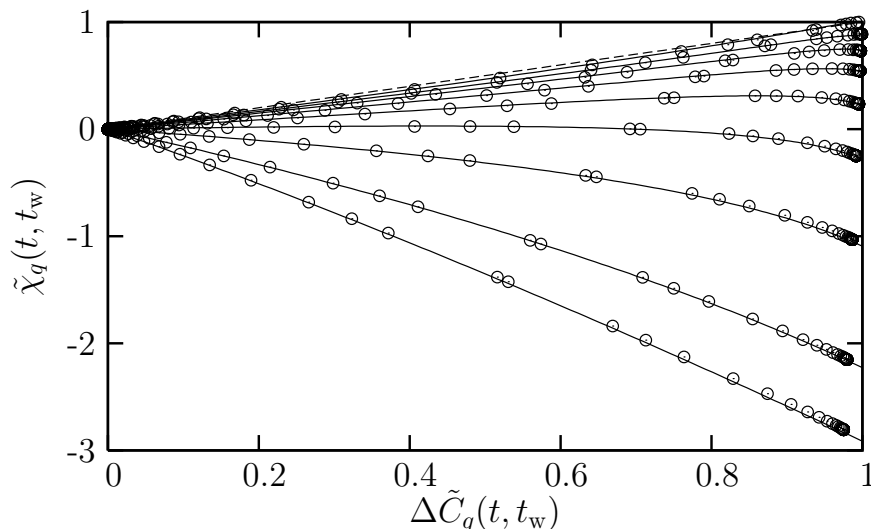


Figure 2. Normalized FD plots for Fourier mode observables n_q in the $d = 1$ FA model. Symbols are simulation data at $T = 0.08$ in a system of linear size $L = 700$, at final time $t = 4.87 \times 10^7$ and wavevector $q = (2\pi/L)j$ with $j = 0, 3, 6, 9, 12, 15, 18, 21$ and 27 (from bottom to top); note that t is given in microscopic units rather than units of $1/c$, as used in the analysis. The dashed line represents equilibrium FDT. Full lines show the theoretical scaling predictions. The lowest curve is for $q = 0$ and gives the FD plot for the energy. It is slightly curved, with slope increasing (in modulus) from $-(1 + \sqrt{2})$ at the origin to X_q^∞ , Eq. (58), on the right.

$\ell \ll \sqrt{t}$, large length scales $\ell \gg \sqrt{t}$ remain far from equilibrium with a well defined violation of FDT corresponding to the case $q = 0$.

The FD plots in Fig. 2 are unusual in two ways: first, they are non-monotonic and second, the step-response functions χ_q can actually become negative. We remark that the non-monotonicity of the plots is genuine and not due to incorrect parameterization with t instead of t_w [112]. As for the local and global observables discussed above, the response function R_q comprises an asymmetric and symmetric contribution. In the regime $\tau \ll t_w$, $R_q^{(a)} > 0$ dominates over $R_q^{(s)} < 0$, see Eqs. (49, 54). One then verifies from Eqs. (44, 49) that $X_q \sim R_q^{(a)}(t, t_w)/\partial_{t_w} C_q(t, t_w) \sim 1$. Equilibrium FDT is satisfied for $\tau \ll t_w$ and all FD plots have slope $X_q \sim 1$ close to the origin. This applies with the exception of $q = 0$ itself; numerically, already for small but nonzero q the initial equilibrium regime is difficult to discern from the plots. In the opposite regime $\tau \gg t_w$, on the other hand, $R_q^{(s)} < 0$ dominates over $R_q^{(a)} > 0$, c.f. Eqs. (50, 55), and the response R_q becomes negative. This causes the non-monotonic FD plots and negative step-response functions χ_q . The resulting asymptotic FDR X_q^∞ for $\tau \gg t_w$ is given by $X_q \sim R_q^{(s)}(t, t_w)/\partial_{t_w} C_q(t, t_w)$, and from the scalings Eqs. (46, 55), takes the value

$$X_q^\infty = -\frac{3\pi}{6\pi - 16} \approx -3.307. \quad (58)$$

All FD plots in Fig. 2 thus end with the same slope X_q^∞ on the right, regardless of q . This is clearly observable in the plots with $\sqrt{t}q \ll 1$ but becomes difficult to detect when $\sqrt{t}q \gg 1$. This reinforces the general point that observables which probe directly large,

non-equilibrated length scales are better suited for measurement of X_q^∞ [125, 136].

Negativity of the response function R_q can be traced back to the activated nature of the dynamics. Perturbations coupling to the n_i affect the energy barriers for creation of defects on these sites. This effect and the associated response functions can be decomposed into symmetric $R_q^{(s)}$ and asymmetric $R_q^{(a)}$ contributions, with the former trapping diffusing excitations but the latter accelerating their dynamics. In the regime $\tau \gg t_w$ the acceleration effect dominates, and the faster relaxation towards $n(t) \rightarrow 0$ decreases the expectation values $\langle n_i(t) \rangle$, thus the negative sign of the response functions R_q . We will see below that similar arguments apply to FA models in dimensions $d > 1$ and also to the East model.

The asymptotic scaling results derived in this section are confronted with numerical data in Fig. 2. The simulations are based on the continuous time BKL algorithm [138]. Step response functions χ_q with $q \neq 0$ are measured using the no-field method of Chatelain [122, 123, 124], while a specialised no-field method is employed for the $q = 0$ case, see Sec. 2.4 below. These no-field methods enable us to construct properly parameterised FD plots with $t_w \in [0, t]$ as the running parameter. It is obvious from Fig. 2 that excellent agreement is obtained between the scaling results and the simulation data.

2.3. Field theoretical approach

In this subsection we describe how to calculate aging properties of the FA model by means of an effective field theory built from the Doi-Peliti [139, 140] formalism for systems with stochastic dynamics. This approach to treat the FA model was first introduced in [21] and developed further in [23, 24]. A summary of the results below, in so far as they relate to aging dynamics for dimensions $d > d_c = 2$, can be found in [125]. The aim of this section is to provide a detailed discussion of the calculations leading to those results, and to consider their extension to $d < d_c$ where a comparison with the exact results from the previous section can be performed.

2.3.1. Effective theory and dynamical action We consider the “bosonic” version of the FA model [21, 23, 24]: we allow for each site of the lattice to contain any number of excitations; that is, $n_i = 0, 1, \dots$ indicates the occupation of site i . Since we are interested in the regime of low temperatures where the equilibrium density of excitations is low, removing the hard-core restriction on site occupation does not change the behaviour of the model significantly [21, 23, 24].

The derivation of the field theory for this version of the FA model was described in detail in Ref. [23] (see also [24]). The effective theory is defined for excitations on a lattice of N sites in d dimensions with integer occupancy per site. As explained above, excitations can effectively diffuse between neighbouring sites with a rate proportional to c ; neighbouring excitations can coalesce with a rate likewise proportional to c [21, 125, 24]. Excitations can also branch into pairs, but the rate for this process

goes as c^2 , and we disregard it in our analysis of aging at low temperatures. Using the Doi-Peliti formalism [139, 140, 141, 142] we can represent this dynamics in terms of complex fields $\phi(\mathbf{r}, t)$, $\bar{\phi}(\mathbf{r}, t)$ with an action [21, 23, 24, 125]

$$S = \int_{\mathbf{r}, t} \bar{\phi}(\partial_t - D\nabla^2)\phi + \lambda\bar{\phi}(1 + \bar{\phi})\phi^2 - n_0\bar{\phi}\delta(t), \quad (59)$$

where $D, \lambda \propto c$. This is the field theory for the $A + A \rightarrow A$ reaction-diffusion process [141, 142]. In this representation the local occupation number operator $\hat{n}(\mathbf{r}, t)$ is given by

$$\hat{n}(\mathbf{r}, t) = [1 + \bar{\phi}(\mathbf{r}, t)] \phi(\mathbf{r}, t). \quad (60)$$

The last term in (59) indicates a Poisson distribution of random initial conditions of density n_0 . Correlation functions are calculated through the path integral: $\langle \hat{A}(t) \rangle = \int D\bar{\phi}D\phi \hat{A}[\hat{n}(t)]e^{-S}$.

2.3.2. Tree-level density and two-time correlations For $d > d_c = 2$ the field theory is finite and a tree level calculation will give the correct behaviour at long times. Such a tree-level analysis amounts to solving the Euler-Lagrange equations. From (59) we have:

$$\frac{\delta S}{\delta \bar{\phi}(t)} = (\partial_t - D\nabla^2)\phi + \lambda(1 + 2\bar{\phi})\phi^2 - n_0\delta(t) = 0, \quad (61)$$

$$\frac{\delta S}{\delta \phi(t)} = -(\partial_t + D\nabla^2)\bar{\phi} + 2\lambda\bar{\phi}(1 + \bar{\phi})\phi = 0. \quad (62)$$

The average density is given by:

$$n(t) \equiv V^{-1} \int_{\mathbf{r}, t} \langle \hat{n}(\mathbf{r}, t) \rangle = V^{-1} \int_{\mathbf{r}, t} \langle \phi(\mathbf{r}, t) \rangle = V^{-1} \langle \phi_0(t) \rangle, \quad (63)$$

where $\phi_{\mathbf{q}}(t)$ is the Fourier transform of $\phi(\mathbf{r}, t)$, $\phi_{\mathbf{q}}(t) = \int_{\mathbf{r}} e^{-i\mathbf{q}\cdot\mathbf{r}}\phi(\mathbf{r}, t)$ [similarly for $\bar{\phi}_{\mathbf{q}}(t)$], and we have used that averages with a factor $\bar{\phi}$ on the left (i.e. at the latest time) vanish. Taking the expectation value of Eq. (61) allows us to calculate $n(t)$ at tree level:

$$\langle \frac{\delta S}{\delta \bar{\phi}(t)} \rangle = 0 \Rightarrow \partial_t \langle \phi_0 \rangle + \lambda V^{-1} \langle \phi_0 \rangle^2 = 0 \Rightarrow n(t) = \frac{n_0}{1 + \lambda n_0 t} \approx \frac{1}{\lambda t}. \quad (64)$$

From (62) we can get the tree-level propagator $G_{\mathbf{q}}(t, t_w) \equiv V^{-1} \langle \phi_{\mathbf{q}}(t) \bar{\phi}_{-\mathbf{q}}(t_w) \rangle$. To $O(\bar{\phi}^2)$, Eq. (62) can be integrated to give:

$$\bar{\phi}_{\mathbf{k}}(t_w) = \frac{n^2(t)}{n^2(t_w)} e^{-Dq^2(t-t_w)} \bar{\phi}_{\mathbf{k}}(t). \quad (65)$$

Making use of the identity $\lim_{\epsilon \rightarrow 0} V^{-1} \langle \phi_{\mathbf{q}}(t + \epsilon) \bar{\phi}_{-\mathbf{q}}(t) \rangle = 1$, we obtain:

$$G_{\mathbf{q}}(t, t_w) = \frac{n^2(t)}{n^2(t_w)} e^{-Dq^2(t-t_w)}. \quad (66)$$

Equations (61) and (66) now allow to compute two-time density correlations,

$$C_q(t, t_w) \equiv \int_{\mathbf{r}} e^{i\mathbf{q}\cdot\mathbf{r}} [\langle \hat{n}(\mathbf{r}, t) \hat{n}(\mathbf{0}, t_w) \rangle - n(t)n(t_w)] \quad (67)$$

$$= V^{-1} \langle \phi_{\mathbf{q}}(t) \phi_{-\mathbf{q}}(t_w) + \phi_{\mathbf{q}}(t) \bar{\phi}_{-\mathbf{q}}(t_w) V^{-1} \phi_0(t_w) \rangle \quad (68)$$

$$= V^{-1} \langle \phi_{\mathbf{q}}(t) \phi_{-\mathbf{q}}(t_w) \rangle + G_q(t, t_w) n(t_w). \quad (69)$$

We now use (61) to obtain the correlations at tree-level from $\langle \phi_{\mathbf{q}}(t) \delta S / \delta \bar{\phi}_{\mathbf{q}}(t_w) \rangle = 0$:

$$\partial_{t_w} C_q(t, t_w) + \lambda n(t_w) (z + 2) C_q(t, t_w) - \lambda n^2(t_w) G_q(t, t_w) (2z + 1) = 0, \quad (70)$$

where

$$z \equiv \frac{Dq^2}{\lambda n(t_w)} \approx Dq^2 t_w. \quad (71)$$

The general form of $C_q(t, t_w)$ that results is

$$C_q(t, t_w) = f(z) n(t_w) G_q(t, t_w), \quad (72)$$

where $f(z)$ obeys $z f'(z) + (2z + 3) f(z) - (2z + 1) = 0$. The solution to this equation is:

$$f(z) = \frac{1}{2z^3} (e^{-2z} - 1) + \frac{1}{z^2} - \frac{1}{z} + 1 \approx \begin{cases} \frac{1}{3} + \frac{z}{3} & (z \ll 1) \\ 1 - \frac{1}{z} & (z \gg 1) \end{cases}, \quad (73)$$

with z given by Eq. (71).

2.3.3. Tree-level response and FDR Consider now a perturbation h_q of wavevector q , cf. Eq. (37). The corresponding change in the rate constants is $D_q \rightarrow D\delta_{q0} + D\beta h_q$ and $\lambda_q \rightarrow \lambda\delta_{q0} + \lambda\beta h_q$. The change in the average density, to linear order in h_q , is given by the linear order correction $\langle \phi_{\mathbf{q}}(t) \rangle^{(1)}$ to the expectation value of ϕ . This can be calculated at tree level by expanding $\langle \delta S / \delta \bar{\phi} \rangle = 0$ to linear order in δh_q :

$$0 = \partial_t \langle \phi_{\mathbf{q}}(t) \rangle^{(1)} + [Dq^2 + 2\lambda n(t)] \langle \phi_{\mathbf{q}}(t) \rangle^{(1)} - \beta h_q(t) \lambda n^2(t) \left[\frac{Dq^2}{\lambda n(t)} - 1 \right]. \quad (74)$$

Here we have used the fact that when the diffusion constant is not uniform, as is the case with a perturbation like the one here, the diffusion term in the action reads $-\int_{\mathbf{r}, t} \bar{\phi} \nabla \cdot (D \nabla \phi - \phi \nabla D)$ [125]. The response, $R_q(t, t_w)$, is given by $R_q(t, t_w) = T \delta \langle \phi_{\mathbf{q}}(t) \rangle^{(1)} / \delta h_q(t_w)$, and obeys the differential equation:

$$\partial_t R_q(t, t_w) + [Dq^2 + 2\lambda n(t)] R_q(t, t_w) - \delta(t - t_w) \lambda n^2(t) \left[\frac{Dq^2}{\lambda n(t)} - 1 \right] = 0, \quad (75)$$

which implies the initial condition $R_q(t_w, t_w) = (z - 1) \lambda n^2(t_w)$. By integrating the above equation we get:

$$R_q(t, t_w) = (z - 1) \lambda n^2(t) e^{-Dq^2(t-t_w)}. \quad (76)$$

From equations (72) and (76) we obtain the FDR for large t and t_w and for all momenta,

$$X_q(t, t_w) = \frac{z - 1}{(1 + \partial_z) z f(z)} = \begin{cases} -3 + 12z & (z \ll 1) \\ 1 - 1/z & (z \gg 1) \end{cases}, \quad (77)$$

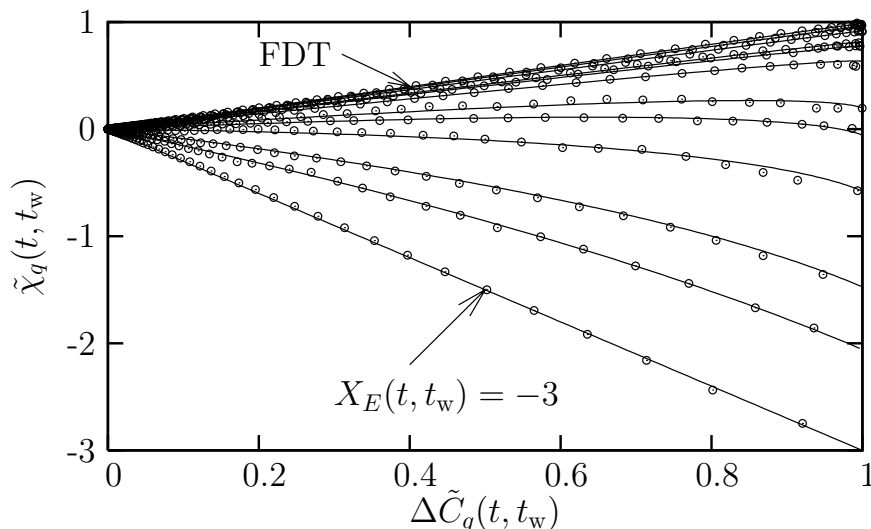


Figure 3. Normalized FD plots for Fourier mode observables n_q in the $d = 3$ FA model. Symbols are simulation data at $T = 0.1$ in a system of linear size $L = 32$, for final time $t = 2 \times 10^5$ and wavevectors $q = \pi/x$ with $x = 1, 2, 2.4, 3, 3.2, 4, 5.33, 6, 8, 12, 16$ and ∞ (top to bottom). Full lines show the field theoretical predictions, accumulating on the equilibrium FDT line at large q . At the other extreme, the lowest curve coincides with the FD plot for the energy at $q = 0$, which is a straight line with slope -3 . From Ref. [125]. Copyright American Physical Society.

where z is given by Eq. (71) as before. At any waiting time t_w , for wavevectors q larger than $1/\sqrt{Dt_w}$, FDT is recovered: $X_q \approx 1$. On the other hand, at small enough wavevectors, $q \ll 1/\sqrt{Dt_w}$, the FDR becomes negative. In the limit $q \rightarrow 0$, we get the FDR for energy fluctuations,

$$X_E(t, t_w) \equiv X_{q=0}(t, t_w) = -3. \quad (78)$$

From (77) this is also the asymptotic FDR $X_q^\infty = \lim_{t_w \rightarrow \infty} \lim_{t/t_w \rightarrow \infty} X_q(t, t_w)$ for *any* wavevector. As for the one-dimensional case, a detailed comparison (see Fig. 3) between these analytical results and direct numerical simulations of the FA model in dimension $d = 3$ shows very good agreement over the complete range of wavevectors, from the straight line of equilibrium FDT for large q to the energy FD plot (straight line of slope $X_E = -3$) for small q .

2.3.4. RG analysis and FDR for $d < d_c$ For dimensions below the critical dimension d_c the field theory needs to be renormalised. Our RG analysis here follows that of Ref. [141, 142]. The theory only requires coupling constant renormalization. The Callan-Symanzik equations for two-time correlation and response functions, in terms of renormalized quantities, read:

$$0 = [2(Dt)\partial_{Dt} + 2(Dt_w)\partial_{Dt_w} - q\partial_q + \beta(g_R)\partial_{g_R} - dn_0\partial_{n_0} + d] C_q(t, t_w; n_0, g_R, \kappa),$$

$$0 = [2(Dt)\partial_{Dt} + 2(Dt_w)\partial_{Dt_w} - q\partial_q + \beta(g_R)\partial_{g_R} - dn_0\partial_{n_0} + (d+2)] R_q(t, t_w; n_0, g_R, \kappa),$$

where we have made explicit the dependence of the functions on the initial density, the renormalized coupling constant, g_R , and the arbitrary scale κ which relates the

dimensional coupling λ to the adimensional one $g = (\lambda/D) \kappa^{d-2}$. The function $\beta(g_R)$ is the exact beta-function [141, 142]. These equations are solved by the method of characteristics [141, 142]

$$C_q(t, t_w; n_0, g_R, \kappa) = \left(\frac{t}{t_0}\right)^{-d/2} C_{q\sqrt{t/t_0}} \left(t_0, t_0 \left(\frac{t_w}{t}\right); n_0 \left(\frac{t}{t_0}\right)^{d/2}, g_R(t), \sqrt{\frac{1}{Dt_0}}\right), \quad (79)$$

$$R_q(t, t_w; n_0, g_R, \kappa) = \left(\frac{t}{t_0}\right)^{-d/2-1} R_{q\sqrt{t/t_0}} \left(t_0, t_0 \left(\frac{t_w}{t}\right); n_0 \left(\frac{t}{t_0}\right)^{d/2}, g_R(t), \sqrt{\frac{1}{Dt_0}}\right), \quad (80)$$

where $g_R(t)$ is the running coupling [141, 142]. In the asymptotic limit $t \rightarrow \infty$ this approaches its fixed-point value, $g_R(t) \rightarrow g_R^*$ ($= 2\pi$ for $d = 1$).

We can now use the tree-level results (72, 76) and Eqs. (79, 80) to obtain the renormalized tree-level correlation and response. To leading order in g_R and for long times we make the replacement $\lambda \rightarrow Dg_R^* \kappa^{2-d}$. Using (79, 80) and setting $d = 1$ we obtain for large t and t_w :

$$C_q(t, t_w) \approx f(Dq^2 t_w) \frac{1}{g_R^* \sqrt{Dt}} \left(\frac{t_w}{t}\right) e^{-Dq^2(t-t_w)}, \quad (81)$$

$$R_q(t, t_w) \approx (Dq^2 t_w - 1) \frac{1}{g_R^* \sqrt{Dt}^{3/2}} e^{-Dq^2(t-t_w)}. \quad (82)$$

The time dependence of these correlations and responses is different from that for $d > d_c$, see Eqs. (72-76). The FDR, however, is the same as that given in (77). The above expressions fail to reproduce the exact results obtained above for $d = 1$ (see Sec. 2.2.3). Eqs. (81, 82) are the renormalized tree-level functions. In principle one could calculate loop corrections which will change the dependence on times and wavevector. It is likely, however, that the discrepancy with the exact results will persist. The problem is similar to what occurs with one-time functions [141, 142]: the RG analysis is based on a $d - d_c$ expansion which is not quantitatively accurate at $d = 1$.

Simulations performed in dimensions $d = 1$ to $d = 4$ fully confirm our results, see Fig. 4. While the $d = 1$ FD plot for the energy is curved and follows perfectly the theoretical predictions obtained in Sec. 2.2.2, the plots in higher dimensions are all compatible with the straight line of slope -3 calculated in this section.

2.4. Simulation methodology

Chatelain proposed a very useful no-field method for measuring response functions in spin systems with Markovian dynamics [122, 123, 124]. The response is re-expressed as a multi-point correlation function, which has the advantage that it can be calculated from unperturbed trajectories. However, the efficiency of this method is poor for long-ranged perturbations: the statistics can become very noisy, especially for the collective quantities we want to study here. It turns out, however, that the response of KCMs to energy/temperature perturbations has special properties that make it possible to derive a more efficient no-field method. Specifically, in any KCM and any dimension [125], the

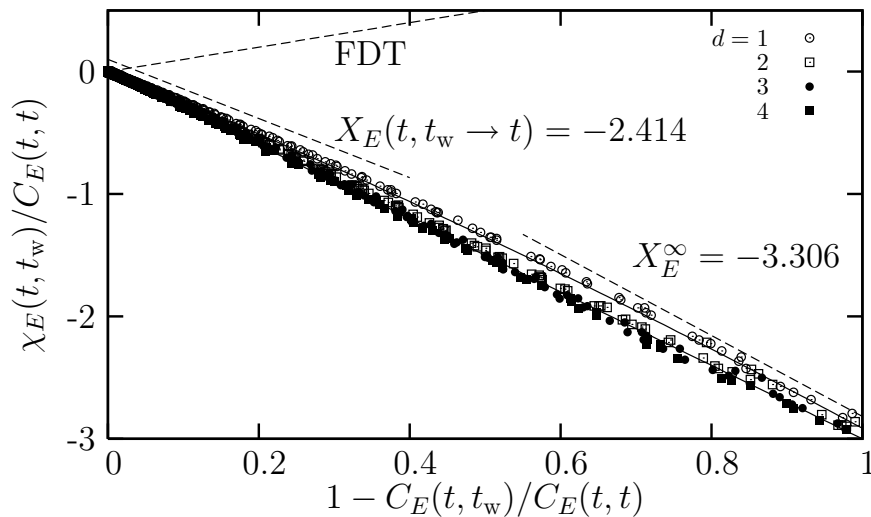


Figure 4. Normalized energy FD plots for the FA model in dimensions $d = 1$ to 4. Symbols show simulation data, all taken in the aging regime for $T = 0.2$ to 0.06 and $t = 10^4$ to 10^8 . Full curves show a straight line with slope -3 and the exact limit plot in $d = 1$ with asymptotic slopes shown as dashed lines. From Ref. [125]. Copyright American Physical Society.

step response can be written as

$$\chi_E(t, t_w) = \frac{1}{2} [(1 - 2c) \tau \partial_t n(t) + C_E(t, t) - C_E(t, t_w) + C_Y(t, t) - C_Y(t, t_w)]. \quad (83)$$

Here $C_Y(t, t_w) = (1/N)(\langle E(t)Y(t_w) \rangle - \langle E(t) \rangle \langle Y(t_w) \rangle)$ is the normalized connected correlation between the energy E and the random variable

$$Y(t) = \int_0^t dt' U(t') \quad \text{with} \quad U = \sum_{i=1}^N f_i(\mathbf{n})(n_i - c). \quad (84)$$

In Monte Carlo simulations the integrand in Eq. (84) is constant between successive spin-flips and hence the integral becomes a sum $Y(t) = \sum_{t_i \leq t} (t - t_{i-1})U(t_i)$, with t_i the sequence of updating events. Equation (84) is easily implemented, especially in event driven code that keeps track of mobile sites i with $f_i(\mathbf{n}) \neq 0$. By recording histories of the energy $E(t)$ and the observable $Y(t)$, step response functions $\chi_E(t, t_w)$ follow immediately from Eq. (83). Importantly, one can obtain values of $\chi_E(t, t_w)$ for arbitrary combinations of t, t_w by averaging over a stored collection of histories. This is crucial for the efficient generation of FD plots with fixed t and running t_w . Without this method, it would have been impossible to obtain the collection of data shown in Fig. 4.

In the remainder of this section we present a derivation of the no-field method Eq. (83). It is convenient to use the operator formalism introduced earlier. We first consider the disconnected correlation $D_E(t, t_w) = \langle E(t)E(t_w) \rangle$ which can be expressed in the form $D_E(t, t_w) = \langle \mathbf{e} | \hat{E} e^{W\tau} \hat{E} e^{Wt_w} | p_0 \rangle$, with $|\mathbf{e}\rangle = \sum_{\mathbf{n}} |\mathbf{n}\rangle$ as before and $|p_0\rangle$ the initial state. Differentiating this with respect to t_w at fixed t (note that $\tau = t - t_w$) gives

$$\partial_{t_w} D_E(t, t_w) = \langle \mathbf{e} | \hat{E} e^{W\tau} [\hat{E}, W] e^{Wt_w} | p_0 \rangle, \quad (85)$$

where $[A, B] = AB - BA$ denotes the commutator. For our derivation we will also need the response $G_E(t, t_w) = T[\delta\langle E(t) \rangle / \delta h(t_w)]$ of the energy to the perturbation $\delta E = -h \sum_i n_i$. In the operator formalism this is

$$G_E(t, t_w) = \langle \mathbf{e} | \hat{E} e^{W\tau} V e^{Wt_w} | p_0 \rangle. \quad (86)$$

The perturbation operator is $V = T\partial_h W(h)|_{h=0}$ where $W(h)$ denotes the master operator in the presence of the field h . The basic idea for deriving a no-field method for the measurement of $G_E(t, t_w)$ is simple: we try to form a linear combination $aG_E(t, t_w) + b\partial_{t_w} D_E(t, t_w) = \langle \mathbf{e} | \hat{E} e^{W\tau} X e^{Wt_w} | p_0 \rangle$ with $X = aV + b[\hat{E}, W]$ so that off-diagonal components in X match the master operator W (there exist no coefficients a, b such that X is purely diagonal). Then this quantity can be expressed as a time derivative. It turns out that the relevant linear combination is $a = 2$ and $b = -1$. To see this let us work out the explicit form of V and $[\hat{E}, W]$. From the master operator Eq. (9) we see that calculation of V only requires $T\partial_h c(h)|_{h=0} = c(1-c)$; the Glauber rate for activation in the presence of the field is $c(h) = 1/[1 + e^{\beta(1-h)}]$. So,

$$V = c(1-c) \sum_{i=1}^N (F_i - 1) \hat{f}_i (1 - 2\hat{n}_i). \quad (87)$$

The calculation of the commutator $[\hat{E}, W]$, on the other hand, essentially reduces to $[\hat{n}_i, F_j]$ and this is $[\hat{n}_i, F_j] = \delta_{i,j} F_i (1 - 2\hat{n}_i)$, whence

$$[\hat{E}, W] = \sum_{i=1}^N F_i \hat{f}_i (c - \hat{n}_i). \quad (88)$$

Based on the last two equations one verifies that $X = 2V - [\hat{E}, W] = (1-2c)W + \hat{U}$, with $\hat{U} = \sum_i \hat{f}_i (\hat{n}_i - c)$ the (diagonal) operator corresponding to the observable U , Eq. (84). This is now a no-field method because

$$\begin{aligned} 2G_E(t, t_w) - \partial_{t_w} D_E(t, t_w) &= \langle \mathbf{e} | \hat{E} e^{W\tau} X e^{Wt_w} | p_0 \rangle \\ &= (1-2c) \langle \mathbf{e} | \hat{E} e^{W\tau} W e^{Wt_w} | p_0 \rangle + \langle \mathbf{e} | \hat{E} e^{W\tau} \hat{U} e^{Wt_w} | p_0 \rangle \\ &= (1-2c) \partial_t \langle E(t) \rangle + \langle E(t) U(t_w) \rangle. \end{aligned} \quad (89)$$

Note that this equation applies to *any* KCM since we have not made any assumptions on the particular form of the kinetic constraint $f_i(\mathbf{n})$. We have only used that the unconstrained flip rates $w_i(\mathbf{n})$ are Glauber rates for $E = \sum_i n_i$ (a similar result can be derived for Metropolis rates). It remains to switch from disconnected to connected correlations in Eq. (89) and to multiply by $1/N$ so that all quantities are intensive. This gives

$$2R_E(t, t_w) = (1-2c) \partial_t n(t) + \partial_{t_w} C_E(t, t_w) + \frac{1}{N} (\langle E(t) U(t_w) \rangle + \langle E(t) \rangle \partial_{t_w} \langle E(t_w) \rangle). \quad (90)$$

Obviously $R_E(t, t_w) = (1/N)G_E(t, t_w)$, $C_E(t, t_w) = (1/N)(D_E(t, t_w) - \langle E(t) \rangle \langle E(t_w) \rangle)$ and $n(t) = (1/N)\langle E(t) \rangle$. But the last term in Eq. (90) is in fact the connected correlation between $E(t)$ and $U(t_w)$ since

$$\partial_{t_w} \langle E(t_w) \rangle = \langle \mathbf{e} | \hat{E} W e^{Wt_w} | p_0 \rangle = -\langle \mathbf{e} | \hat{U} e^{Wt_w} | p_0 \rangle = -\langle U(t_w) \rangle. \quad (91)$$

The identity $\langle \mathbf{e} | \hat{E}W = -\langle \mathbf{e} | \hat{U}$ is most easily seen from Eq. (88) by multiplying both sides with $\langle \mathbf{e} |$ and using conservation of probability $\langle \mathbf{e} | W = 0$ as well as completeness of the projection state $\langle \mathbf{e} | F_i = \langle \mathbf{e} |$. Equation (91) makes intuitive sense: according to its definition, Eq. (84), U is a measure for how much the concentration over *mobile* spins (with $f_i(\mathbf{n}) = 1$) differs from the equilibrium concentration c . Thus, if $\langle U(t_w) \rangle > 0$ there is an excess of mobile $n_i = 1$ spins and $\langle E(t_w) \rangle$ will decrease, and vice versa. Our no-field method Eq. (83), finally, follows by integrating Eq. (90) to obtain the step response $\chi_E(t, t_w) = \int_{t_w}^t dt' R_E(t, t')$.

For completeness we add that this no-field method of course reduces to the standard FDT in equilibrium. This is most easily seen from Eq. (89). In equilibrium the term $\partial_t \langle E(t) \rangle = 0$ drops out since the energy is stationary. Further, $\partial_{t_w} D_E(t, t_w) = -\langle \mathbf{e} | \hat{E}W e^{W(t-t_w)} \hat{E} | p_{\text{eq}} \rangle = \langle \mathbf{e} | \hat{U} e^{W(t-t_w)} \hat{E} | p_{\text{eq}} \rangle = \langle U(t) E(t_w) \rangle = \langle E(t) U(t_w) \rangle$, where the last equality expresses time-reversal symmetry. Thus Eq. (89) retrieves the FDT $G_E(t, t_w) = \partial_{t_w} D_E(t, t_w)$ in equilibrium.

3. East model

In the second part of this paper we move to the East model, a directed variant of the FA model. It is defined on a one-dimensional lattice, i.e. a chain of N spins, and differs from the FA model only in the choice of facilitation factor:

$$f_i(\mathbf{n}) = n_{i-1}. \quad (92)$$

Compared to $f_i = n_{i-1} + n_{i+1}$ in the FA case, this allows facilitation only from the left; the spin to the “East” of each defect is mobile. This seemingly harmless change has profound consequences. In particular, there are no finite groups of defects that can diffuse unimpeded over a defect-free (all down-spin) background. This is clear because the leftmost up-spin of any such group will never be able to change its state, due to the absence of a facilitating neighbour on the left. The East model therefore has much more cooperative dynamics, and its relaxation times correspondingly diverge more quickly as c decreases towards zero. In fact, when expressed in terms of temperature, relaxation times to equilibrium after a quench diverge as an exponential of inverse temperature *squared*, $\ln t_{\text{rel}} \propto 1/T^2 \propto \ln^2(1/c)$ [27, 28, 116, 117, 143], compared to the Arrhenius dependence $\ln t_{\text{rel}} \propto \ln(1/c) \approx 1/T$ for the FA case.

We consider again the dynamics after a quench from equilibrium at infinite temperature, where every spin is up independently with probability 1/2, to some low final temperature T . On timescales of $O(1)$ the system will reach a state where all up-spins are isolated. Further reduction in the defect density proceeds via thermally activated fluctuations, but now in a much more non-local manner than for the FA model: each up-spin can flip down only when, starting from the nearest up-spin on the left, a fluctuating “front” of up-spins has extended sufficiently far to the right to mobilize it. To be specific, consider an up-spin at site d , and let the nearest up-spin on the left be at site 0. To relax this “domain” of length d , a front of defects needs to propagate from n_0

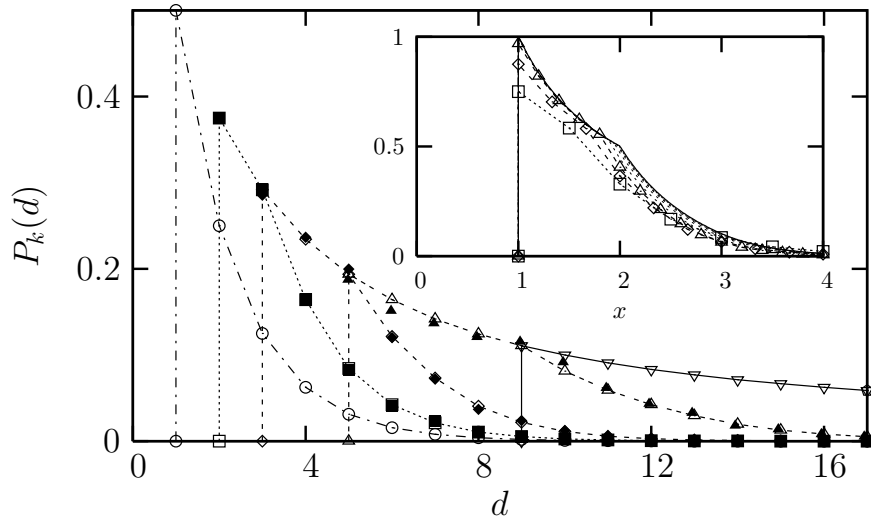


Figure 5. Domain size distribution in the East model in the first few plateaus of the dynamics. Open symbols are the theoretical prediction for the irreversible coarsening regime, filled symbols are from simulations. Circles: $k = -1$ (initial condition), squares: $k = 0$, diamonds: $k = 1$, upward triangles: $k = 2$, downward triangles: $k = 3$. The inset shows $d_{\min} P_k(d)$ versus $x = d/d_{\min}$ to show the approach to the predicted scaling form $\tilde{P}(x)$ (solid line) for large k .

so that it creates a defect at site $d - 1$, thus mobilizing n_d . Naively one might suspect that the creation of this front takes an energy $d - 1$, with spins n_1, n_2, \dots, n_{d-1} simply flipped up in sequence. However, further reflection [6, 116, 117] shows that the most efficient way of creating a front is hierarchical on lengthscales increasing as powers of two: after flipping up n_1 and n_2 , n_1 can be flipped down; then n_3 and n_4 are flipped up, n_3 is flipped down, and finally n_2 is eliminated by reversing the initial part of the process. Pictorially, one has

$$\begin{aligned} 10000 &\rightarrow 11000 \rightarrow 11100 \rightarrow 10100 \rightarrow 10110 \rightarrow 10111 \rightarrow 10101 \rightarrow \\ &\rightarrow 11101 \rightarrow 11001 \rightarrow 10001 \rightarrow \dots \end{aligned}$$

Effectively one creates a “stepping stone” at site 2, steps from there to site 4, and removes the stepping stone at site 2; this process can then be continued by creating a stepping stone at site 8 from the one at site 4 and so on. Keeping track of the maximum number of extra defects that exist at any one time, one shows that the energy barrier for flipping down the up-spin at site d (via creation of an up-spin at site $d - 1$) is

$$k \text{ for } 2^{k-1} < d \leq 2^k, \quad (93)$$

where $k = 0, 1, 2, \dots$ [116, 117]. Such relaxation processes therefore take place on timescales $t \approx \exp(k/T) \approx c^{-k}$. Importantly, in the limit of small c the ratio of any two of these timescales diverges, and the dynamics separates naturally into “stages” labelled by the value of k . We can include in this picture the initial relaxation after the quench, where domains of length $d = 1$ disappear without activation; this is stage $k = 0$.

To understand the non-equilibrium dynamics in more detail, it is useful to view it as a coarsening process: when the up-spin at the right boundary of a domain disappears,

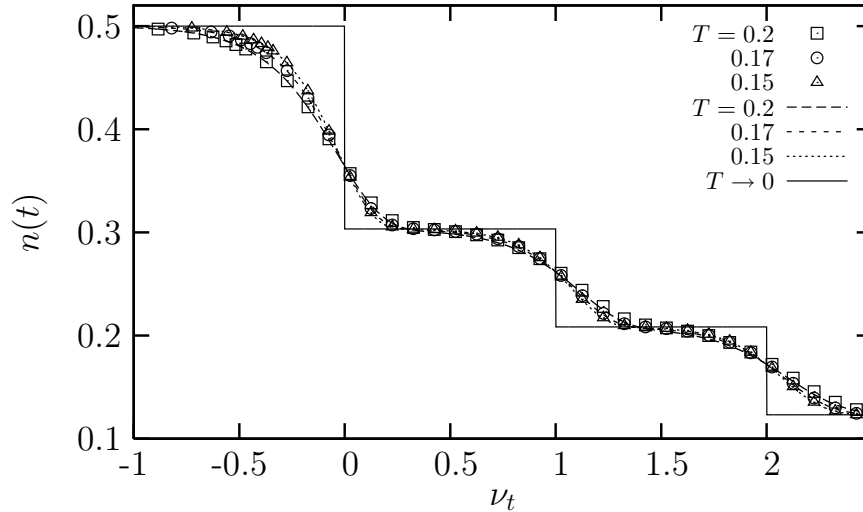


Figure 6. Defect density $n(t)$ versus ν_t for three different temperatures. Symbols represent the simulation results. The theoretical prediction (118) is shown at finite T with dotted lines, while its $T \rightarrow 0$ limit is shown as a full line.

this domain merges with the neighbouring domain on the right. Because the rate for disappearance of an up-spin depends only on the length d of the domain it bounds, it is clear that no correlations between neighbouring domain lengths can ever develop during such a process [116, 117]. For low c , the evolution of the domain size distribution, $P(d, t)$, can therefore be calculated without approximation by an “independent interval” approach. In stage k of the dynamics one finds the equation of motion (for $d > 2^k$)

$$\frac{\partial}{\partial t} P(d, t) = \sum_{2^{k-1} < d' \leq 2^k} P(d - d', t) \left[-\frac{\partial}{\partial t} P(d', t) \right]. \quad (94)$$

The sum runs over the “active” domain sizes d' that are eliminated during stage k . The rate for creating longer “inactive” domains is then the product of the rate $[-(\partial/\partial t)P(d', t)]$ at which domains of size d' disappear, and the probability of having a domain of length $d - d'$ on the right. As shown in Appendix B, this equation can be solved to relate the domain size distributions at the beginning and the end of stage k , and this relation can then be iterated numerically, starting from the initial $P(d, t = 0) = 2^{-d}$ [116]. The results are shown in Fig. 5 for the domain size distributions $P_k(d)$ in the first few “plateaus” of the dynamics. Here we label each plateau by the stage which it follows, i.e. plateau 0 refers to times $1 \ll t \ll c^{-1}$. More generally we will use the notation

$$\nu = T \ln t, \quad k = \lfloor \nu \rfloor, \quad a = \nu - k, \quad (95)$$

so k denotes the plateau that has been reached (and the stage of the dynamics that has finished) at time t . To avoid confusion we note that plateaus were labelled by $k + 1$ in previous work [116, 117]; in our convention, the initial condition corresponds to plateau $k = -1$.

As Fig. 5 shows, the predicted domain size distributions agree well with simulation data at low T . From the domain size distribution one can predict in particular the defect density, giving $n(t) = 1/\bar{d}_k$ where $\bar{d}_k = \sum_d dP_k(d)$ is the average domain length in plateau k . Again this agrees well with simulation data (Fig. 6), though the sharp steps that are predicted for $T \rightarrow 0$ in a plot of n vs ν at the integer values $\nu = 0, 1, 2, \dots$ are obviously rounded at nonzero T . By analysing the dynamics in more detail (see Appendix B and Eq. (118) below) also this effect can be predicted, and then gives a very good description of the data.

A further observation from Fig. 5 is that the domain size distributions approach a scaling form for large k . This is obtained by scaling with the minimum domain size present at time t ,

$$d_{\min}(t) = 2^k + 1, \quad (96)$$

so that $d_{\min}(t)P_k(d)$ is plotted versus $x = d/d_{\min}(t)$. The limiting distribution $\tilde{P}(x)$ can in fact be worked out explicitly [116, 117]: its Laplace transform is $1 - \exp[-\text{Ei}(s)]$ where $\text{Ei}(s) = \int_1^\infty dz \exp(-zs)/z$ is the exponential integral. Expanding in powers of $\text{Ei}(s)$ and inverting the transform gives then

$$\tilde{P}(x) = \sum_{l=1}^{\infty} \frac{(-1)^l}{l!} f_l(x), \quad (97)$$

where the functions $f_l(x)$ can be defined recursively by successive convolutions,

$$f_0(x) = \delta(x), \quad f_1(x) = \Theta(x-1)\frac{1}{x}, \quad f_{l+1}(x) = (f_l * f_1)(x). \quad (98)$$

Here $\Theta(x)$ and $\delta(x)$ are the standard Heaviside step and Dirac delta functions. Explicitly one has $f_2(x) = \Theta(x-2)(2/x) \ln(x-1)$, while for $l \geq 3$ the $f_l(x)$ cannot be expressed in any simple closed form. Fortunately each $f_k(x)$ contains a factor $\Theta(x-k)$ so for realistic ranges of x only the first few functions are needed. The mean value of x across the distribution (97) is $\exp(\gamma) = 1.78\dots$, with γ being Euler's constant. Converting back to the unscaled defect density gives then

$$n(t) = e^{-\gamma} 2^{-k}, \quad (99)$$

for large k . Because of the logarithmic dependence of k on t , this scales as $n(t) \sim t^{-T \ln 2}$: the East model exhibits anomalously slow coarsening, with the decay exponent $T \ln 2$ that governs the decay of the defect density decreasing towards zero at low temperature.

We will refer to the above analysis of the East model dynamics after a quench to low c (or equivalently low T) as “irreversible coarsening”. It becomes exact in the limit $c \rightarrow 0$ taken at fixed stage k , i.e. with typical domain sizes d kept fixed and of order unity. This way of taking the limit ensures that up-spins do indeed flip down irreversibly: the probability of observing, at some given point in time and within a domain of length d , an up-spin as part of a fluctuating up-spin front is $O(dc)$ and can be neglected in the limit. Also, even though within a given stage k there can and will in general be multiple relaxation timescales because active domains cover a range of lengths and can be eliminated by passing through different sequences of intermediate configurations, the

timescales for different stages do always separate by much more than this spread for low c .

Both of the above simplifying properties no longer apply if we wish to look at typical domain sizes of the order of the equilibrium domain length $\bar{d}_{\text{eq}} = 1/c$. We would then take c small at fixed $\delta = dc$, rather than at fixed d . For δ of order unity and larger, this gives information on the eventual crossover to equilibrium behaviour. For the purposes of this paper we will only be concerned with the earliest stages of this crossover, $\delta \ll 1$. This should connect appropriately with the large- d limit of the irreversible coarsening regime, where from (93) the timescale for relaxation of a domain of length d is $t \sim c^{-k} \sim c^{-\ln d / \ln 2} \approx d^{1/(T \ln 2)}$. A simple scaling hypothesis, supported by numerical evaluation of first passage times for the elimination of domains of large d , then gives the following picture [117]. The splitting into discrete stages of the dynamics is lost because the spectrum of relaxation times within the stages becomes so broad that a clear separation no longer exists. However, there is now a *continuous* form of timescale separation: the time t for eliminating a domain of scaled size δ is again $t \sim (\delta/c)^{1/(T \ln 2)}$. Comparing two different domain sizes δ_1 and δ_2 then shows that one always has $t_2/t_1 \gg 1$ in the limit $T \rightarrow 0$, as long as $\delta_2/\delta_1 > 1$. As a consequence, each up-spin has a sharply (on the spatial scale $d \sim 1/c$) defined “equilibration zone” to its right, of size $\delta \sim ct^{-T \ln 2}$. As t increases these zones grow; when an equilibration zone reaches the next up-spin to the right the latter is eliminated and the two domains either side merge. Put differently, the dynamics consists of always eliminating the shortest domain and “pasting” all of its length on to the domain on the right. This “paste-all” model has been studied independently in the literature [144]. Remarkably, the domain size distribution it produces in the scaling limit is exactly identical [117] to the one we found in Eq. (97). This shows that the irreversible coarsening regime of the East model connects smoothly to the paste-all regime just discussed, as it should: in the large- k limit of irreversible coarsening the domain size distribution approaches (97), and this form is preserved – apart from a trivial scaling with the minimum domain length d_{min} – in the paste-all dynamics. The paste-all regime has two advantages for theoretical analysis: only the smallest domain length is “active” and hence the temporal order in which domains disappear is deterministic; this is not the case in the irreversible coarsening regime, where two neighbouring domains of different lengths can be simultaneously active so that either can disappear first. Secondly, the role of the clock is played by d_{min} , so that effectively diverging timescales,

$$t \sim d_{\text{min}}^{1/(T \ln 2)}, \quad (100)$$

can be considered. Even where predictions cannot be extracted analytically, they are then relatively easy to obtain by numerical simulation.

After this overview of the theoretical tools used to analyse the low- T out-of-equilibrium dynamics of the East model we turn as in the FA case to specific correlation and response function pairs, first for local observables, then for the global one (which is just the energy), and finally for non-local observables. Because we need to deal with

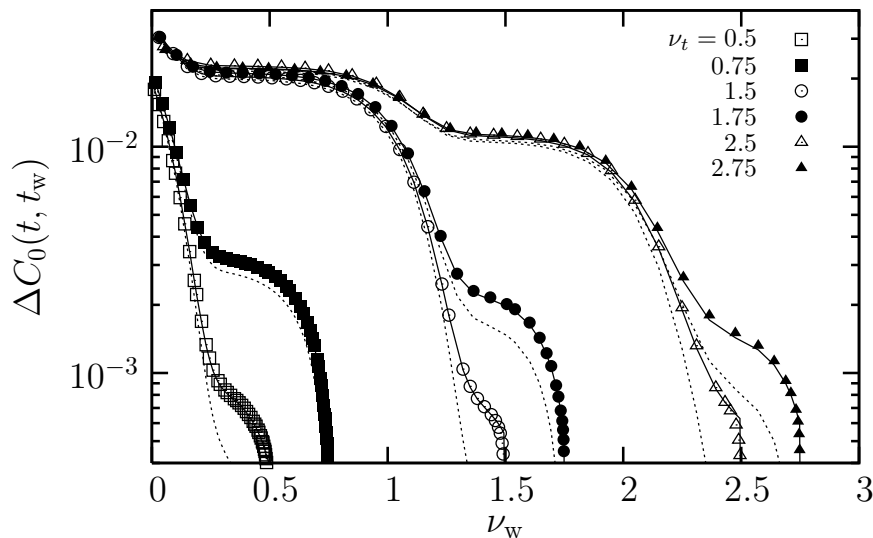


Figure 7. Local correlation function difference from simulations, for ν_t as indicated and $T = 0.15$ (symbols). Dotted lines: leading order prediction (103). Solid lines: theory including quasi-equilibrium corrections (113). Note the logarithmic y -axis; on a linear axis the correction terms would be difficult to discern.

two-time functions in all cases it will be useful to refine our notation from (95) to

$$\nu_t = T \ln t, \quad k_t = \lfloor \nu_t \rfloor, \quad a_t = \nu_t - k_t, \quad (101)$$

with analogous quantities defined for t_w (giving ν_w , k_w , a_w) and the time difference $\tau = t - t_w$ (giving ν_τ , k_τ , a_τ). Simulations are carried out for system sizes $N = 250$ and for temperatures $T = 0.2, 0.17, 0.15$, with corresponding equilibrium up-spin concentrations of $c = 6.69 \times 10^{-3}, 2.78 \times 10^{-3}$ and 1.27×10^{-3} . For numerical convenience we mainly restrict ourselves to waiting times $t_w \geq 1$ when simulating two-time quantities.

3.1. Local correlation and response

We begin with the local correlation function $C_0(t, t_w) = \langle n_i(t_w)n_i(t) \rangle - n(t_w)n(t)$. Within the irreversible coarsening regime the time-dependence of this quantity is easy to determine: any spin that is up at time t must also have been up at time t_w since to leading order in c spins never flip back up. This implies $\langle n_i(t_w)n_i(t) \rangle = \langle n_i(t) \rangle = n(t)$ and so

$$C_0(t, t_w) = n(t)[1 - n(t_w)]. \quad (102)$$

Simulation data are compared with this prediction – which is, trivially, exact for $t_w = t$ – in Fig. 7. To make our later understanding of the FD behaviour easier we plot the data in the same form as required in an FD plot, showing the correlation function difference $\Delta C_0(t, t_w) = C_0(t, t) - C_0(t, t_w)$ for which the prediction (102) takes the form

$$\Delta C_0(t, t_w) = n(t)[n(t_w) - n(t)]. \quad (103)$$

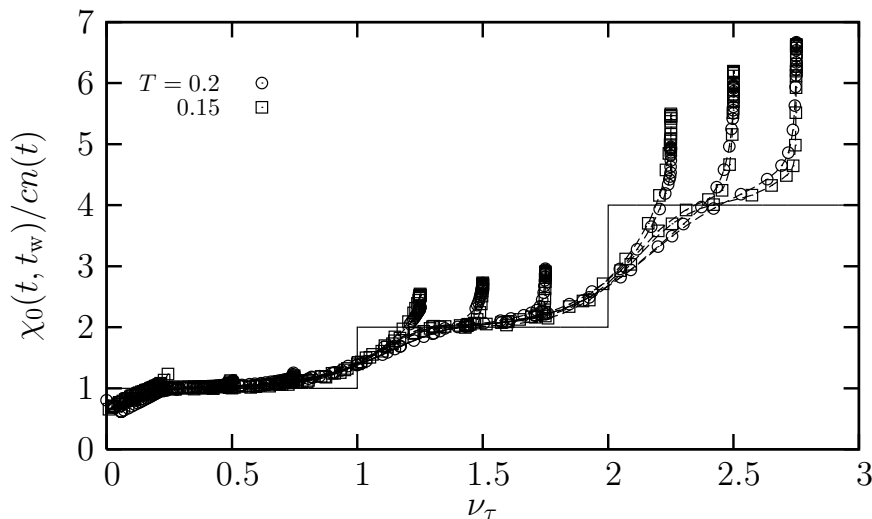


Figure 8. Local susceptibility $\chi_0(t, t_w)$ in the quasi-equilibrium regime, scaled by $cn(t)$ and plotted against $\nu_\tau = T \ln(t - t_w)$. The steps show the theoretical prediction (108) for $c \rightarrow 0$. Squares correspond to $T = 0.15$, circles to $T = 0.2$. For both temperatures we show data for $\nu_t = 0.25, 0.5, 0.75, 1.25, 1.5, 1.75, 2.25, 2.5$ and 2.75 (from left to right).

This is plotted against t_w or, more precisely, ν_w . The theoretical estimate (103) rationalizes the simulation data quite well, but there clearly are small corrections for nonzero c . These are most noticeable when t and t_w are close together inside the same plateau of the dynamics; Eq. (103) then predicts a very small correlation function difference because $n(t_w) \approx n(t)$. The actual values are somewhat larger because there is an additional quasi-equilibrium contribution in this regime. This correction can be most easily determined via FDT from the local susceptibility χ_0 , to which we turn next.

To understand the effect of a field h_i applied at time t_w on the evolution of spin n_i , let us take the history $n_{i-1}(t')$ of its facilitating left neighbour as given in the time interval $t' = t_w \dots t$. Spin n_i then behaves like an isolated spin except for the fact that it cannot change state whenever $n_{i-1}(t') = 0$: the time interval available for it to relax from the state $n_i(t_w)$ is reduced from $t - t_w$ to $\int_{t_w}^t dt' n_{i-1}(t')$. Since with Glauber rates (6) the relaxation time of an isolated spin is unity, we thus have

$$\langle n_i(t) \rangle = c' + [n_i(t_w) - c'] \exp \left(- \int_{t_w}^t dt' n_{i-1}(t') \right). \quad (104)$$

Here, c' is the perturbed up-spin density at site i . To linear order in the field strength h_i it can be expanded as

$$c' = \frac{1}{1 + e^{\beta(1-h_i)}} = c + \beta h_i c(1 - c) + \dots \quad (105)$$

Inserting into (104) and differentiating w.r.t. βh_i , the initial value $n_i(t_w)$ drops out. After averaging over the history of n_{i-1} one thus gets for the local susceptibility the general expression

$$\chi_0(t, t_w) = c(1 - c) \left[1 - \left\langle \exp \left(- \int_{t_w}^t dt' n_{i-1}(t') \right) \right\rangle \right] \equiv c(1 - c)[1 - r(t, t_w)]. \quad (106)$$

For low c the factor $1 - c$ can be dropped, and it remains to understand the behaviour of the “relaxation integral” $r(t, t_w)$. The average over the dynamics in its definition can, for a large system, be replaced by an average over sites $j = i - 1$:

$$r(t, t_w) = \frac{1}{N} \sum_j \exp \left(- \int_{t_w}^t dt' n_j(t') \right). \quad (107)$$

Sites where a spin has been up for a total time larger than unity make a negligible contribution, so $r(t, t_w)$ is to a good approximation the fraction of sites with spins that have remained persistently down between t_w and t ; in other words, $\chi_0(t, t_w)/c$ is the fraction of sites that have been up at some point between t_w and t . From this we can predict its dependence on $t - t_w$ in the quasi-equilibrium regime, where t_w and t remain in the same plateau of the dynamics so that no domains disappear and the up-spins defining them can be regarded as fixed. As long as $\tau = t - t_w \gg 1$ but $\tau \ll c^{-1}$, only these fixed up-spins contribute to χ_0 ; since these also determine the overall up-spin density, one predicts $\chi_0/c = n(t_w)$. Once τ increases past c^{-1} , the right neighbour of each fixed up-spin will have had time to flip up once or more, so that $\chi_0/c = 2n(t_w)$. This process then proceeds: for $\tau \gg c^{-k}$, the relation (93) between energy barriers and distances implies that the $2^k - 1$ spins to the right of each fixed up-spin will have been up at some point. (The “ -1 ” arises because we are considering flipping spins *up*; the energy barrier for flipping a spin at distance d *down*, as written in (93), is the same as that for flipping a spin at distance $d - 1$ *up*.) Adding the contribution from the fixed up-spin back on gives overall

$$\chi_0(t, t_w) = c n(t_w) 2^{k\tau} = c n(t) 2^{k\tau}. \quad (108)$$

(Either $n(t_w)$ or $n(t)$ can be used in the prefactor since by assumption we remain in the same plateau.) This quasi-equilibrium prediction is checked against simulations in Fig. 8, with good agreement. Our use of the term “quasi-equilibrium” is justified by the fact that exactly the same step-like structure in χ_0 would be observed in equilibrium, except for the replacement of the density of “fixed” up-spins, $n(t)$, by the appropriate equilibrium value c . The simple scaling (108) of the step heights with powers of two does not seem to have been noticed in previous analyses of the equilibrium dynamics [6, 145, 117].

The quasi-equilibrium regime lasts while t and t_w remain in the same plateau of the dynamics, i.e. $k_t = k_w$. In the limit of low c we have $k_t = \max(k_w, k_\tau)$, so an equivalent condition for quasi-equilibrium is $k_\tau \leq k_w$. When t is held fixed as in Fig. 8, the limit $k_\tau = k_w$ corresponds to $\tau \approx t_w \approx t/2$ and so, again for low c , $k_\tau = k_t$. We thus expect to see k_t steps in χ_0 within the quasi-equilibrium regime, as confirmed by the data in Fig. 8.

Beyond the quasi-equilibrium regime we can continue to identify χ_0/c with the fraction of the chain swept by up-spins, but this now becomes more difficult to calculate as domains and the corresponding “swept out” areas merge. Within the paste-all regime, however, it is a relatively simple matter to get accurate predictions by simulating the paste-all dynamics and keeping track of the swept out areas within each domain. The

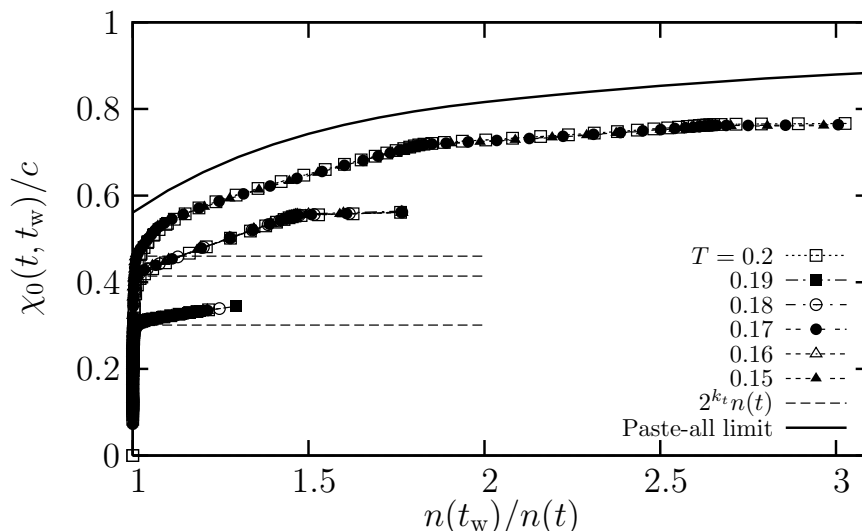


Figure 9. Local susceptibility χ_0 in units of c , plotted against $\theta = n(t_w)/n(t)$ to show the out-of-equilibrium regime. From bottom to top, we have $\nu_t = 0.5, 1.5$ and 2.75 . Horizontal lines indicate the predicted height of the quasi-equilibrium regime for the three cases. Solid line: theoretical prediction for the paste-all limit ($\nu_t \gg 1$).

clock variable for this simulation is $d_{\min}(t)/d_{\min}(t_w)$. Since in the paste-all regime the up-spin density scales with the inverse of d_{\min} , we can equivalently write

$$\chi_0(t, t_w)/c = \mathcal{F}(\theta), \quad \theta = n(t_w)/n(t). \quad (109)$$

We explain in Appendix F how the initial part of the scaling function can be calculated analytically, with the result

$$\mathcal{F}(\theta) = e^{-\gamma} \left(1 + \ln \theta - \frac{1}{2} \ln^2 \theta \right), \quad \text{for } \theta \leq 2. \quad (110)$$

This is in very good agreement with the numerical values extracted from the paste-all simulations, as demonstrated in more detail in Fig. 12 below. We show in Fig. 9 the overall prediction for χ_0/c versus $n(t_w)/n(t)$ and compare with numerical data. Even though the simulations are performed within the first few plateaus, i.e. far from the paste-all regime, the data for increasing ν_t clearly do approach the theoretical prediction. The initial discontinuity of the theory represents the contribution from the initial quasi-equilibrium regime, which in the limit of low c shrinks to the point $n(t_w)/n(t) = 1$. The value of χ_0/c at this point is $\exp(-\gamma) \approx 0.56$: each domain contains a swept-out equilibration zone of length $d_{\min}(t_w)$, and the density of domains is $n(t_w) = \exp(-\gamma)/d_{\min}(t_w)$, giving a swept out fraction $d_{\min}(t_w)n(t_w) = \exp(-\gamma)$ of the chain. This is entirely consistent with extrapolating to the same point from the quasi-equilibrium regime: as discussed above, the latter ends where $k_\tau = k_w$. At this point, from (108), $\chi_0/c = n(t_w)2^{k_w}$ which for large k_w approaches $\exp(-\gamma)$ from (99).

Before combining correlation and susceptibility data to get the FD plots we return to the quasi-equilibrium corrections to the local correlation function. To determine these

we use the following relation between local susceptibility and correlation:

$$\chi_0(t, t_w) = n(t)[1 - n(t_w)] - C_0(t, t_w) + c[n(t_w) - n(t)]. \quad (111)$$

This is derived in Appendix C; remarkably, it is *exact* and applies not just to the East model but in fact to all spin models with directed constraints. We used it to obtain the numerical data for the susceptibility in the simulations, but also checked it against direct susceptibility measurements. From the theoretical point of view we note that the first two terms on the r.h.s. of (111) cancel to leading order because of (102); this of course must be so because from (106) the susceptibility never becomes larger than c . Because the $O(c)$ -corrections to the correlation function are difficult to estimate directly, Eq. (111) would not be useful to deduce accurate estimates for χ_0 . We can, however, turn it around to get an expression for the correlation function (difference):

$$\Delta C_0(t, t_w) = n(t)[n(t_w) - n(t)] + \chi_0(t, t_w) - c[n(t_w) - n(t)]. \quad (112)$$

The last two contributions on the r.h.s. are the exact corrections to the irreversible coarsening estimate (103). They will be significant only in the quasi-equilibrium regime $n(t_w) \approx n(t)$, where furthermore the last term is negligible compared to the second one. The remaining dominant contribution to $\Delta C_0(t, t_w)$ is simply $\chi_0(t, t_w)$, as expected from FDT for dynamics in the quasi-equilibrium regime. Using (108) gives explicitly

$$\Delta C_0(t, t_w) \approx n(t)[n(t_w) - n(t)] + cn(t)2^{k\tau}. \quad (113)$$

This improved prediction is included in Fig. 7 above and now shows very good agreement with the numerical data. As expected, the correction term only affects the outcome when t and t_w are close together and the correlation function is still close to its equal-time value; elsewhere it is negligible.

We can now combine the above results to obtain the FD plot for the local observable in the East model. The raw results, with both axes scaled by $C_0(t, t)$ to produce the normalized two-time correlation $\tilde{C}_0(t, t_w) = C_0(t, t_w)/C_0(t, t)$ and susceptibility $\tilde{\chi}_0(t, t_w) = \chi(t, t_w)/C_0(t, t)$, are shown in Fig. 10, for fixed t with t_w varying along the curves. The data show clearly the initial quasi-equilibrium regime. The curves depart from this where t_w becomes small enough to have left the plateau that time t is in. The kinks in this out-of-equilibrium part of the curves, where points accumulate, correspond to t_w being well within a plateau; the next line segment begins when this plateau is being left and t_w moves (backwards) through the previous stage of the dynamics. The segments between the kinks appear straight to a good approximation, but close inspection of the data for larger ν_t (as included in Fig. 9, and Fig. 11 below) does show a small amount of curvature, as observed also in the not dissimilar triangular plaquette model [126]. The slopes of the segments, which give the local FDR $X_0(t, t_w)$, are indicated in the plot. They are significantly smaller than unity but do not, in this raw form, follow a clear pattern.

To determine a more appropriate scaling for the FD plot we recall from (109) that χ_0/c is a scaling function of $n(t_w)/n(t)$, at least in the paste-all limit. For the correlation function difference we see from (103) that $\Delta C_0(t, t_w)/n^2(t) = n(t_w)/n(t) - 1$ is a function

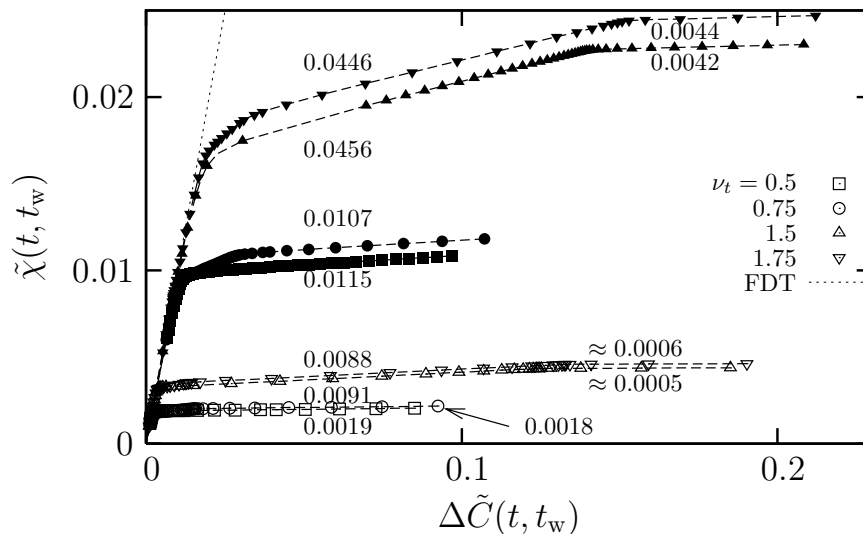


Figure 10. Normalized FD plot for the local observable for $T = 0.2$ (full symbols) and $T = 0.15$ (open symbols). The numbers indicate the value of the fluctuation-dissipation ratio X_0 in the various straight-line segments. For $T \rightarrow 0$ one expects the plot to depend only on $k_t = \lfloor \nu_t \rfloor$, while for nonzero T the sharp change at integer values of ν_t will be replaced by a smooth crossover. This is visible in the additional short linear segments just beyond the departure from quasi-equilibrium (dotted line) in the plots for $T = 0.2$ and $\nu_t = 0.75, 1.75$.

of the same scaling variable. (Since we are concerned with understanding the scaling in the non-equilibrium regime, we ignore here the small quasi-equilibrium corrections.) These considerations motivate one to plot, as we do in Fig. 11 (top), $\chi_0(t, t_w)/c$ vs $\Delta C_0(t, t_w)/n^2(t)$. The curves for different temperatures now collapse reasonably well, except for small shifts caused by the presence of the initial quasi-equilibrium regime. If these are removed by subtracting from both χ_0 and ΔC_0 the relevant contribution $cn(t)2^{k_t}$, as done in Fig. 11 (bottom), the collapse is really quite good.

Looking more quantitatively at the local FDR and comparing with the FA case, the most striking feature is that for the East model X_0 is never negative, even though the dynamics is activated. This is not just because any negative values are hard to see on the scale of the FD plot, as was the case for the FA model at late times. In fact, from (106) one has

$$R_0(t, t_w) = -\frac{\partial}{\partial t_w} \chi_0(t, t_w) = c(1-c) \left\langle n_{i-1}(t_w) \exp\left(-\int_{t_w}^t dt' n_{i-1}(t')\right) \right\rangle, \quad (114)$$

and because this local impulse response is always positive, the same is true of the local FDR. The magnitude of X_0 , on the other hand, is very small: the scaling of Fig. 11 shows that X_0 is roughly of the order of $c/n^2(t)$ for small c . To be precise, the expected scaling outside the trivial quasi-equilibrium regime is

$$X_0(t, t_w) = \frac{c}{n^2(t)} S_{k_t, \nu_w}. \quad (115)$$

This contains the overall prefactor from the scaling of the FD plot. The remaining coefficient S_{k_t, ν_w} depends only on the plateau k_t in which t is located, and the stage ν_w

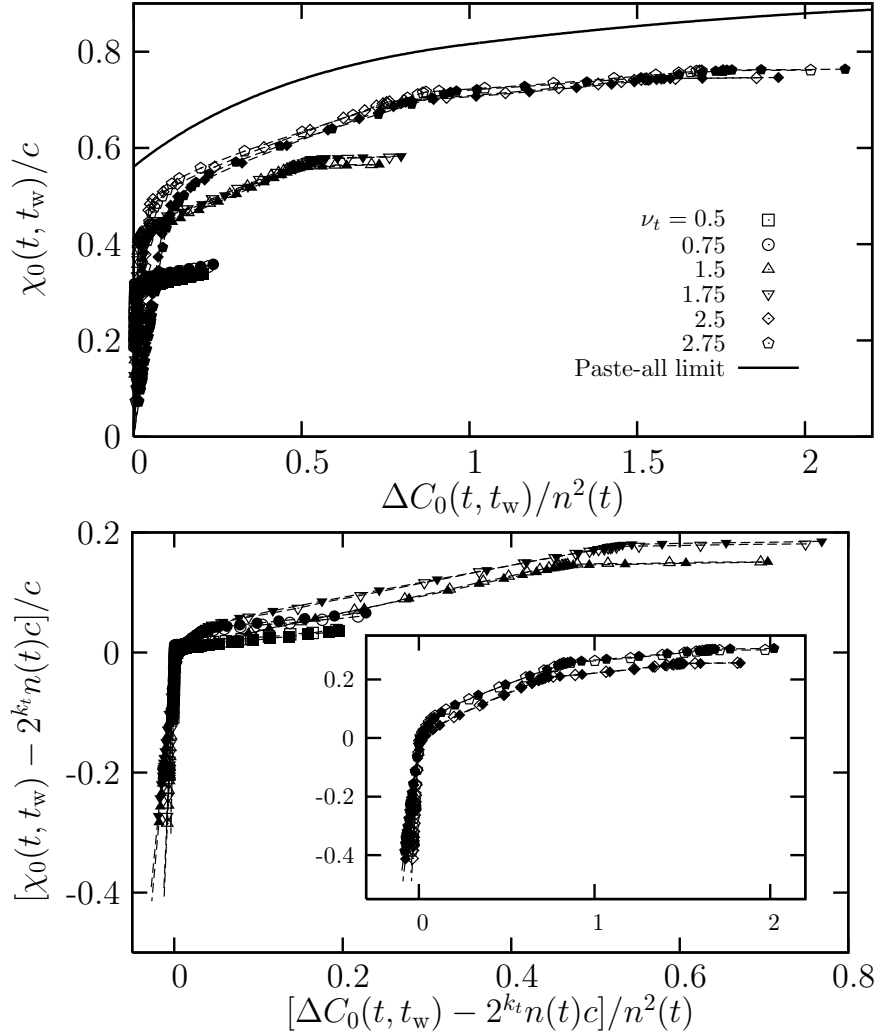


Figure 11. (Top) Scaled local FD plot for $T = 0.15$ (open symbols) and $T = 0.17$ (full symbols) for different values of ν_t . (Bottom) Same with quasi-equilibrium correction subtracted; the data for $\nu_t = 2.5, 2.75$ are shown separately in the inset for better visibility.

of the dynamics that t_w is traversing. Note here that the FDR is defined only for integer ν_w in the limit $c \rightarrow 0$: for all other values, t_w lies within a plateau and C_0 and $\Delta\chi_0$ are both constant. Table 1 shows the values of S determined from our numerical data. They show a relatively weak dependence on temperature, consistent with the expected approach to nonzero limits for $T \rightarrow 0$; as temperature decreases, also the expected independence from the non-integer part a_t of ν_t becomes manifest.

In our simulations we are necessarily restricted to exploring only the first few plateaus. Theoretically, we can also study the interesting paste-all limit where domain sizes are much larger than unity but still small compared to the average equilibrium domain length $1/c$; this could be viewed as the true asymptotic non-equilibrium regime. We have included in Fig. 11 (top) the paste-all prediction for the scaled FD plot. It is obtained by combining the predicted scaling (109) with $\Delta C_0(t, t_w)/n^2(t) =$

S_{k_t, ν_w}	T	$\nu_w = 0$	$\nu_w = 1$
$k_t = 0$	0.2	0.155	—
	0.17	0.149	—
	0.15	0.135	—
$k_t = 1$	0.2	0.0269	0.295
	0.17	0.0235	0.301
	0.15	0.0166	0.306
S_{k_t, ν_w}	T	$\nu_w = 0$	$\nu_w = 1$
$k_t = 0$	0.2	0.134	—
	0.17	0.132	—
	0.15	0.122	—
$k_t = 1$	0.2	0.0257	0.263
	0.17	0.0203	0.266
	0.15	0.0154	0.276

Table 1. Numerical values of S_{k_t, ν_w} for $a_t = 0.5$ (top) and $a_t = 0.75$ (bottom).

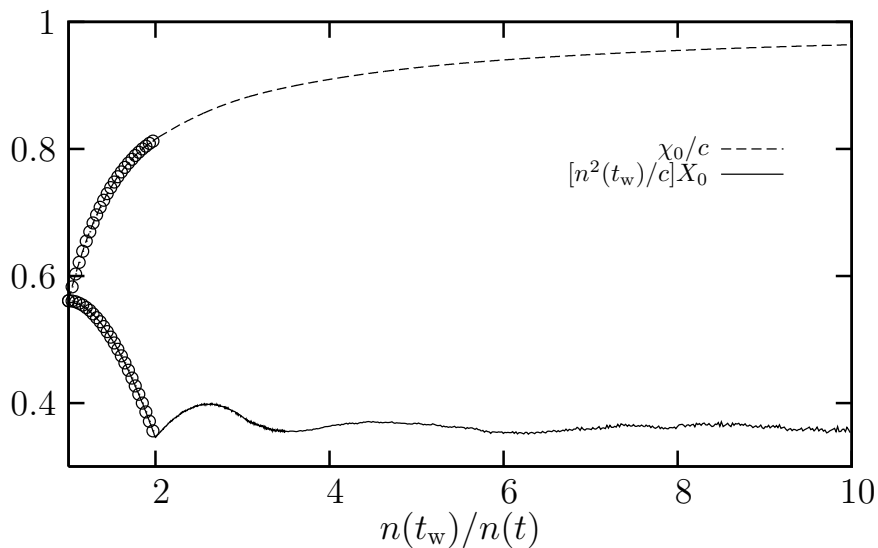


Figure 12. Paste-all prediction for $\chi_0(t, t_w)/c$ (dashed line) and $[n^2(t_w)/c]X_0(t, t_w)$ (solid line), plotted against $\theta = n(t_w)/n(t)$. The lines show the results of numerical simulations of the paste-all dynamics; the circles give the closed-form prediction for $\theta \leq 2$.

$n(t_w)/n(t) - 1 = \theta - 1$. Beyond the quasi-equilibrium regime the limiting scaled FD plot is a smooth curve (although from the theoretical analysis in Appendix F one expects discontinuities in higher-order derivatives at integer values of θ). Within a mean-field picture, this would be interpreted as arising from an infinite hierarchy of relaxation timescales, each “responsible” for an infinitesimal segment of the FD plot, as found for instance in the infinite range Sherrington-Kirkpatrick spin glass model [62]. Remarkably,

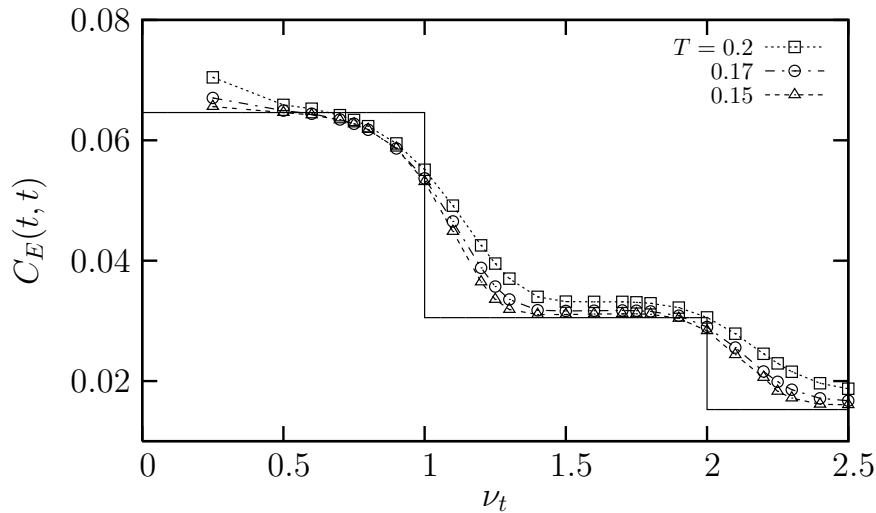


Figure 13. Energy variance $C_E(t, t)$ versus ν_t for three different temperatures. The solid line shows the theoretical prediction for the limit $T \rightarrow 0$.

even though the East model with its purely local and directed interactions is very far from mean field, this is exactly the scenario here. Along the x -axis of the plot we have $\theta - 1 = n(t_w)/n(t) - 1 = d_{\min}(t)/d_{\min}(t_w) - 1$; two different points θ and $\theta' > \theta$ then correspond to waiting times with, from (100), a ratio $t'_w/t_w = (\theta'/\theta)^{1/(T \ln 2)}$ that diverges exponentially for $T \rightarrow 0$.

We note finally that for the closely related triangular plaquette model, approximate relations for correlation and response functions have recently been derived by assuming that relaxations in the different stages of the dynamics are independent of each other [126]. The resulting factorization of the local correlation functions does hold in the East model for small c , as already discussed in [126]. The local FDR was also predicted to be independent of the later time t . To check the quality of this approximation at least in the paste-all regime, we differentiate (109) w.r.t. $\Delta C_0(t, t_w)/n^2(t) = \theta - 1$ to get $X_0(t, t_w) = [c/n^2(t)]\mathcal{F}'(n(t_w)/n(t))$. Independence of t would then require that $[n^2(t_w)/c]X_0(t, t_w) = [n(t_w)/n(t)]^2\mathcal{F}'(n(t_w)/n(t))$ be independent of $n(t)$, i.e. constant. As Fig. 12 shows, this is a reasonable approximation when $n(t_w)/n(t)$ is large, but for smaller values there are deviations which are in fact oscillatory in $n(t_w)/n(t)$. In the earlier, irreversible coarsening stages of the dynamics, t -independence is also not a very accurate approximation. To check this one can consider, instead of S_{k_t, ν_w} from Table 1, the combination $X_0/c = S_{k_t, \nu_w} n^2(t)$. Fixing for example $\nu_w = 0$ and comparing $k_t = 0$ and $k_t = 1$ one finds values which, while closer than those of S_{k_t, ν_w} itself, still differ by a factor around three.

3.2. Global observable

We now switch from the local observable n_i to its global analogue $E = \sum_i n_i$; as in the FA case, this is just the energy function of the system. The associated correlation and response are defined in (29, 30).

$C_E(t, t_w)$		$k_w = -1$	$k_w = 0$	$k_w = 1$	$k_w = 2$
$k_t = 0$	$T = 0.2$	0.0739	0.0659	—	—
	$T = 0.17$	0.0744	0.0649	—	—
	$T = 0.15$	0.0748	0.0646	—	—
	Theory	0.0758	0.0646	—	—
$k_t = 1$	$T = 0.2$	0.0254	0.0141	0.0332	—
	$T = 0.17$	0.0254	0.0138	0.0316	—
	$T = 0.15$	0.0256	0.0137	0.0310	—
	Theory	0.0261	0.0137	0.0305	—
$k_t = 2$	$T = 0.2$	0.00395	0.00240	0.000580	0.0188
	$T = 0.17$	0.00376	0.00226	0.000148	0.0167
	$T = 0.15$	0.00367	0.00232	-0.000110	0.0160
	Theory	0.00385	0.00232	-0.000233	0.0153

Table 2. Numerical values of energy correlation $C_E(t, t_w)$ by plateau of the dynamics, labelled by k_w and $k_t \geq k_w$. Data for three temperatures are shown alongside the theoretical prediction for $T \rightarrow 0$. In this limit, $k_w = -1$ corresponds to $t_w = 0$; the simulation data were in fact taken at a nonzero t_w corresponding for each T to $\nu_w = -0.8$, hence the slightly more noticeable deviation from theory in the first column.

We start in Fig. 13 with simulation results for the equal-time correlation $C_E(t, t)$. Plotting against ν_t reveals that this has a plateau structure similar to the defect density $n(t)$, and for $c \rightarrow 0$ one expects sharp transitions to occur at integer values of ν_t . This can be confirmed by a calculation within the irreversible coarsening regime, as outlined in Appendix D. It produces values in very good agreement with the simulation data, as indicated graphically in Fig. 13. The theory shows that, not unexpectedly, energy fluctuations are related to the variance of the domain size distribution, via

$$C_E(t, t) = \frac{\overline{d^2} - \bar{d}^2}{\bar{d}^3}. \quad (116)$$

The same calculational approach can in fact also be used to predict the two-time energy correlations $C_E(t, t_w)$, which have a plateau structure in both t and t_w . Table 2 summarizes the predictions as a function of k_w and k_t : good convergence of the simulation results to the theory is observed as c is reduced. The only exception is ($k_w = 1, k_t = 2$), where the predicted *negative* correlation is too small to be accurately determined from the simulation data. That such negative correlations could arise can be motivated by considering e.g. configurations with atypically many short domains at time t_w , i.e. a high value of the energy; in the next stage of the dynamics these will have to merge and so can lead to unusually many large domains at a later time t .

One may wonder whether negative energy-energy correlations are only a quirk of the first few stages of the dynamics. To check this we calculate in Appendix D the behaviour in the paste-all limit, where $C_E(t, t_w)/n(t)$ becomes a scaling function $\mathcal{G}(\theta)$

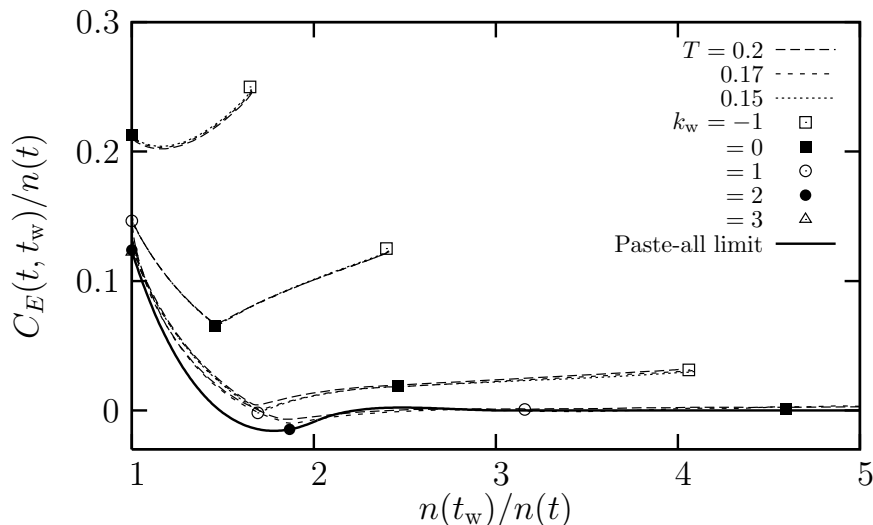


Figure 14. $C_E(t, t_w)/n(t)$ from simulations, plotted against $n(t_w)/n(t)$. The various dashed lines show simulation data for $\nu_t = 0.5, 1.5, 2.5$ and 3.5 (top to bottom). Results are displayed for temperatures $T = 0.15$ (except for $\nu_t = 3.5$), 0.17 and 0.2 but the variation with temperature is almost invisible on the scale of the graph. As ν_t increases, convergence towards the curve predicted in the paste-all regime (solid line) is observed. For finite ν_t , i.e. in the irreversible coarsening regime, only the plateau values can be predicted theoretically (see Table 2); these are shown by the symbols and agree closely with the simulation results.

of $\theta = n(t_w)/n(t)$. In terms of the functions $f_l(x)$ defined in (98) this scaling function reads

$$\mathcal{G}(\theta) = e^{-\gamma}(\theta + 1) - \left(1 + \sum_{l=1}^{\infty} \frac{1}{l!} \int_1^{\theta} d\theta' f_l(\theta') \right). \quad (117)$$

It is plotted in Fig. 14 and shows that (weak) negative correlations do persist even in the paste-all limit. The figure also shows graphically the simulation data, with symbols indicating the predicted plateau values from Table 2. In spite of the relatively low values of ν_t reached, the data are clearly already moving towards the paste-all limit.

The excursion of $C_E(t, t_w)$ to negative values as illustrated in Fig. 14 implies in particular that the two-time energy correlations are not monotonic in t_w (at fixed t) as one would usually expect. An additional source of non-monotonicity is the behaviour around $\nu_w = 0$, where in both simulations and theory we find that C_E starts to rise again as t_w decreases. We attribute this unusual behaviour to the relatively large value of the equal-time correlation $C_E(t_w, t_w) = 1/4$ in the initial plateau ($k_w = -1$).

Next we look at the energy susceptibility $\chi_E(t, t_w)$. By definition this is the response of the defect density $n(t)$ when the equilibrium up-spin concentration is changed at time t_w from c to c' , given in (105). To gain some qualitative insight we exploit the plateau structure of $n(t)$ in the unperturbed dynamics. With successive relaxations taking place

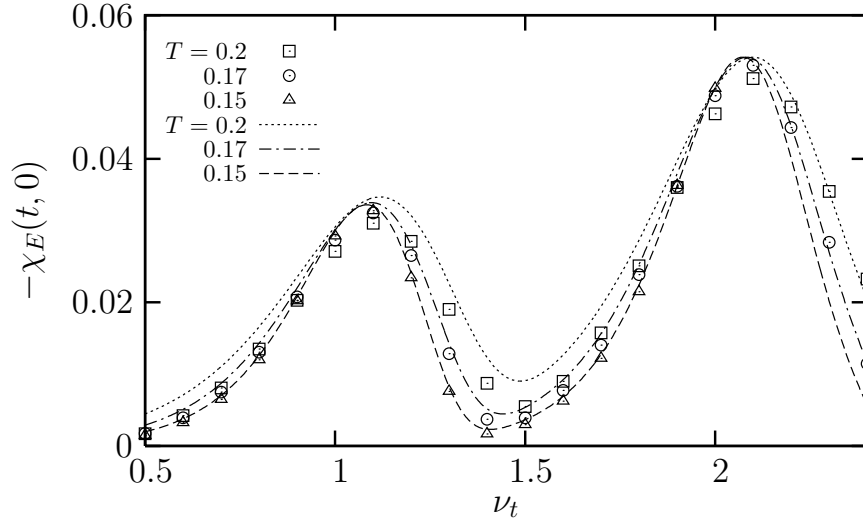


Figure 15. $-\chi_E(t, 0)$, plotted against ν_t for three temperatures. Symbols: simulation data; lines: theoretical prediction, Eq. (122).

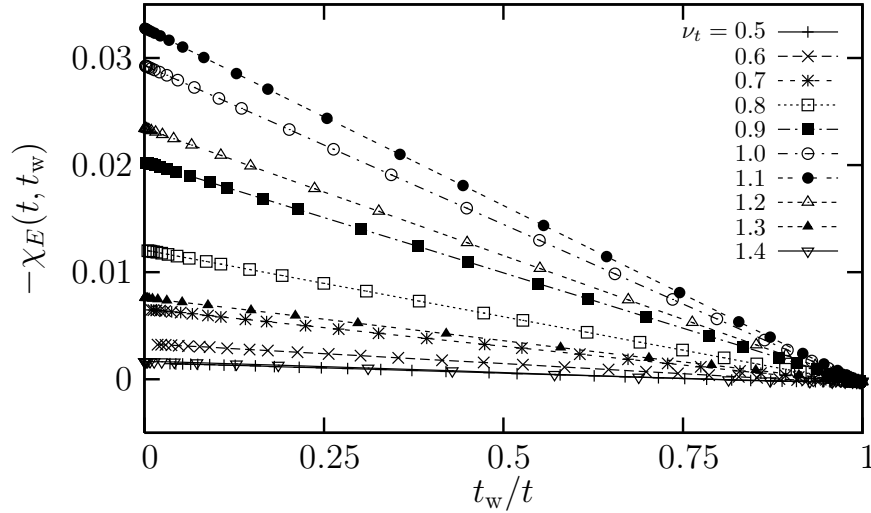


Figure 16. Negative energy susceptibility $-\chi_E(t, t_w)$ for $T = 0.15$ and several ν_t , plotted against t_w/t . The proportionality to $(1 - t_w/t)$ expected from theory, Eq. (122), is well verified.

on timescales $\sim c^{-k}$, $k = 0, 1, 2, \dots$ we can write (see Appendix B)

$$\ln \left(\frac{n(t)}{n(0)} \right) = - \sum_{k=0}^{\infty} g_k(c^k t), \quad (118)$$

where the functions $g_k(\cdot)$ describe the relaxation within stage k and are independent of c to leading order. Each $g_k(\zeta)$ increases from zero at $\zeta = 0$ and exponentially approaches a finite limit for large ζ . For the first few stages one can calculate explicitly (see Appendix B)

$$g_0(\zeta) = \frac{1}{2} (1 - e^{-\zeta}), \quad (119)$$

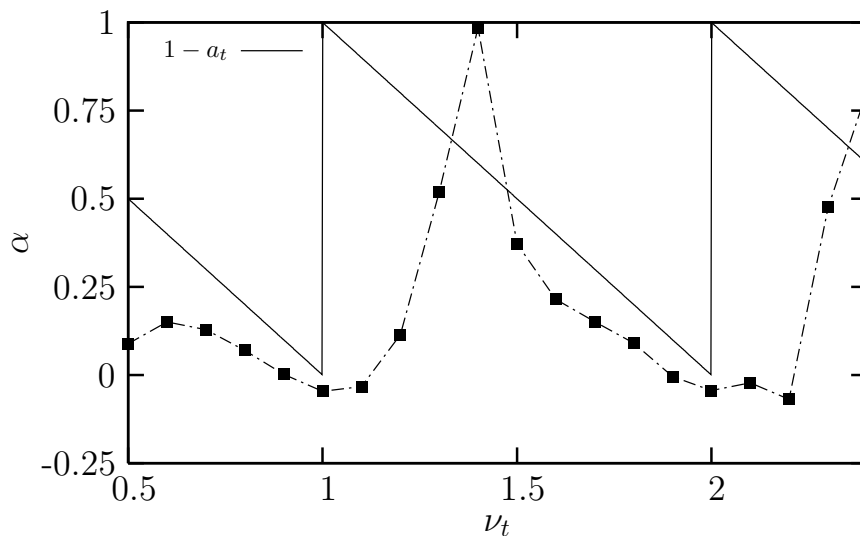


Figure 17. The exponent α as obtained by fitting the c -dependence of $\chi_E(t, 0)$ for fixed ν_t , compared with the theoretical prediction $\chi_E(t, 0) \sim c^\alpha$ with $\alpha = 1 - a_t$.

$$g_1(\zeta) = \frac{3}{8} (1 - e^{-\zeta/2}), \quad (120)$$

$$g_2(\zeta) = \frac{7}{24} (1 - e^{-2\zeta/3}) + \frac{15}{64} (1 - e^{-\zeta/4}). \quad (121)$$

Now when the field is switched on, the effective time interval appearing in the argument of these functions will be replaced by $c^k t_w + (c')^k (t - t_w)$. (For $t_w \neq 0$ this will not necessarily be exact except when the g_k 's are single exponentials, but should give a reasonable approximation nonetheless.) Using (105) and differentiating w.r.t. βh then produces the following estimate for the energy susceptibility:

$$\chi_E(t, t_w) = -(1 - t_w/t)n(t) \sum_{k \geq 0} k c^k t g'_k(c^k t). \quad (122)$$

Each of the terms in the sum produces a ‘‘bump’’ in $\chi_E(t, 0)$ at $t \sim c^{-k}$ with a height of order unity; the dependence on t_w is only through the simple factor $1 - t_w/t$. Simulation results are in very good agreement with this prediction: see Fig. 15. We plot $-\chi_E(t, 0)$ because the susceptibility is predicted to be *negative* – recall that the $g_k(\cdot)$ are increasing functions – in a clear signature of activated dynamics. Also the predicted linear dependence on t_w is well verified by our data, as shown in Fig. 16.

The bumps correspond to the various stages of the dynamics; indeed, within the plateaus between these stages the defect density is independent of c for small c and so one expects the susceptibility to vanish for $c \rightarrow 0$. More precisely, if we write $T \ln t = k_t + a_t$ as usual with $0 < a_t < 1$, we have the scaling

$$-\chi_E(t, 0) \sim c^\alpha, \quad \alpha = 1 - a_t. \quad (123)$$

To see this, note that all terms with $k \leq k_t$ in the sum (122) are exponentially suppressed because the argument of $g_k(\cdot)$ is large. In the remaining terms, on the other hand, the function argument vanishes for $c \rightarrow 0$; since the derivatives $g'_k(0)$

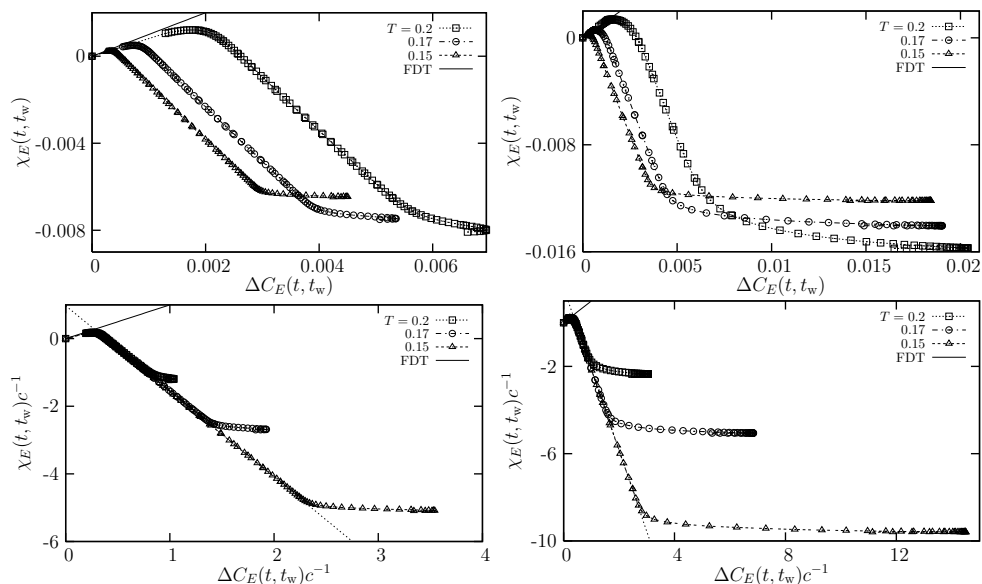


Figure 18. Top: Energy FD plots for $\nu_t = 0.7$ (left) and 1.7 (right) for three different temperatures. Bottom: Same plots with each axis rescaled by $1/c$; fits to the linear parts give slopes of $-2.55(2)$ and $-3.77(5)$, respectively.

are constants of order unity, each term scales as $c^k t$. The dominant contribution thus comes from $k = k_t + 1$, giving $-\chi_E(t, 0) \sim c^{k_t+1} c^{-k_t - a_t} = c^{1-a_t}$, as claimed. Intuitively, the dominant contribution to $-\chi_E$ is from the bump on whose uphill flank t is situated. The scaling (123) is checked against numerical fits of the c -dependence in Fig. 17. Qualitatively we clearly observe the expected non-monotonic dependence of the exponent α on ν_t . Quantitatively there are deviations which arise from the fact that we only fit across three different values of c , and that (compare Fig. 15) we are not yet in the asymptotic low- c regime where the different bumps become well separated in time.

We note briefly that in the paste-all regime, where the dynamics no longer separates into discrete stages, one can argue as above that the unperturbed defect density decays as $n(t) \sim t^{-T \ln 2}$. Perturbing $T = \ln(1/c)$ to $T' = \ln(1/c') = T + T^2(\beta h) + \dots$ then shows that

$$-\chi_E(t, 0) \sim T^2 (\ln t) t^{-T \ln 2} = T \nu_t 2^{-\nu_t} \propto T \nu_t n(t). \quad (124)$$

At constant ν_t this is proportional to $T = \ln(1/c)$: this logarithmic scaling is effectively a “smoothed” version across bumps of the dependence on c^α with $\alpha = 1 - a_t \in [0, 1]$ in the irreversible coarsening regime.

We can now combine χ_E and C_E into FD plots. Sample results from the numerical simulations are shown in Fig. 18. Three regimes can be discerned. Initially, for t_w close to t , $\chi_E(t, t_w)$ is positive and of order c . This is a quasi-equilibrium response which we ignored in our estimates above. There follows a section where the predicted negative activated response becomes dominant; $|\chi_E(t, t_w)|$ increases here as t_w decreases, as expected from the dependence on $1 - t_w/t$. For small c , this factor can get close to unity before t_w leaves the plateau that t is in. Only when this happens does $C_E(t, t_w)$

start to change significantly, and we enter the third regime where $\chi_E(t, t_w)$ is essentially constant and the FD plot therefore horizontal. (Within this regime the FD plot then eventually reverses direction in the peculiar initial stage where t_w is of order unity, when $C_E(t, t_w)$ starts to increase again.)

Our above theoretical estimates do not allow us to predict the precise behaviour of the FD plot around the initial quasi-equilibrium regime. Nevertheless, the fact that χ_E reaches values of order c suggests scaling both axes of the plot with c^{-1} ; Fig. 18 indicates that a limit plot is then approached as c gets small at constant ν_t . This describes the initial quasi-equilibrium regime and the crossover to negative values of χ_E . In the second regime that follows, the numerically obtained FD plots are straight with negative slopes of order unity. To rationalize this, consider t and t_w within the same plateau. Both are then small compared to the timescale governing the following stage of the dynamics ($k = k_t + 1$), and we can linearize the evolution of the $C_E(t, t_w)$ in both times. This then leads to a linear dependence on $t - t_w$ of $\Delta C_E(t, t_w) = C_E(t, t) - C_E(t, t_w)$. Combined with the similarly linear relation $\chi_E \propto (t - t_w)/t$, the FD plot should then be a straight line as observed numerically. Working out the relevant prefactors of $t - t_w$ for ΔC_E and χ_E one can predict for the energy-FDR in this regime as (we omit the details)

$$X_E = -(k_t + 1) \left[\frac{\overline{\Gamma d}}{\overline{\Gamma}} - \left(\frac{\overline{d^2}}{\overline{d}^2} - 1 \right) \right]^{-1}. \quad (125)$$

Here the averages are over the domain size distribution, $\Gamma(d)$ is the relaxation rate of domains of size d (see Appendix B) and all quantities are evaluated at the beginning of the current plateau. The numerical value of (125) can be found relatively easily for the first few plateaus. For $k_t = 0$, there is only one nonzero rate, $\Gamma(2)$. It follows that $\overline{\Gamma d}/\overline{\Gamma} = 2$, and evaluating the remaining moments \overline{d} and $\overline{d^2}$ of $P_0(d)$ gives the prediction $X_E = -2.54\dots$, in full agreement with the value $X_E = -2.55(2)$ obtained from the simulations shown in Fig. 18. For $k_t = 1$ one predicts similarly, by using that $\Gamma(3) = 2c^2/3$ and $\Gamma(4) = c^2/4$ (see Appendix B), the value $X_E = -3.79\dots$, again in agreement with the simulation estimate $X_E = -3.77(5)$. In the paste-all limit, where $\Gamma(d)$ is significant only for the shortest domains, one has $\overline{\Gamma d}/\overline{\Gamma} = d_{\min}$ so that the energy FDR $X_E = -(k_t + 1)/[1 - \exp(-\gamma)]$ grows linearly with the index of the stage of the dynamics. Intuitively this dependence arises because timescales grow as c^{-k_t-1} and as k_t grows so does the perturbation arising from the change in c .

So far we have discussed the initial quasi-equilibrium regime of the energy FD plot and the straight line section with negative FDR X_E that follows. Because the ‘‘height’’ of the FD plot scales as $\chi_E(t, 0) \sim c^{1-a_t}$ and X_E is of order unity there, this section only extends by a small amount $\sim c^{1-a_t}$ of the same order along the C_E -axis. In the remaining ‘‘third’’ section, X_E vanishes for $c \rightarrow 0$ as explained above. More precisely, this section can be divided further into subsections where the FDR scales as $X_E \sim c$, $X_E \sim c^2$ etc (up to c^{k_t+1}) as t_w moves backwards through the various plateaus of the dynamics. To see this, recall that $X_E = -(\partial\chi_E/\partial t_w)/(\partial C_E/\partial t_w)$. The numerator equals $-\partial\chi_E/\partial t_w = \chi_E(t, 0)/t$ from (122) which scales as $c^{1-a_t+(k_t+a_t)} = c^{1+k_t}$. For the

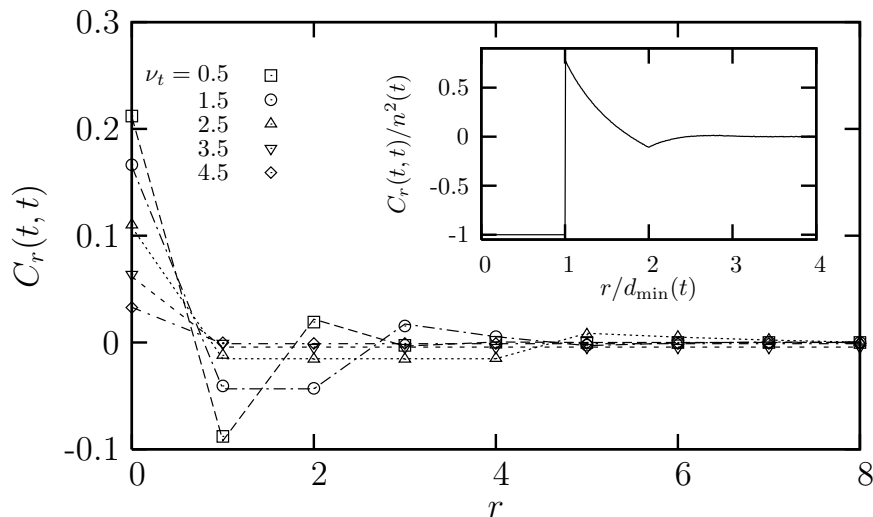


Figure 19. Non-local equal-time correlations $C_r(t, t)$ from simulations (symbols) for $T = 0.15$ and different values of ν_t ; these compare well with the irreversible coarsening predictions shown as dashed lines. Inset: paste-all prediction for the same quantity, from Eq. (130).

correlation function we do not have an explicit result that interpolates between plateaus but it seems reasonable to assume a smooth dependence on $n(t_w)$. This then gives the estimate $\partial C_E / \partial t_w \sim (\partial / \partial t_w) n(t_w)$ which from (118) will scale as c^{k_w+1} to leading order. Putting this together gives $X_E \sim c^{k_t - k_w}$ and hence scalings $\sim c, c^2, \dots, c^{k_1+1}$ as claimed. The case where t_w is still in the same plateau as t ($k_w = k_t$) is included and leads to the FDRs of order unity discussed above.

3.3. Non-local observables

In the previous subsections we found that both for local and global observables the correlation functions have values of order unity and exhibit a plateau structure that reflects the splitting of the dynamics into discrete stages (in the irreversible coarsening regime). The susceptibilities of local and global observables differ more strongly: for the local case, χ_0 is always positive and of order c , and the local FDR is positive and of the order of $c/n^2(t_w)$ (cf. the discussion at the end of Sec. 3.1). The global susceptibility, on the other hand, is negative save for an initial quasi-equilibrium part of $O(c)$, and the associated FDR X_E is negative with values of order unity before dropping to zero – more precisely $O(c), O(c^2), \dots$ – in the final segment of the FD plot. The question naturally arises of how these results relate to each other.

Based on experience with the FA model we initially experimented with Fourier component observables. These, however, lead to FD plots that are very difficult to interpret; also, the limit of short wavevectors does not give direct access to the quantities for local observables. Instead we consider observables defined by random staggered fields ϵ_i with Gaussian correlations $\langle \epsilon_i \epsilon_{i+r} \rangle = \exp(-r^2/2\ell^2)$ in space. These have correlation

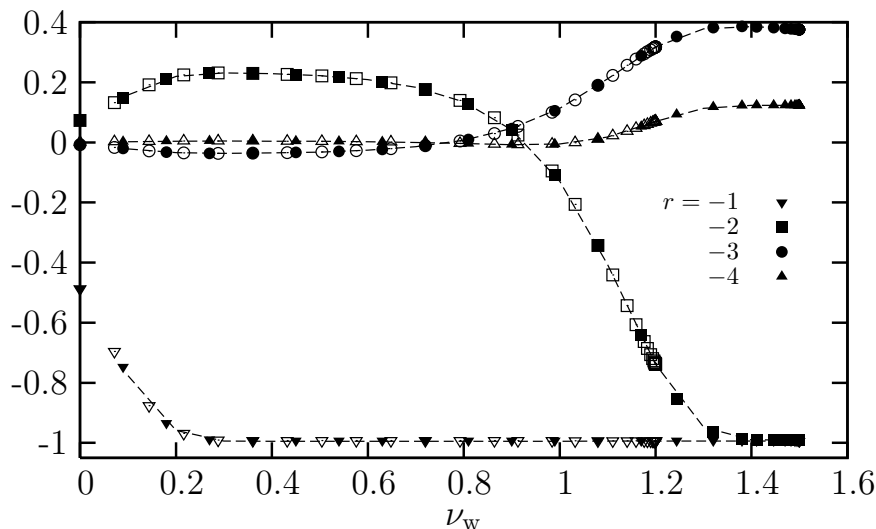


Figure 20. Non-local correlation function $C_r(t, t_w)/[n(t)n(t_w)]$ for various negative r , plotted against ν_w . Symbols: simulation data for $T = 0.15$, for fixed $\nu_t = 1.2$ (open symbols) and $\nu_t = 1.5$ (full symbols). Dashed lines: theoretical prediction in terms of equal-time correlations, $C_r(t_w, t_w)/n^2(t_w)$, from eq. (132).

and susceptibility

$$C_\ell(t, t_w) = \sum_r e^{-r^2/2\ell^2} C_r(t, t_w), \quad (126)$$

$$\chi_\ell(t, t_w) = \sum_r e^{-r^2/2\ell^2} \chi_r(t, t_w). \quad (127)$$

As ℓ is increased from 0 to ∞ we can thus directly interpolate between local and global observables. Before looking at this ℓ -dependence we turn to the non-local functions C_r and χ_r as these are the building blocks from which C_ℓ and χ_ℓ are constructed.

The equal-time correlations $C_r(t, t)$ are simple to predict in the irreversible coarsening regime. Because the dynamics is of an independent interval type, domains from the domain size distribution $P_k(d)$ for the current plateau $k = k_t$ are arranged in random order. Summing the probability of having an up-spin one, two (etc) domains along one gets

$$C_r(t, t) = \langle n_i(t)n_{i+r}(t) \rangle - n^2(t) \quad (128)$$

$$= n(t) \left[-n(t) + \delta_{r,0} + P_k(r) + \sum_d P_k(d)P_k(r-d) + \dots \right]. \quad (129)$$

This is simple to evaluate by numerical convolution given that we know $P_k(d)$; only the first few terms are needed since the m -th order convolution term is nonzero only for $r \geq md_{\min}(t) = m(2^k + 1)$. The result is shown in Fig. 19 for the first few plateaus and is in very good agreement with numerical data. The negative initial section for $0 < r < d_{\min}(t)$ arises because no up-spins exist in this distance range. This strong short-range repulsion also leads to oscillations in the correlation for larger values of r , including weak anti-correlations at some distances. In the paste-all limit one can

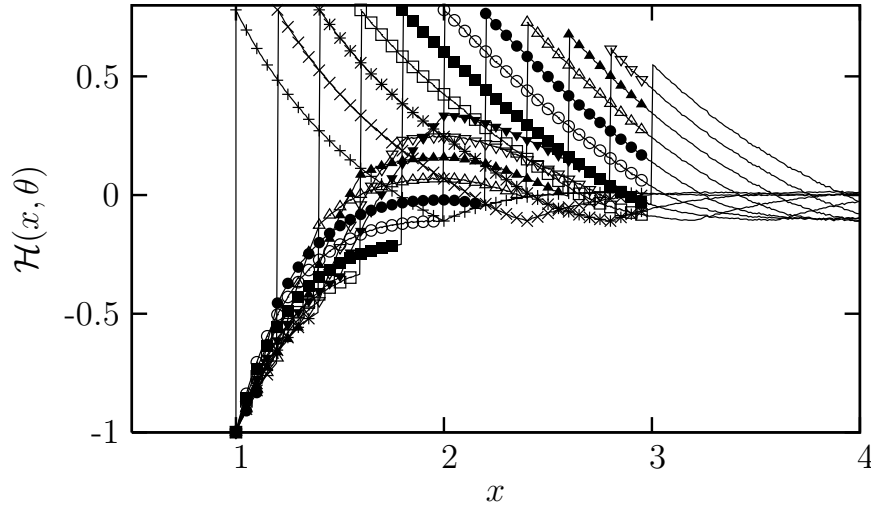


Figure 21. Scaling function $\mathcal{H}(x, \theta)$ for the non-local correlation function in the paste-all regime. Curves are for $\theta = 1, 1.2, \dots, 3$ from left to right. Lines: Simulations of paste-all dynamics; symbols: analytical prediction (134).

exploit that the infinite sum of convolutions in (129) becomes a simple geometric series for the Laplace transforms. The result is proportional to $\exp(\text{Ei}(s))$, and inverting the transform gives in terms of the functions (98)

$$\frac{C_r(t, t)}{n^2(t)} = \mathcal{H}(r/d_{\min}(t), 1), \quad \mathcal{H}(x, 1) = -1 + e^\gamma \sum_{l \geq 1} \frac{1}{l!} f_l(x). \quad (130)$$

A plot of this is included in Fig. 19 and clearly shows that small negative values occur e.g. around $x = 2$, outside the main “repulsion zone” $0 < x < 1$.

The two-time correlations

$$C_r(t, t_w) = \langle n_{i+r}(t) n_i(t_w) \rangle - n(t) n(t_w) \quad (131)$$

are more difficult but can still be obtained relatively simply for $r < 0$. The survival of an up-spin at site $i + r$ from time t_w to time t depends only on the arrangement of domain lengths to the *left* of this site; in particular, it does *not* depend on whether an up-spin is present at site i (to the right of $i + r$) at time t_w . Since the overall survival probability of an up-spin is just $n(t)/n(t_w)$, this implies $\langle n_{i+r}(t) n_i(t_w) \rangle = [n(t)/n(t_w)] \langle n_{i+r}(t_w) n_i(t_w) \rangle$ or, in terms of $C_r(t, t_w)$,

$$\frac{C_r(t, t_w)}{n(t) n(t_w)} = \frac{C_r(t_w, t_w)}{n^2(t_w)}, \quad \text{for } r < 0. \quad (132)$$

This prediction is very well verified by our simulation results in Fig. 20, which confirm for various negative r that the left hand side of Eq. (132) is both independent of t and varies with t_w in the manner predicted.

For positive values of r , no similar simple argument applies. However, one can still calculate $C_r(t, t_w)$ within the paste-all regime; this involves keeping track of which

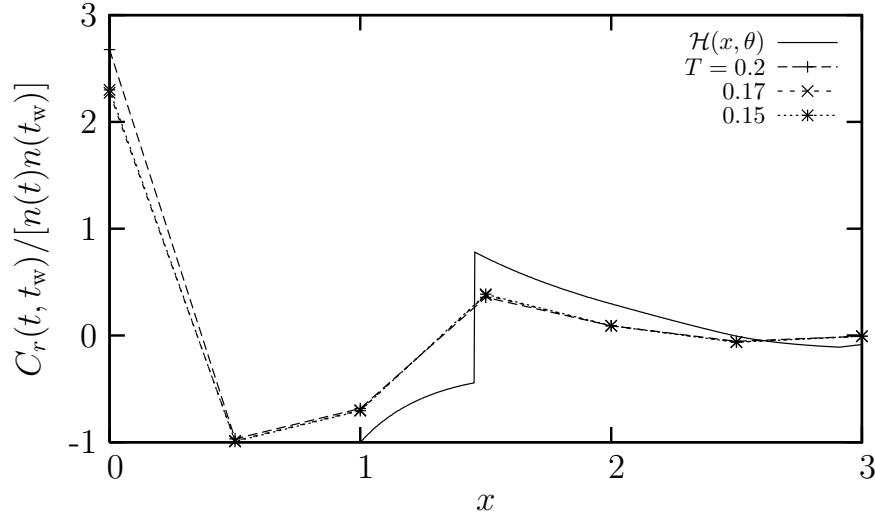


Figure 22. Non-local correlation function $C_r(t, t_w)$, as obtained from simulations at $\nu_t = 1.5$ and $\nu_w = 0.5$ and for the three temperatures indicated. The axes are as in Fig. 21, showing the correlations scaled by $n(t)n(t_w)$ against the scaled distance $x = r/d_{\min}(t_w)$. The solid line graphs the paste-all prediction for the limit of large ν_w and ν_t .

domain lengths from time t_w have been swallowed up into the larger domains at time t (see Appendix E). One finds the following scaling:

$$\frac{C_r(t, t_w)}{n(t)n(t_w)} = \mathcal{H}(x, \theta), \quad x = \frac{r}{d_{\min}(t_w)}, \quad \theta = \frac{n(t_w)}{n(t)}. \quad (133)$$

The scaling function \mathcal{H} can be calculated explicitly in the range $0 \leq x \leq 3$ and $1 \leq \theta \leq 3$, with the result:

$$\begin{aligned} \mathcal{H}(x, \theta) = & -1 + e^\gamma \frac{\theta}{x} \left\{ 1 - \frac{\Theta(\theta - x)}{x} \right. \\ & + \Theta(x - 2) \left[-\frac{x-1}{x} \ln(x-1) + 1 - \frac{2}{x} \right] \\ & + \Theta(x - \theta - 1) \left[\frac{x-1}{x} \ln \left(\frac{(x-\theta)(x-1)}{\theta} \right) - \frac{x-\theta-1}{x-\theta} \right] \\ & + \Theta(x - 2\theta) \left[\frac{1}{x} \ln \left(\frac{x-\theta}{\theta} \right) + \frac{2}{x} - \frac{1}{x-\theta} \right] \\ & + \Theta(\theta - x - 1) \frac{1}{x} \ln \left(\frac{\theta}{(x+1)(\theta-x)} \right) \\ & \left. + \Theta(\theta - 2x) \frac{1}{x} \ln \left(\frac{2(\theta-x)}{\theta} \right) \right\}. \quad (134) \end{aligned}$$

(Notice that for negative distances, the scaling is independent of t from (132): $\mathcal{H}(-x, \theta) = \mathcal{H}(-x, 1)$, and due to the spatial symmetry of the equal-time correlation this is identical to $\mathcal{H}(x, 1)$ from (130).) We plot $\mathcal{H}(x, \theta)$ for positive x in Fig. 21 for a range of values of θ , comparing also with data from direct simulations of the paste-all dynamics. The two-time correlations are seen to have an extremely rich spatial structure, which

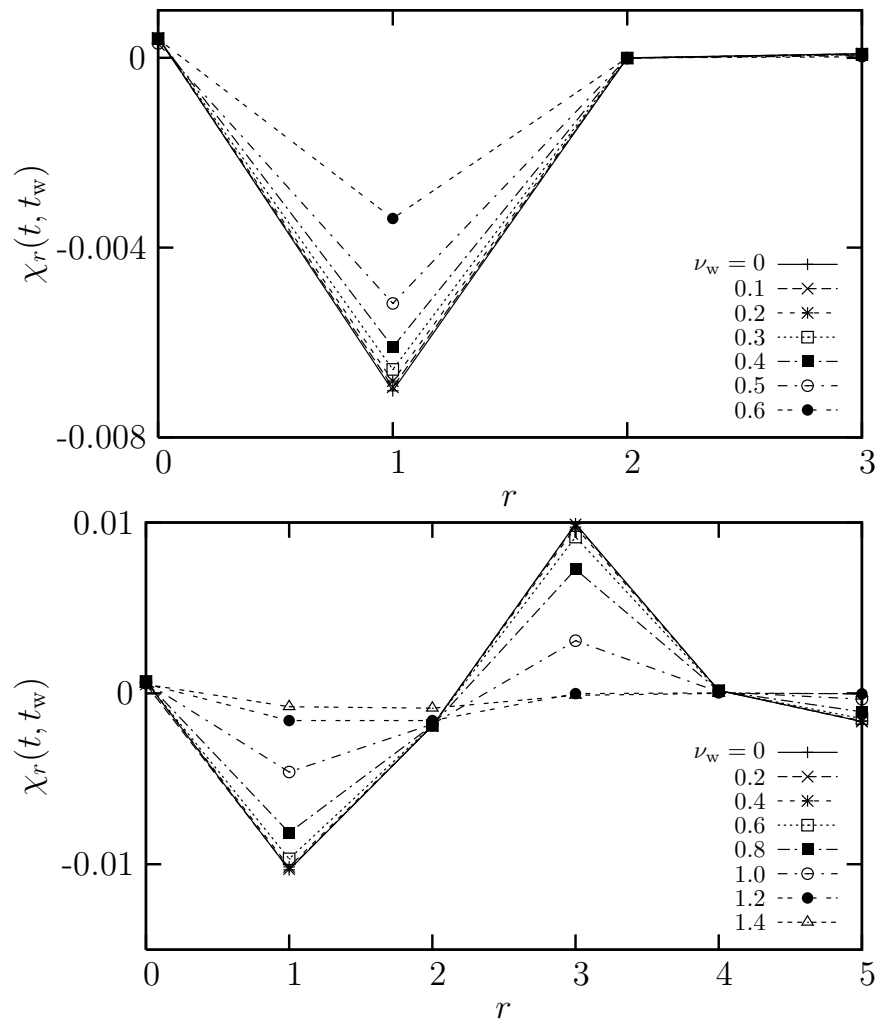


Figure 23. Non-local susceptibility from simulations at $T = 0.15$ and for $\nu_t = 0.7$ (top) and $\nu_t = 1.5$ (bottom). We plot $\chi_r(t, t_w)$ against r for a range of waiting times as indicated by the legend.

arises from the interplay of the different lengthscales $d_{\min}(t_w)$ and $d_{\min}(t)$. The strict exclusion zone for $r < d_{\min}(t_w)$ ($x < 1$) remains at the later time t . Larger distances r can separate spins at the two different times t_w and t ($\mathcal{H} > -1$), but correlations only become positive beyond the lengthscale $r = d_{\min}(t)$ ($x = \theta$). Simulation data in the first plateaus (Fig. 22) qualitatively follow these predicted trends; later plateaus would evidently need to be considered to see more quantitative agreement with the paste-all limit of large k_w and k_t .

Next we consider the non-local susceptibility $\chi_r(t, t_w)$. Here again the case of negative r is simpler: $\chi_r(t, t_w)$ then has to vanish. This is because the evolution of spin $n_{i+r}(t)$ is only affected by the spins to its left; in particular, it remains unperturbed by a field applied at site $i > i + r$. For positive r , on the other hand, $\chi_r(t, t_w)$ will be nonzero but there are competing effects governing its sign and magnitude, making theoretical analysis difficult. We show selected simulation data for $\chi_r(t, t_w)$ in Fig. 23,

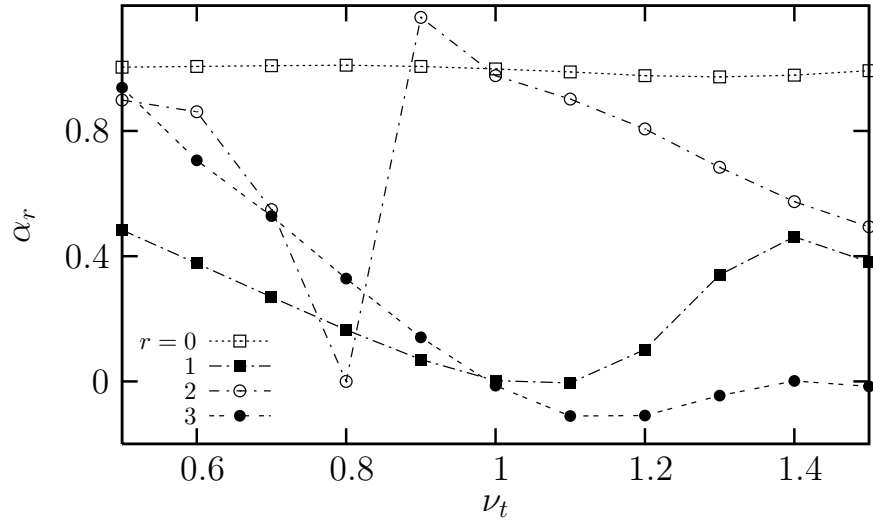


Figure 24. Scaling exponent α_r obtained from fits of simulation data to $\chi_r(t, 0) \sim c^{\alpha_r}$ at fixed ν_t . The exponent is plotted against ν_t for r as indicated by the legend.

and the exponent α_r extracted by fits to the expected scaling $\chi_r(t, 0) \sim c^{\alpha_r}$ at fixed ν_t in Fig. 24.

To develop some intuition, consider $r = 1$ and a local spin configuration $(n_{-1}, n_0, n_1) = (1, 0, 1)$ at time $t_w = 0$ when the field is applied to site 0. This will increase the chances of n_0 flipping up, after a time $\sim c^{-1}$, and hence increase the probability of n_1 flipping down. The resulting contribution to $\chi_1(t, 0)$ is a “bump” around $t = c^{-1}$ with negative sign and amplitude of order unity. If the next up-spin to the left of n_0 is further away, a similar effect occurs but with a longer delay because an up-spin front needs to propagate to n_{-1} . Overall this should give rise to a series of negative bumps in $\chi_1(t, 0)$ centred around $t = c^{-1}, c^{-2}$ etc, similarly to $\chi_E(t, 0)$. At constant ν_t the scaling with c is then $\sim c^{1-a_t}$ as argued after (123). This is in reasonable agreement with the data (Fig. 24). For $r = 2$, an argument based on initial configurations such as $(n_{-1}, n_0, n_1, n_2) = (1, 0, 0, 1)$ suggests a similar structure but with the bump around $t = c^{-1}$ absent, giving the scaling $\chi_2(t, 0) \sim c^{2-\nu_t}$ for $\nu_t < 2$ (and $\sim c^{1-a_t}$ thereafter). This is again in general accord with the numerical trends seen in Fig. 24. Closer inspection reveals, however, that $\chi_2(t, 0)$ is in fact *positive* below $\nu_t \approx 0.8$. This sign change, which also makes the measurements of the exponent α_r in this region rather unreliable, is not accounted for by our naive argument. For $r = 3$ this issue becomes more pronounced still; in fact, $\chi_3(t, 0)$ is positive throughout the range that we can explore (Fig. 23). The dominant contribution for $t < c^{-3}$ is in this case an effect *across* domains: starting from $(n_{-1}, n_0, n_1, n_2, n_3) = (1, 0, 1, 0, 1)$, a field at site 0 will speed up the disappearance of the domain formed by the first three spins. This causes n_3 to survive for *longer*, giving a positive contribution to $\chi_3(t, 0)$. The timescale $t \sim c^{-1}$ on which this term becomes significant is set by the rate for the first domain to disappear. One would expect, then, the scaling $\chi_3(t, 0) \sim c^{1-a_t}$ for $\nu_t < 1$. In fact, the relevant scaling function – which for short chains can be calculated explicitly

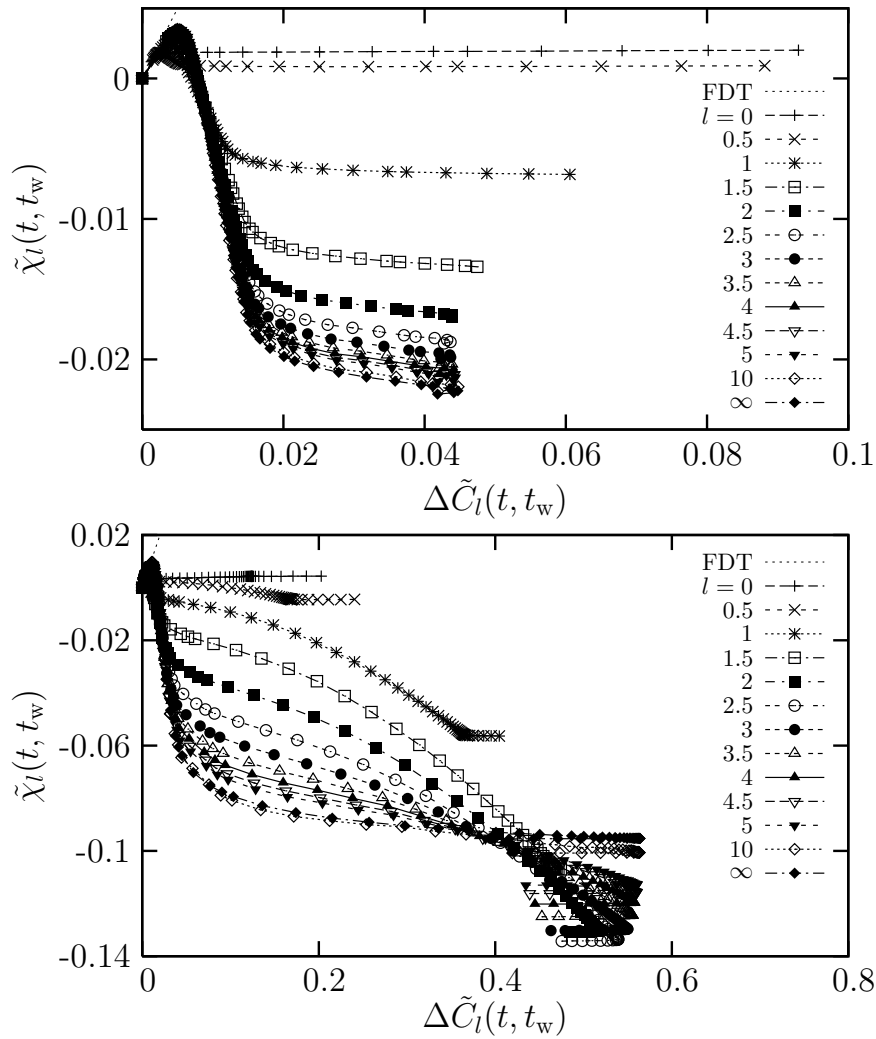


Figure 25. Normalized FD plot for observables defined by Gaussian staggered fields, for $T = 0.15$ and $\nu_t = 0.5$ (top), $\nu_t = 1.5$ (bottom). The lengthscale ℓ of the field correlation is given in the legend.

– turns out to start off quadratically for small values of its argument, so that instead $\chi_3(t, 0) \sim c^{2(1-a_t)}$, in good agreement with our numerics (Fig. 24). It is not clear to us at present how to systematically account for effects of this type to get an overall prediction for the low- c scaling of $\chi_r(t, 0)$. Also the inclusion of the full t_w -dependence of $\chi_r(t, t_w)$ is not trivial: for $k_t = 0$ (Fig. 23 top) a simple proportionality to $(1 - t_w/t)$ can be checked to describe the data well, whereas for $k_t = 1$ (Fig. 23 bottom) this is no longer the case.

Finally we show in Fig. 25 the FD plots for the ℓ -dependent correlation and response defined in (127). These interpolate between the local ($\ell = 0$) and global limits ($\ell \rightarrow \infty$) as they must. For the times considered here the dynamical lengthscales (typical domain sizes) are short enough that the global behaviour is approached already for moderate values of ℓ . The approach to the local limit $\ell = 0$, on the other hand, must be expected to become singular for small c . This can be seen as follows. Consider

$\chi_E(t, t_w) = \sum_r \chi_r(t, t_w)$. We know that for $t_w = 0$ and fixed ν_t this quantity scales as c^{1-at} for $c \rightarrow 0$. There must therefore be one or several values of r for which $\chi_r(t, 0)$ scales in the same way. But then these values will dominate the sum over r in $\chi_\ell(t, 0)$; in particular, they will always dominate over the local term ($r = 0$) with its $O(c)$ contribution. Thus, for any nonzero ℓ we expect $\chi_\ell(t, 0) \sim c^{1-at}$, whereas at $\ell = 0$ itself the scaling is $\sim c$. Assuming that similar arguments apply also to the two-time quantities $\chi_\ell(t, t_w)$, one expects the FD plots for sufficiently small c to switch effectively discontinuously from the local FD relation for $\ell = 0$ to behaviour dominated by non-local effects for $\ell > 0$.

4. Discussion and Conclusions

We have studied two paradigmatic kinetically constrained models (KCMs) of glassy dynamics: the FA (Fredrickson-Andersen) and East models. Deploying a variety of analytical techniques and comparing with detailed numerical simulations, we have analysed in particular the correlation and response functions during the aging after a quench to low temperature, along with the resulting fluctuation-dissipation ratios (FDRs). Local as well as global observables were considered, and Fourier mode and Gaussian staggered field observables respectively allowed us to interpolate between these two limiting cases.

In the FA model, with its effective dynamics of diffusing and coagulating defects, a clear physical scenario emerges: the asymptotic FDR X^∞ for well-separated times $t \gg t_w$ is *negative*. Its precise value depends on whether one is above or below the critical dimension $d_c = 2$, with $X^\infty = -3$ for $d > 2$ and $X^\infty = -3\pi/(6\pi - 16)$ in $d = 1$. The underlying physics is, however, the same: the negative FDR arises from the activated nature of the aging dynamics. Where a temperature increase would, in equilibrium, increase the defect density n , here its main effect is to speed up the decrease of $n(t)$ and so reduce its value. The asymptotic FDR can be determined from observables of any wavelength or characteristic lengthscale, although for local observables this is very awkward because the interesting aging effects are buried underneath a dominant quasi-equilibrium signal. Much better suited is the global observable, i.e. the energy or total number of defects, which produces a fluctuation-dissipation (FD) plot that is close (in $d = 1$) or exactly equal (in $d > 2$) to a straight line of slope X^∞ .

The East model has a more strongly cooperative behaviour than the FA model, and a correspondingly more subtle pattern of violations of the fluctuation-dissipation theorem (FDT). For the local observable, the FDR $X_0(t, t_w)$ is always positive but small, of order $c/n^2(t_w)$, where c is the (small) equilibrium defect concentration. In the paste-all limit of large domain sizes, which corresponds to a long-time limit taken within the aging regime, we find an intriguing similarity with mean-field predictions for spin glass dynamics: a continuous hierarchy of relaxation timescales leads to a curved FD plot that is effectively composed of a sequence of infinitesimal straight line segments.

For global observables, on the other hand, also the East model displays the negative

FDRs characteristic of activated aging dynamics. For times t and t_w in the same “plateau” of the dynamics, the FDR has (negative) values of order unity which we can predict theoretically; as t_w becomes smaller it then drops to $O(c)$, $O(c^2)$ and so on. The contrast to the local observable can be traced to the different scaling with c , and different signs, of the distance dependent susceptibilities χ_r . Observables probing intermediate lengthscales ℓ can interpolate between the local and global cases, although we argued that for $c \rightarrow 0$ the non-local effects would dominate for any $\ell > 0$.

The apparent decoupling of the local response from activation effects in the East model can be understood as follows. The response of a spin to a local field is governed by the history of its facilitating neighbour on the left. The field does not affect this “clock” because of the directed nature of the East model, and so one does not get any speed-up effects: the susceptibility only reflects the direct influence of the field and is positive. For spins at some distance $r > 0$ from the site where the field is applied, one has the opposite scenario. These spins have a pure “speed-up” response: the spin at the field site will be up more often, thus accelerating the dynamics of all spins on the right.

We already alluded in the introduction (Sec. 1.4) to the wider implications of our results. The non-trivial FDRs we have found in the aging regime reflect the growth of a purely dynamic lengthscale and cannot be related to the (trivial) equilibrium properties of KCMs. For most observables the FDRs are negative, precluding an interpretation in terms of an effective temperature. The negative sign nevertheless has a clear physical interpretation as arising from the activated nature of the aging dynamics. In the FA case, also the actual value of the asymptotic FDR (in the sense of widely separated times $t \gg t_w$) is robust among observables probing the entire range of lengthscales, from purely local behaviour to system-spanning global observables. In the East model the situation is more subtle, with the FD behaviour of local observables decoupled from activation effects. The latter do show up, however, in appropriate non-local and global observables. Because the East model has a hierarchy of relaxation timescales, the (negative) value of the FDR then also varies depending on which stage of the dynamics is being considered.

To what extent will our results apply to other KCMs? One suspects that the strictly directed KCMs might form a somewhat separate group with regard to FD behaviour, because the effects of a local field can never propagate back to the site where it was applied. Qualitatively similar effects to those seen here for the East model would therefore be expected in, for example, the analogous three-dimensional model studied in Ref. [40]. The local FD plot shown in Fig. 26 demonstrates that this is indeed the case. In $d = 3$ there is again a hierarchy of timescales in the non-equilibrium dynamics, with the defect density relaxing in steps as in Fig. 6. This leads to FD plots that are (approximately) piecewise linear, with a number of segments depending on the position of t in the hierarchy (compare Fig. 10 for $d = 1$). The two-dimensional triangular plaquette model [126] also shows some broad similarities to the East model, but with additional subtleties because one now has to choose between studying the dynamics of the defects or of the underlying spin system. When the direction of facilitation is itself

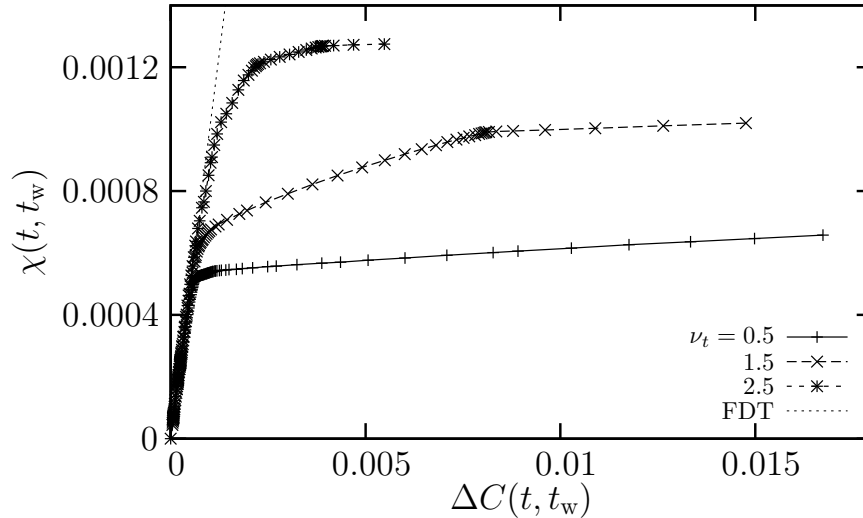


Figure 26. FD plot for the local observable in the three-dimensional analogue of the East model, for $T = 0.15$ and $\nu_t = 0.5, 1.5, 2.5$ (from bottom to top). As in $d = 1$, the FD plot consists of approximately straight segments whose number increases with t (see Fig. 10).

treated as a dynamical variable [37], the model becomes isotropic overall and one might expect the connection between local and global observables to be restored as for the FA model. It would therefore be very interesting to study the aging dynamics of such a model.

A significant open question concerns the FD behaviour of undirected but highly cooperative KCMs, for example the FA model in $d = 2$ with two rather than one up-spin neighbours required to facilitate a move. Numerical studies on similar models with conserved dynamics [106, 107] indicate a mean-field-like scenario without any apparent activation effects. It seems clear, however, that such effects should be present, certainly for global observables: the relaxation to lower defect densities must, as for our simpler one-spin facilitated FA models, proceed more quickly for higher c and result in a negative susceptibility. Here and also more widely in experimental studies we hope that our study will stimulate the search for well-defined negative FDRs. Arising as they do from activated dynamics, they should be essentially ubiquitous among systems exhibiting glassy dynamics.

Acknowledgments

LB, JPG and PS are grateful to the Newton Institute, Cambridge, for providing a stimulating environment in which to discuss some of the central questions of this paper. JPG acknowledges financial support from EPSRC (grants GR/R83712/01 and GR/S54074/01) and the University of Nottingham (grant FEF 3024). We thank Robert Jack for useful discussions and collaborations on the subject of this article.

Appendix A. Functions used in Section 2.2

Two functions appearing throughout Sec. 2.2 are the modified Bessel function $I_n(t)$ of integer order n [127, 146],

$$I_n(t) = \int_0^{2\pi} \frac{d\varphi}{2\pi} \cos(n\varphi) e^{t \cos(\varphi)}, \quad (\text{A.1})$$

and the function $H_n(t)$,

$$H_n(t) = \frac{1}{2} \int_0^t dt' e^{-t'} [I_{n-1}(t') - I_{n+1}(t')]. \quad (\text{A.2})$$

Elementary properties that can be read off from these equations are $I_n(0) = \delta_{n,0}$, $I_{-n}(t) = I_n(t)$, $H_0(t) = 0$ and $H_{-n}(t) = -H_n(t)$. In our analysis we make extensive use of the asymptotic scalings of these functions. At fixed order n and in the limit $t \rightarrow \infty$,

$$e^{-t} I_n(t) \sim \frac{1}{\sqrt{2\pi t}} \quad \text{and} \quad H_n(t) \sim 1, \quad (\text{A.3})$$

whereas for $t, n \rightarrow \infty$ simultaneously with n^2/t fixed,

$$e^{-t} I_n(t) \sim \frac{1}{\sqrt{2\pi t}} e^{-n^2/(2t)} \quad \text{and} \quad H_n(t) \sim \Phi\left(\frac{n}{\sqrt{2t}}\right). \quad (\text{A.4})$$

Here $\Phi(z) = (2/\sqrt{\pi}) \int_z^\infty du e^{-u^2}$ denotes the complementary error function as in the main text. The following functional relations are also of great value for our analysis,

$$\partial_t I_n(t) = \frac{1}{2} [I_{n-1}(t) + I_{n+1}(t)], \quad (\text{A.5})$$

$$\frac{n}{t} I_n(t) = \frac{1}{2} [I_{n-1}(t) - I_{n+1}(t)]. \quad (\text{A.6})$$

To calculate Fourier transforms we use the identities ($t \geq t_w \geq 0$)

$$\sum_{n=-\infty}^{\infty} e^{-iqn} I_{n+i}(t) I_{n+j}(t) = e^{i\frac{1}{2}(i+j)q} I_{i-j}\left(2t \cos \frac{q}{2}\right), \quad (\text{A.7})$$

$$\begin{aligned} & \sum_{n=-\infty}^{\infty} e^{-iqn} I_n(t - t_w) [I_{n-m} + I_{n+m}](t + t_w) \\ &= 2T_m \left(\frac{t \cos(q/2)^2 + t_w \sin(q/2)^2}{A} \right) I_m(2A), \end{aligned} \quad (\text{A.8})$$

$$\begin{aligned} & \sum_{n=-\infty}^{\infty} e^{-iqn} [I_{n-1} - I_{n+1}](t - t_w) [I_{n-1} - I_{n+1}](t + t_w) \\ &= 2 \left[\cos(q) I_0(2A) - \frac{t^2 \cos(q/2)^2 - t_w^2 \sin(q/2)^2}{A^2} I_2(2A) \right], \end{aligned} \quad (\text{A.9})$$

where $A = \sqrt{t^2 \cos(q/2)^2 + t_w^2 \sin(q/2)^2}$ and $T_n(x) = \cos(n \arccos x)$ is the Chebyshev polynomial of degree n . Equations (A.7) and (A.8) follow from the integral representation Eq. (A.1) and trigonometric identities. The sum Eq. (A.9) can be reduced to Eq. (A.8) by using Eq. (A.6) and expressing the resulting factor n^2 as a second derivative with respect to q .

Appendix B. Initial stages of irreversible coarsening dynamics

In this section we give further details of the solution of the irreversible coarsening dynamics, leading in particular to the explicit expressions for the scaling functions (119–121) for stages $k = 0, 1, 2$ of the dynamics.

The dynamical equations (94) for stage k can be solved in terms of the generating functions [116]

$$G(z, t) = \sum_d P(d, t) z^d, \quad H(z, t) = \sum_{2^{k-1} < d \leq 2^k} P(d, t) z^d, \quad (\text{B.1})$$

where H is the analogue of G restricted to the active domains. Bearing in mind that (94) applies only for the inactive domain lengths d , one has

$$\frac{\partial}{\partial t} [G(z, t) - H(z, t)] = G(z, t) \left(-\frac{\partial}{\partial t} \right) H(z, t), \quad (\text{B.2})$$

and hence

$$G(z, t) = 1 + [G(z, 0) - 1] \exp[H(z, 0) - H(z, t)]. \quad (\text{B.3})$$

In the limit $t \rightarrow \infty$, where all active domains have disappeared ($H \rightarrow 0$), this gives a relation between the generating functions in plateaus $k - 1$ and k :

$$G_k(z) = 1 + [G_{k-1}(z) - 1] \exp[H_{k-1}(z)]. \quad (\text{B.4})$$

If we define $h_k(d)$ as the inverse transform of $\exp[H_k(z)] - 1$, i.e. $\exp[H_k(z)] - 1 = \sum_d h_k(d) z^d$, this gives the following recursion for the domain length distributions

$$P_k(d) = P_{k-1}(d) - h_{k-1}(d) + (P_{k-1} * h_{k-1})(d). \quad (\text{B.5})$$

Starting from the initial condition $P_{-1}(d) = 2^{-d}$ one finds easily the particular values that we will need later:

$$P_{-1}(1) = \frac{1}{2}, \quad P_0(2) = \frac{3}{8}, \quad P_1(3) = \frac{7}{24}, \quad P_2(4) = \frac{15}{64}. \quad (\text{B.6})$$

The overall distributions, which were obtained by evaluating the recursion numerically, are graphed in Fig. 5.

To get a prediction for the evolution of the defect density $n(t)$ during stage k , we exploit that $1/n(t) = \bar{d}(t) = (\partial/\partial z)G(z = 1, t)$. From (B.3) this gives

$$n(t) = n(0) \exp[H(1, t) - H(1, 0)], \quad (\text{B.7})$$

and we need the evolution of $H(1, t)$. Since active domains cannot be recreated during the coarsening process, we can write

$$H(1, t) = \sum_{2^{k-1} < d \leq 2^k} P(d, t) = \sum_{2^{k-1} < d \leq 2^k} P(d, 0) S(d, t), \quad (\text{B.8})$$

where $S(d, t)$ is the survival probability of a domain of length d . In stage $k = 0$ this is very simple: the disappearance of a domain of length $d = 1$ corresponds to a mobile up-spin flipping down, so $S(1, t) = \exp[-(1 - c)t] \approx \exp(-t)$ for $c \rightarrow 0$. Also $P_{-1}(1) = 1/2$ at the beginning of stage 0, so $H(1, t) = \exp(-t)/2$. Inserting into (B.7) directly leads

to the expression (119) for $g_0(\zeta)$. For later stages and correspondingly larger d one can proceed using a “leaky” Markov chain that exits as soon as spin n_d flips down. Taking $k = 1$ as an example, active domains have length $d = 2$. The initial state of the domain is 101 (i.e. $n_0 = 1, n_1 = 0, n_2 = 1$). The only other possible state that can be reached before spin n_2 flips down is 111. The leaky transition matrix between these two states is

$$W = \begin{pmatrix} -c & 1 - c \\ c & -2(1 - c) \end{pmatrix}. \quad (\text{B.9})$$

The first column represents the transition at rate c from 101 to 111; the second column has the reverse transition, with rate $1 - c$, and in addition the rate $1 - c$ for exiting via $111 \rightarrow 110$. The survival probability is just the probability of remaining in the chain, starting in state 101:

$$S(2, t) = (1, 1)e^{Wt} \begin{pmatrix} 1 \\ 0 \end{pmatrix} = \left(\frac{1}{2} + \frac{2 - c}{4D}\right) e^{\lambda_1 t} + \left(\frac{1}{2} - \frac{2 - c}{4D}\right) e^{\lambda_2 t}, \quad (\text{B.10})$$

with $D = \sqrt{1 - 2c + 5c^2/4}$ and the eigenvalues $\lambda_{1,2} = -1 + c/2 \pm D$. To get $g_1(\zeta)$ we need to consider the survival probability on the timescale $t = \zeta/c$, taking the limit $c \rightarrow 0$ at fixed ζ . Since λ_2 stays of order unity, the second exponential then disappears. In the first one, $\lambda_1 = -c/2$ to leading order while the prefactor tends to 1 so that overall $S(2, t = \zeta/c) \rightarrow \exp(-\zeta/2)$. Inserting into (B.8) and using (B.6) for the prefactor $P_0(2)$ then gives the result (120) for $g_1(\zeta)$. One proceeds similarly for $g_2(\zeta)$ to derive (121), the main difference being that there are now two active domain lengths, $d = 3$ and $d = 4$. The required leaky transition matrices are of size 4×4 and 8×8 , respectively, and the survival probability is evaluated in the regime $t = \zeta/c^2$. By taking derivatives of the survival functions at $\zeta = 0$ one further obtains the rates $\Gamma(d)$ required for the prediction of the negative energy FDR (125), as

$$\Gamma(1) = 1, \quad \Gamma(2) = \frac{c}{2}, \quad \Gamma(3) = \frac{2c^2}{3}, \quad \Gamma(4) = \frac{c^2}{4}. \quad (\text{B.11})$$

Appendix C. Exact relation between local correlation and response

We outline the derivation of the exact relation (111) between the local correlation C_0 and susceptibility χ_0 in the East model. For the latter we have the expression (106), $\chi_0(t, t_w) = c(1 - c)[1 - r(t, t_w)]$, in terms of the relaxation integral

$$r(t, t_w) = \langle \hat{r}(t, t_w) \rangle, \quad \hat{r}(t, t_w) = \exp\left(-\int_{t_w}^t dt' n_{i-1}(t')\right). \quad (\text{C.1})$$

For the correlation function we need to evaluate $\langle n_i(t)n_i(t_w) \rangle$. As in the derivation of χ_0 we first take the history of spin n_{i-1} from time 0 to t as fixed. If also $n_i(t_w)$ is given, the average value of $n_i(t)$ is $c + [n_i(t_w) - c]\hat{r}(t, t_w)$, using the same argument as for χ_0 . Thus

$$\langle n_i(t)n_i(t_w) \rangle_{n_i(t_w), n_{i-1}(0..t)} = n_i(t_w)[c + (1 - c)\hat{r}(t, t_w)], \quad (\text{C.2})$$

where the subscript indicates the fixed quantities. Now we average over $n_i(t_w)$, which has evolved from the initial average defect density $n(0)$ at time 0 to a later value governed by the relaxation integral $\hat{r}(t_w, 0)$:

$$\langle n_i(t)n_i(t_w) \rangle_{n_{i-1}(0..t)} = \{c + [n(0) - c]\hat{r}(t_w, 0)\}[c + (1 - c)\hat{r}(t, t_w)] \quad (\text{C.3})$$

$$\begin{aligned} &= c^2 + c(1 - c)\hat{r}(t, t_w) + c[n(0) - c]\hat{r}(t_w, 0) \\ &\quad + (1 - c)[n(0) - c]\hat{r}(t, 0), \end{aligned} \quad (\text{C.4})$$

where we have exploited that $\hat{r}(t, t_w)\hat{r}(t_w, 0) = \hat{r}(t, 0)$. Still at fixed history of n_{i-1} , the same arguments as above give the average densities at times t_w and t as

$$\langle n_i(t_w) \rangle_{n_{i-1}(0..t)} = c + [n(0) - c]\hat{r}(t_w, 0), \quad (\text{C.5})$$

$$\langle n_i(t) \rangle_{n_{i-1}(0..t)} = c + [n(0) - c]\hat{r}(t, 0). \quad (\text{C.6})$$

These can be used to eliminate the occurrences of $\hat{r}(t_w, 0)$ and $\hat{r}(t, 0)$ from (C.4):

$$\begin{aligned} \langle n_i(t)n_i(t_w) \rangle_{n_{i-1}(0..t)} &= c^2 + c(1 - c)\hat{r}(t, t_w) + c[\langle n_i(t_w) \rangle_{n_{i-1}(0..t)} - c] \\ &\quad + (1 - c)[\langle n_i(t) \rangle_{n_{i-1}(0..t)} - c]. \end{aligned} \quad (\text{C.7})$$

Averaging over the history of n_{i-1} gives then

$$\langle n_i(t)n_i(t_w) \rangle = -c(1 - c)[1 - r(t, t_w)] + cn(t_w) + (1 - c)n(t), \quad (\text{C.8})$$

and so finally for the autocorrelation function $C_0(t, t_w) = \langle n_i(t)n_i(t_w) \rangle - n(t)n(t_w)$:

$$C_0(t, t_w) = -c(1 - c)[1 - r(t, t_w)] + cn(t_w) + (1 - c)n(t) - n(t)n(t_w). \quad (\text{C.9})$$

The first term on the r.h.s. is $-\chi_0(t, t_w)$, and rearranging slightly gives the promised result (111). It is clear from the derivation that this exact relation will hold for all kinetically constrained spin models with directed constraints, as long as we replace $n_{i-1}(t)$ by the appropriate facilitation factor $f_i(t)$ for spin n_i . The key ingredient is that n_i does not affect the evolution of this facilitation factor; this is why we can first fix the facilitation history and average over the dynamics of n_i .

Appendix D. Energy correlations

Here we sketch how the energy correlations for the East model can be calculated within the irreversible coarsening regime. The energy $E = N/\bar{d}$ is inversely proportional to the average domain length. Since the latter has fluctuations $\delta\bar{d}$ of order $N^{-1/2}$ we can write

$$C_E(t, t_w) = \frac{N\langle\delta\bar{d}(t)\delta\bar{d}(t_w)\rangle}{\bar{d}^2(t)\bar{d}^2(t_w)}. \quad (\text{D.1})$$

The fluctuations $\delta\bar{d}$ arise from the corresponding fluctuations $\delta P(d)$ in the domain size distribution. At equal times, $t_w = t$, the latter are easy to obtain because of the independent interval nature of the dynamics: the actual arrangement of domain lengths at some given time can be obtained by repeatedly sampling domain lengths from the (average) domain length distribution $P(d)$ and lining them up along the chain until the

total length N is reached. By a relatively simple combinatorial calculation one then finds for large N the following expression for the covariance of the $\delta P(d)$:

$$N\langle\delta P(d)\delta P(d')\rangle = \bar{d}[P(d)\delta_{d,d'} - P(d)P(d')]. \quad (\text{D.2})$$

Summing over d and d' , this implies $\langle[\sum_d \delta P(d)]^2\rangle = 0$ as it must be because the distribution is always normalized. By multiplying with dd' first and then summing, on the other hand, one obtains the variance of \bar{d} as $\bar{d}(\bar{d}^2 - \bar{d}^2)$ and hence the expression (116) for the equal-time energy correlations.

For the two-time correlations one exploits that the recursion (B.5) for the domain size distribution in the plateaus of the dynamics holds whatever the initial shape of this distribution. We can apply it, in particular, to a domain size distribution $P_{k_w}(d) + \delta P_{k_w}(d)$ in plateau k_w perturbed by a small fluctuation. Linearization in the small quantities $\delta P_{k_w}(d) \sim N^{-1/2}$ then tells us how this fluctuation propagates into the later plateau k_t . We can write the outcome in the generic form

$$\delta P_{k_t}(d) = \sum_{d'} M_{k_t k_w}(d, d') \delta P_{k_w}(d'), \quad (\text{D.3})$$

with an appropriate (infinite) matrix $M_{k_t k_w}$ depending on both the initial and final plateau. Inserting into (D.1) gives then

$$C_E(t, t_w) = \bar{d}_{k_w}^{-2} \bar{d}_{k_t}^{-2} \sum_{d, d', d''} dd'' M_{k_t k_w}(d, d') N \langle \delta P_{k_w}(d') \delta P_{k_w}(d'') \rangle \quad (\text{D.4})$$

$$= \bar{d}_{k_w}^{-1} \bar{d}_{k_t}^{-2} \sum_{d, d', d''} dd'' M_{k_t k_w}(d, d') [P_{k_w}(d') \delta_{d', d''} - P_{k_w}(d') P_{k_w}(d'')] \quad (\text{D.5})$$

$$= \bar{d}_{k_w}^{-1} \bar{d}_{k_t}^{-2} \sum_{d, d'} d M_{k_t k_w}(d, d') P_{k_w}(d') (d' - \bar{d}_{k_w}). \quad (\text{D.6})$$

To evaluate the sum numerically without explicitly calculating and storing $M_{k_t k_w}$, we perturb the domain size distribution in plateau k_w from $P_{k_w}(d)$ to $P_{k_w}(d)[1 + \epsilon(d - \bar{d}_{k_w})]$ with some small “field” ϵ , and find the resulting small change (proportional to ϵ) in the average domain length in plateau k_t . Multiplying by the prefactor $\bar{d}_{k_w}^{-1} \bar{d}_{k_t}^{-2}$ then gives the results shown in Table 2.

A closed form solution for the propagation of perturbations from t_w to t can be obtained in the paste-all regime of large domain lengths. We work with the normalized lengths $x = d/d_{\min}(t_w)$ as before; the clock variable is $\theta = d_{\min}(t)/d_{\min}(t_w)$ so that at “time” θ there are no domains of length $x < \theta$. The distribution $P_\theta(x)$ of domain lengths at time θ obeys the master equation

$$\frac{\partial}{\partial \theta} P_\theta(x) = -\delta(x - \theta) P_\theta(\theta) + P_\theta(x - \theta) P_\theta(\theta). \quad (\text{D.7})$$

The first term on the right captures the disappearance of domains of length $x = \theta$; these merge with their right neighbours into larger domains as represented by the second term. (Because $x \geq \theta$ always, $P_\theta(x)$ has a step discontinuity at $x = \theta$; the $P_\theta(\theta)$ in the master equation is to be understood as the nonzero probability $P_\theta(x = \theta^+)$ to the right of this discontinuity, i.e. the probability density of the shortest domains present.) The initial condition $P_1(x)$ at $\theta = 1$ is the scaling distribution $\tilde{P}(x)$ from (97).

To solve (D.7) one goes to Laplace transforms

$$\hat{P}_\theta(s) = \int_0^\infty dx e^{-sx} P_\theta(x), \quad (\text{D.8})$$

to find

$$\frac{\partial}{\partial \theta} \hat{P}_\theta(s) = e^{-\theta s} P_\theta(\theta) [\hat{P}_\theta(s) - 1]. \quad (\text{D.9})$$

Integrating w.r.t. θ gives explicitly

$$\hat{P}_\theta(s) = 1 + [\hat{P}_1(s) - 1] \exp\left(\int_1^\theta d\theta' e^{-\theta' s} P_{\theta'}(\theta')\right). \quad (\text{D.10})$$

The initial condition is the Laplace transform of $\tilde{P}(x)$, given by $\hat{P}_1(s) = 1 - \exp[-\text{Ei}(s)]$. Since the paste-all limit is a scaling regime one expects $P_\theta(x) = P_1(x/\theta)/\theta$ and in particular $P_\theta(\theta) = P_1(1)/\theta = 1/\theta$. This is indeed the correct solution of (D.10) as the integral over θ' then becomes $\text{Ei}(s) - \text{Ei}(\theta s)$ so that $\hat{P}_\theta(s) = 1 - \exp[-\text{Ei}(\theta s)] = \hat{P}_1(\theta s)$.

To apply the above description of the paste-all dynamics to the calculation of the energy correlation function, we substitute $P_\theta(x) \rightarrow P_\theta(x) + \delta P_\theta(x)$ everywhere and linearize in the small perturbation δP_θ . In the Laplace transform version (D.10) this yields

$$\delta \hat{P}_\theta(s) = \delta \hat{P}_1(s) e^{\text{Ei}(s) - \text{Ei}(\theta s)} + [\hat{P}_1(s) - 1] e^{\text{Ei}(s) - \text{Ei}(\theta s)} \int_1^\theta d\theta' e^{-\theta' s} \delta P_{\theta'}(\theta'), \quad (\text{D.11})$$

or

$$e^{\text{Ei}(\theta s)} \delta \hat{P}_\theta(s) = e^{\text{Ei}(s)} \delta \hat{P}_1(s) - \int_1^\theta d\theta' e^{-\theta' s} \delta P_{\theta'}(\theta'). \quad (\text{D.12})$$

As explained above, we need to insert as the initial perturbation $\delta P_1(x) = P_1(x)(x - \bar{x}) = P_1(x)(x - e^\gamma)$, i.e.

$$\delta \hat{P}_1(s) = -\frac{\partial}{\partial s} \hat{P}_1(s) - e^\gamma \hat{P}_1(s) = \frac{e^{-s}}{s} e^{-\text{Ei}(s)} - e^\gamma [1 - e^{-\text{Ei}(s)}]. \quad (\text{D.13})$$

This gives for the Laplace transform (D.12) of the perturbed domain size distribution at time θ

$$e^{\text{Ei}(\theta s)} \delta \hat{P}_\theta(s) = \frac{e^{-s}}{s} - e^\gamma [e^{\text{Ei}(s)} - 1] - \int_1^\theta d\theta' e^{-\theta' s} \delta P_{\theta'}(\theta'). \quad (\text{D.14})$$

It remains to determine $\delta P_{\theta'}(\theta')$ from the condition that $\delta P_\theta(x) = 0$ for $x < \theta$. On the l.h.s. of (D.14) we have the (Laplace transform of) a convolution of $P_\theta(x)$ with another function; this convolution then also vanishes for $x < \theta$. The same must therefore be true of the r.h.s., which is the Laplace transform of

$$\Theta(x - 1) - e^\gamma \sum_{l \geq 1} \frac{1}{l!} f_l(x) - \Theta(\theta - x) \delta P_x(x). \quad (\text{D.15})$$

The condition that this must vanish for $x < \theta$ implies that in this range

$$\delta P_x(x) = \Theta(x - 1) - e^\gamma \sum_{l \geq 1} \frac{1}{l!} f_l(x). \quad (\text{D.16})$$

Because we can make θ as large as desired, this expression must then hold for all x . We can now reinsert this result into (D.14) and take the limit $s \rightarrow 0$ to obtain the perturbation $\delta\bar{x}_\theta$ in the average domain length, using that $\delta\hat{P}_\theta(s) = -s\delta\bar{x}_\theta + O(s^2)$ and $\text{Ei}(s) = -\ln s - \gamma + s + O(s^2)$:

$$-\frac{\delta\bar{x}_\theta}{e^{\gamma\theta}} = -2 + e^\gamma - \int_1^\theta d\theta' \delta P_{\theta'}(\theta'), \quad (\text{D.17})$$

or, after inserting (D.16),

$$\delta\bar{x}_\theta = e^{\gamma\theta} \left(1 - e^\gamma + \theta - e^\gamma \sum_{l \geq 1} \frac{1}{l!} \int_1^\theta d\theta' f_l(\theta') \right). \quad (\text{D.18})$$

From (D.6) we can then finally write down the two-time energy correlation. By considering the combination $C_E(t, t_w)/n(t)$ we remove one factor of $\bar{d}_{\kappa t}^{-1}$ and also ensure that all factors of $d_{\min}(t_w)$ arising from our length rescaling cancel from the result. The remainder of the prefactor is $1/(e^\gamma e^{\gamma\theta})$ so that overall

$$C_E(t, t_w)/n(t) = e^{-\gamma}(\theta + 1) - 1 - \sum_{l \geq 1} \frac{1}{l!} \int_1^\theta d\theta' f_l(\theta'). \quad (\text{D.19})$$

This is the scaling function $\mathcal{G}(\theta)$ given in (117); for $\theta \leq 2$ it can be written explicitly as

$$\mathcal{G}(\theta) = e^{-\gamma}(\theta + 1) - 1 - \ln \theta. \quad (\text{D.20})$$

For $\theta = 1$ in particular one obtains the scaling of the equal-time correlations in the paste-all limit as $C_E(t, t)/n(t) = 2e^{-\gamma} - 1 = 0.1229 \dots$. This value gives the y -axis intercept of the paste-all curve in Fig. 14.

Appendix E. Non-local correlations

In this appendix we describe how the non-local two-time correlations in the East model can be calculated in the paste-all regime. The aim is to derive the scaling function $\mathcal{H}(x, \theta)$ defined in (133), in the nontrivial region of positive x .

As explained in the main text, two-time spatial correlations require one to keep track of which domains from time t_w have been merged into the domains at time t . We can then characterize a domain at t by the (scaled) lengths of the t_w -domains it contains. If these lengths are, in order, x_1, \dots, x_l , we write the fraction of such t -domains as $P_\theta^{(l)}(x_1, \dots, x_l)$; here $\theta = n(t_w)/n(t) = d_{\min}(t)/d_{\min}(t_w)$ as before. For this more detailed description of the domains, the master equation (D.7) becomes

$$\begin{aligned} \frac{\partial}{\partial \theta} P_\theta^{(l)}(x_1, \dots, x_l) = & -\delta(x_1 + \dots + x_l - \theta) P_\theta^{(l)}(x_1, \dots, x_l) \\ & + \sum_{l'=1}^{l-1} \delta(x_1 + \dots + x_{l'} - \theta) P_\theta^{(l')}(x_1, \dots, x_{l'}) P_\theta^{(l-l')}(x_{l'+1}, \dots, x_l). \end{aligned} \quad (\text{E.1})$$

The first term represents the usual disappearance of domains of total length θ . The second one keeps track of the appearance of new domains; as two domains merge, the

lists of the lengths of the t_w -domains which they contain are simply appended to each other.

It turns out that the above equations for the $P_\theta^{(l)}$ can be solved explicitly, but it is useful to check first how they enter the scaling function $\mathcal{H}(x, \theta)$. From the definition (133), $\mathcal{H} + 1$ is the density of t_w -spins a distance $-x$ from a t -spin, divided by the overall density of t_w -spins. The latter is $1/\bar{x} = e^{-\gamma}$ in the paste-all regime, so $e^{-\gamma}(\mathcal{H} + 1)$ for positive x is the density of t_w -spins that are a distance x to the left of a t -spin. This can be written as

$$e^{-\gamma}(\mathcal{H} + 1) = Q_\theta(x) + (Q_\theta * P_\theta)(x) + (Q_\theta * P_\theta * P_\theta)(x) + \dots \quad (\text{E.2})$$

The terms in this series represent t_w -spins that are within (or on the left boundary of) the first, second, third etc. t -domain to the left of the t -spin considered, hence the appearance of the length distribution $P_\theta(x)$ of t -domains. The factor $Q_\theta(x)$ records the positions of t_w -spins *within* t -domains:

$$Q_\theta(x) = \sum_{m=1}^{\infty} Q_\theta^{(m)}(x), \quad (\text{E.3})$$

$$Q_\theta^{(m)}(x) = \sum_{l=m}^{\infty} \int dx_1 \cdots dx_l P_\theta^{(l)}(x_1, \dots, x_l) \delta(x_{l-m+1} + \dots + x_l - x), \quad (\text{E.4})$$

where $Q_\theta^{(m)}(x)$ accounts for the contributions from the m -th t_w -spin within a t -domain, counting leftwards from the t -spin on its right boundary. We see that we do not need *all* details of the $P_\theta^{(l)}$; the $Q_\theta^{(m)}$ are sufficient. Unfortunately, the latter do not obey closed equations because they do not contain information about the total length of the t -domain. We therefore generalize so that this is also kept track of and define the quantities

$$\begin{aligned} \tilde{Q}_\theta^{(m)}(x, x_{\text{tot}}) &= \sum_{l=m}^{\infty} \int dx_1 \cdots dx_l P_\theta^{(l)}(x_1, \dots, x_l) \times \\ &\quad \times \delta(x_{l-m+1} + \dots + x_l - x) \delta(x_1 + \dots + x_l - x_{\text{tot}}). \end{aligned} \quad (\text{E.5})$$

These give the fraction of t -domains of length x_{tot} for which the m rightmost t_w -domains contained within add up to a length x . Taking the simplest case $m = 1$ as an example, one now derives from (E.1) the evolution equation

$$\frac{\partial}{\partial \theta} \tilde{Q}_\theta^{(1)}(x, x_{\text{tot}}) = -\delta(x_{\text{tot}} - \theta) \tilde{Q}_\theta^{(1)}(x, x_{\text{tot}}) + \frac{1}{\theta} \tilde{Q}_\theta^{(1)}(x, x_{\text{tot}} - \theta). \quad (\text{E.6})$$

The factor $1/\theta$ here is the total rate of disappearance of domains; formally it is calculated from

$$\sum_{l'=1}^{\infty} \int dx_1 \cdots dx_{l'} \delta(x_1 + \dots + x_{l'} - \theta) P_\theta^{(l')}(x_1, \dots, x_{l'}), \quad (\text{E.7})$$

which just gives the density $P_\theta(\theta) = 1/\theta$ of t -domains of length θ (as enforced by the delta function) at time θ .

The initial condition for (E.6) at $\theta = 1$, i.e. $t = t_w$, is $\tilde{Q}_1^{(1)}(x, x_{\text{tot}}) = P_1(x)\delta(x - x_{\text{tot}}) = \tilde{P}(x)\delta(x - x_{\text{tot}})$ because there is then no distinction between t_w -domains and t -domains. (It is only through this initial condition that the x -dependence enters.) Going to Laplace transforms $x_{\text{tot}} \rightarrow s$, integrating with respect to θ and transforming back gives then

$$\int_0^\infty \frac{dx'}{\theta} \mathcal{E}\left(\frac{x_{\text{tot}} - x'}{\theta}\right) \tilde{Q}_\theta^{(1)}(x, x') = \tilde{P}(x) \mathcal{E}(x_{\text{tot}} - x) - \int_1^\theta \frac{d\theta'}{\theta'} \mathcal{E}\left(\frac{x_{\text{tot}} - \theta'}{\theta'}\right) \tilde{Q}_{\theta'}^{(1)}(x, \theta'), \quad (\text{E.8})$$

where

$$\mathcal{E}(x) = \delta(x) + \sum_{l \geq 1} \frac{1}{l!} f_l(x) \quad (\text{E.9})$$

is the inverse Laplace transform of $\exp[\text{Ei}(s)]$. We now need to find $\tilde{Q}_{\theta'}^{(1)}(x, \theta')$ from the condition that $\tilde{Q}_\theta^{(1)}(x, x')$ vanishes for $x' < \theta$. Since $\mathcal{E}(\cdot)$ is zero for negative argument, the l.h.s. of (E.8) vanishes for $x_{\text{tot}} < \theta$ so that in this regime

$$\tilde{P}(x) \mathcal{E}(x_{\text{tot}} - x) = \int_1^\theta \frac{d\theta'}{\theta'} \mathcal{E}\left(\frac{x_{\text{tot}} - \theta'}{\theta'}\right) \tilde{Q}_{\theta'}^{(1)}(x, \theta'). \quad (\text{E.10})$$

Again because of the vanishing of $\mathcal{E}(\cdot)$ for negative argument we can restrict the integration to $\theta' \leq x_{\text{tot}}$. Also $\tilde{Q}_{\theta'}^{(1)}(x, \theta')$ must vanish for $\theta' < x$ – the total length cannot be smaller than the length of the rightmost t_w -domain within – so the lower integration limit can be raised from $\theta' = 1$ to $\theta' = x$. After relabelling $x_{\text{tot}} \rightarrow \theta$ our condition becomes

$$\tilde{P}(x) \mathcal{E}(\theta - x) = \int_x^\theta \frac{d\theta'}{\theta'} \mathcal{E}\left(\frac{\theta - \theta'}{\theta'}\right) \tilde{Q}_{\theta'}^{(1)}(x, \theta'). \quad (\text{E.11})$$

It is from this expression that $\tilde{Q}_{\theta'}^{(1)}(x, \theta')$ is to be found. The simplest regime is $\theta/x < 2$. Then the argument of $\mathcal{E}(\cdot)$ on the right is always less than 1 and so only the first term in (E.9) contributes, giving

$$\tilde{Q}_\theta^{(1)}(x, \theta) = \tilde{P}(x) \mathcal{E}(\theta - x), \quad \text{for } \theta/x < 2. \quad (\text{E.12})$$

Since $x \geq 1$ this solution applies, in particular, whenever $\theta < 2$, where it simplifies further to

$$\tilde{Q}_\theta^{(1)}(x, \theta) = \tilde{P}(x) \delta(\theta - x). \quad (\text{E.13})$$

This makes sense: a t -domain of size $\theta < 2$ cannot contain two or more t_w -domains, so that necessarily $\theta = x$. Inserting (E.13) into (E.8) yields

$$\int_0^\infty \frac{dx'}{\theta} \mathcal{E}\left(\frac{x_{\text{tot}} - x'}{\theta}\right) \tilde{Q}_\theta^{(1)}(x, x') = \tilde{P}(x) \left[\mathcal{E}(x_{\text{tot}} - x) - \frac{\Theta(\theta - x)}{x} \mathcal{E}\left(\frac{x_{\text{tot}} - x}{x}\right) \right] \quad (\text{E.14})$$

One can now integrate over x_{tot} , or equivalently go back to Laplace transforms and take $s \rightarrow 0$, to find

$$Q_\theta^{(1)}(x) = \int dx' \tilde{Q}_\theta^{(1)}(x, x') = \theta \tilde{P}(x) \left[1 - \frac{\Theta(\theta - x)}{x} \right]. \quad (\text{E.15})$$

This expression is exact for $\theta < 2$. If also $x < 2$, then it is the only contribution to (E.2) because all other terms involve two or more t_w -domains whose combined length will be above 2. We have thus obtained the first line of (134). To get the full expression valid for $\theta < 3$ and $x < 3$ one has to extend the above calculation for $Q_\theta^{(1)}(x)$ to the range $2 < \theta < 3$; one also needs to calculate $Q_\theta^{(2)}(x)$. We omit the details.

Appendix F. Persistence function

Here we outline how to calculate the persistence function of down-spins (110) in the paste-all regime of the East model. From the discussion before (109) this governs the behaviour of the local susceptibility χ_0 in the East model.

As discussed in Sec. 3, in the paste-all regime each domain contains an equilibration zone on its left, of size θ . (We use the same definitions of x and θ as in previous sections.) Each equilibration zone has been fully “swept” by up-spins, i.e. it contains no persistent down-spins. However, regions to the right of the current equilibration zone may already have been swept previously. For example, when two domains merge, only the equilibration zone of the original domain on the left remains, but we have to keep track of the fact that the equilibration zone in the domain on the right has already been swept by up-spins. We therefore define $P_\theta(u, x)$ as the fraction of domains that have length x and an unswept zone of length u (on their right end). This has two components:

$$P_\theta(u, x) = P'_\theta(x)\delta(x - \theta - u) + P''_\theta(u, x). \quad (\text{F.1})$$

The first part represents domains where the swept area is exactly the equilibration zone and so $u = x - \theta$; the second part describes domains where the swept zone is larger and correspondingly $u < x - \theta$. Initially, at $\theta = 1$, only the first part is present, and so $P'_1(x) = \tilde{P}(x)$ and $P''_1(u, x) = 0$. This is because we want to count persistence from time t_w , i.e. the swept zones are reset to the current equilibration zones at that point. At some later “time” θ , the fraction of the chain occupied by persistent down-spins is $\langle u \rangle_\theta$ divided by the average domain length $e^\gamma \theta$. The function $\mathcal{F}(\theta)$ is the complement of this, i.e. the fraction of swept areas

$$\mathcal{F}(\theta) = 1 - \frac{\langle u \rangle_\theta}{e^\gamma \theta}. \quad (\text{F.2})$$

To calculate the required average $\langle u \rangle_\theta$ we start from the evolution equations for P' and P'' ,

$$\frac{\partial}{\partial \theta} P'_\theta(x) = -\delta(x - \theta) P'_\theta(x) + P''_\theta(x - \theta, x), \quad (\text{F.3})$$

$$\frac{\partial}{\partial \theta} P''_\theta(u, x) = -\delta(x - \theta - u) P''_\theta(x - \theta, x) + \frac{1}{\theta} P_\theta(u, x - \theta). \quad (\text{F.4})$$

In (F.3) the first term describes disappearance of domains of length θ ; note that only domains in the P' -part of the distribution can disappear in this way because at disappearance the equilibration zone covers the whole of the domain and is therefore identical to the swept zone. The second term accounts for the fact that when the

equilibration zone (length θ) grows long enough to cover all of the existing swept zone (length $x - u = x - (x - \theta) = \theta$), domains are counted in P' rather than P'' . The first term in (F.4) records the corresponding loss of domains from P'' . The last term, finally, accounts for the creation of new domains as domains of length θ disappear and merge with their right neighbours. The factor $1/\theta$ is the total rate of disappearance of domains as in (E.6); the length u of the unswept zone remains unchanged during a merger while the overall domain lengths θ and $x - \theta$ add.

The first evolution equation (F.3) can be integrated directly to give

$$P'_\theta(x) = \Theta(x - \theta) \left[\tilde{P}(x) + \int_1^\theta d\theta' P''_\theta(x - \theta', x) \right], \quad (\text{F.5})$$

while for the second one we insert (F.1) and then proceed as in the derivation of (E.8) to obtain

$$\begin{aligned} \int_0^\infty \frac{dx'}{\theta} \mathcal{E}\left(\frac{x - x'}{\theta}\right) P''_\theta(u, x') &= \int_1^\theta \frac{d\theta'}{\theta'} \left[-\mathcal{E}\left(\frac{x - \theta' - u}{\theta'}\right) P''_{\theta'}(u, \theta' + u) \right. \\ &\quad \left. + \frac{1}{\theta'} \mathcal{E}\left(\frac{x - 2\theta' - u}{\theta'}\right) P'_{\theta'}(\theta' + u) \right]. \end{aligned} \quad (\text{F.6})$$

One sees that all quantities are determined once we know $P''_{\theta'}(u, \theta' + u)$. Fortunately, this *vanishes* for $\theta' < 2$. The reason is that domains that have not yet merged have identical swept and equilibration zones and so are counted in P' . Domains in the P'' -part of the distribution must then be the product of a merger of at least two of the domains that were present at time t_w . Their swept zone is, as a consequence, the result of a merger of at least two equilibration zones and must have length at least 2. It follows that $P''_{\theta'}(u, x) = 0$ for $u > x - 2$, and substituting $x = \theta' + u$ with $\theta' < 2$ proves our claim.

With the above simplification for $\theta < 2$ we get $P'_\theta(x) = \Theta(x - \theta)\tilde{P}(x)$ and

$$\int_0^\infty \frac{dx'}{\theta} \mathcal{E}\left(\frac{x - x'}{\theta}\right) P''_\theta(u, x') = \int_1^\theta \frac{d\theta'}{(\theta')^2} \mathcal{E}\left(\frac{x - 2\theta' - u}{\theta'}\right) \tilde{P}(\theta' + u), \quad (\text{F.7})$$

or, after integration over x ,

$$\int_0^\infty dx' P''_\theta(u, x') = \theta \int_1^\theta \frac{d\theta'}{(\theta')^2} \tilde{P}(\theta' + u). \quad (\text{F.8})$$

Putting everything together gives for the average of u

$$\langle u \rangle_\theta = \int dx du u P_\theta(u, x) \quad (\text{F.9})$$

$$= \int dx (x - \theta) P'_\theta(x) + \int dx du u P''_\theta(u, x) \quad (\text{F.10})$$

$$= \int dx (x - \theta) \Theta(x - \theta) \tilde{P}(x) + \int du u \theta \int_1^\theta \frac{d\theta'}{(\theta')^2} \tilde{P}(\theta' + u) \quad (\text{F.11})$$

$$= I(\theta) + \theta \int_1^\theta \frac{d\theta'}{(\theta')^2} I(\theta'), \quad (\text{F.12})$$

where

$$I(\theta) = \int_{\theta}^{\infty} dx(x - \theta)\tilde{P}(x) \quad (\text{F.13})$$

$$= \int_1^{\infty} dx(x - \theta)\tilde{P}(x) - \int_1^{\theta} dx(x - \theta)\tilde{P}(x) \quad (\text{F.14})$$

$$= e^{\gamma} - \theta - \int_1^{\theta} dx \left(1 - \frac{\theta}{x}\right) \quad (\text{F.15})$$

$$= e^{\gamma} + 1 - 2\theta + \theta \ln \theta. \quad (\text{F.16})$$

Carrying out the remaining θ' -integration in (F.12) yields

$$\langle u \rangle_{\theta} = (e^{\gamma} - 1)\theta - \theta \ln \theta + \frac{\theta}{2} \ln^2 \theta, \quad (\text{F.17})$$

and, after inserting into (F.2), the result (110) from the main text. One can push the calculation further, certainly up to $\theta < 3$, but the resulting expressions become very unwieldy and so are not given here.

References

- [1] E. Donth. *The glass transition*. Springer, Berlin, 2001.
- [2] A P Young, editor. *Spin Glasses and Random Fields*. World Scientific, Singapore, 1998.
- [3] L. Cipelletti and L. Ramos. *J. Phys. Cond. Matt.*, 17:R253, 2005.
- [4] F. Ritort and P. Sollich. *Advances in Physics*, 52:219, 2003.
- [5] G. H. Fredrickson and H. C. Andersen. *Phys. Rev. Lett.*, 53:1244, 1984.
- [6] J. Jäckle and S. Eisinger. *Z. Phys. B Cond. Matt.*, 84:115, 1991.
- [7] G. H. Fredrickson and H. C. Andersen. *J. Chem. Phys.*, 83:5822, 1985.
- [8] G. H. Fredrickson and S. A. Brawer. *J. Chem. Phys.*, 84:3351, 1986.
- [9] G. H. Fredrickson. *Annals NY Acad. of Sci.*, 484:185, 1986.
- [10] C. Toninelli, G. Biroli, and D. S. Fisher. *Phys. Rev. Lett.*, 92:185504, 2004.
- [11] C. Toninelli, G. Biroli, and D. S. Fisher. *J. Stat. Phys.*, 120:167, 2005.
- [12] S. Butler and P. Harrowell. *J. Chem. Phys.*, 95:4454, 1991.
- [13] S. Butler and P. Harrowell. *J. Chem. Phys.*, 95:4466, 1991.
- [14] P. Harrowell. *Phys. Rev. E*, 48:4359, 1993.
- [15] M. Foley and P. Harrowell. *J. Chem. Phys.*, 98:5069, 1993.
- [16] W. Ertel, K. Froböse, and J. Jäckle. *J. Chem. Phys.*, 88:5027, 1988.
- [17] J. Reiter, F. Mauch, and J. Jäckle. *Physica A*, 184:458, 1992.
- [18] J. P. Garrahan and D. Chandler. *Phys. Rev. Lett.*, 89:035704, 2002.
- [19] M. D. Ediger. *Annu. Rev. Phys. Chem.*, 51:99, 2000.
- [20] M. Schulz and S. Trimper. *J. Stat. Phys.*, 94:173, 1999.
- [21] S. Whitelam, L. Berthier, and J. P. Garrahan. *Phys. Rev. Lett.*, 92:185705, 2004.
- [22] G. Szamel. *J. Chem. Phys.*, 121:3355, 2004.
- [23] S. Whitelam, L. Berthier, and J. P. Garrahan. *Phys. Rev. E*, 71:026128, 2005.
- [24] R. L. Jack, P. Mayer, and P. Sollich. *J. Stat. Mech.*, page P03006, 2006.
- [25] R. L. Jack, J. P. Garrahan, and D. Chandler. *J. Chem. Phys.*, 125:184509, 2006.
- [26] R. L. Jack, L. Berthier, and J. P. Garrahan. *Phys. Rev. E*, 72:016103, 2005.
- [27] N. Cancrini, F. Martinelli, C. Roberto, and C. Toninelli. Preprint cond-mat/0603745.
- [28] N. Cancrini, F. Martinelli, C. Roberto, and C. Toninelli. Preprint math.PR/0610106.
- [29] L. Berthier, G. Biroli, J.-P. Bouchaud, W. Kob, K. Miyazaki, and D. R. Reichman. Preprint cond-mat/0609656.

- [30] L. Berthier, G. Biroli, J.-P. Bouchaud, W. Kob, K. Miyazaki, and D. R. Reichman. Preprint cond-mat/0609658.
- [31] L. Berthier and J. P. Garrahan. *Phys. Rev. E*, 68:041201, 2003.
- [32] L. Berthier and J. P. Garrahan. *J. Chem. Phys.*, 119:4367, 2003.
- [33] Y. J. Jung, J. P. Garrahan, and D. Chandler. *Phys. Rev. E*, 69:061205, 2004.
- [34] W. Van Ketel, C. Das, and D. Frenkel. *Phys. Rev. Lett.*, 94:135703, 2005.
- [35] L. Berthier, D. Chandler, and J. P. Garrahan. *Europhys. Lett.*, 69:320, 2005.
- [36] S. Léonard and L. Berthier. *J. Phys. Cond. Matt.*, 17:S3571, 2005.
- [37] J. P. Garrahan and D. Chandler. *Proc. Natl. Acad. Sci.*, 100:9710, 2003.
- [38] C. Toninelli, G. Biroli, and D. S. Fisher. *Phys. Rev. Lett.*, 96:035702, 2006.
- [39] M. Sellitto, G. Biroli, and C. Toninelli. *Europhys. Lett.*, 69:496, 2005.
- [40] L. Berthier and J. P. Garrahan. *J. Phys. Chem. B*, 109:3578, 2005.
- [41] P. L. Geissler and D. R. Reichman. *Phys. Rev. E*, 71:031206, 2005.
- [42] A. J. Moreno and J. Colmenero. *J. Chem. Phys.*, 125:016101, 2006.
- [43] R. Yamamoto and A. Onuki. *Phys. Rev. Lett.*, 81:4915, 1998.
- [44] C. Benneman, C. Donati, J. Baschnagel, and S. C. Glotzer. *Nature*, 399:246, 1999.
- [45] N. Lacevic, F. W. Starr, T. B. Schroder, and S. C. Glotzer. *J. Chem. Phys.*, 119:7372, 2003.
- [46] L. Berthier. *Phys. Rev. E*, 69:020201, 2004.
- [47] C. Toninelli, M. Wyart, G. Biroli, L. Berthier, and J.-P. Bouchaud. *Phys. Rev. E*, 71:041505, 2005.
- [48] G. Szamel and E. Flenner. *Phys. Rev. E*, 74:021507, 2006.
- [49] X. H. Qiu and M. Ediger. *J. Phys. Chem. B*, 107:459, 2003.
- [50] L. Berthier, G. Biroli, J.-P. Bouchaud, L. Cipelletti, D. El Masri, D. L'Hôte, F. Ladieu, and M. Pierno. *Science*, 310:1797, 2005.
- [51] O. Dauchot, G. Marty, and G. Biroli. *Phys. Rev. Lett.*, 95:265701, 2005.
- [52] A. Lefèvre, L. Berthier, and R. Stinchcombe. *Phys. Rev. E*, 72:010301, 2005.
- [53] A. M. Puertas, M. Fuchs, and M. E. Cates. *J. Chem. Phys.*, 121:2813, 2004.
- [54] E. Weeks, J. C. Crocker, and D. A. Weitz. Preprint cond-mat/0610195.
- [55] D. R. Reichman, E. Rabani, and P. L. Geissler. *J. Phys. Chem. B*, 109:14654, 2005.
- [56] P. Mayer, H. Bissig, L. Berthier, L. Cipelletti, J.-P. Garrahan, P. Sollich, and V. Trappe. *Phys. Rev. Lett.*, 93:115701, 2004.
- [57] A. Duri and L. Cipelletti. *Europhys. Lett.*, 76:972, 2006.
- [58] P. I. Hurtado, L. Berthier, and W. Kob. Preprint cond-mat/0612513.
- [59] C. J. Dibble, M. Kogan, and M. J. Solomon. *Phys. Rev. E*, 74:041403, 2006.
- [60] L. C. E. Struik. *Physical aging in amorphous polymers and other materials*. Elsevier, Amsterdam, 1978.
- [61] L. F. Cugliandolo and J. Kurchan. *Phys. Rev. Lett.*, 71:173, 1993.
- [62] L. F. Cugliandolo and J. Kurchan. *J. Phys. A*, 27:5749, 1994.
- [63] J. Kurchan and L. Laloux. *J. Phys. A*, 29:1929, 1996.
- [64] L. F. Cugliandolo, J. Kurchan, and L. Peliti. *Phys. Rev. E*, 55:3898, 1997.
- [65] J. Kurchan. *Nature*, 433:222, 2005.
- [66] S. Franz, M. Mézard, G. Parisi, and L. Peliti. *Phys. Rev. Lett.*, 81:1758, 1998.
- [67] A. Crisanti and F. Ritort. *J. Phys. A*, 36:R181, 2003.
- [68] T. S. Grigera and N. E. Israeloff. *Phys. Rev. Lett.*, 83:5038, 1999.
- [69] B. Abou and F. Gallet. *Phys. Rev. Lett.*, 93:160603, 2004.
- [70] P. Wang, C. M. Song, and H. A. Makse. *Nat. Phys.*, 2:526, 2006.
- [71] L. Bellon, S. Ciliberto, and C. Laroche. *Europhys. Lett.*, 53:511, 2001.
- [72] L. Bellon and S. Ciliberto. *Physica D*, 168:325, 2002.
- [73] L. Buisson, L. Bellon, and S. Ciliberto. *J. Phys. Cond. Matt.*, 15:S1163, 2003.
- [74] L. Buisson, S. Ciliberto, and A. Garcimartin. *Europhys. Lett.*, 63:603, 2003.
- [75] M. Nicodemi. *Phys. Rev. Lett.*, 82:3734, 1999.

- [76] F Corberi, A De Candia, E Lippiello, and M Zannetti. 65:046114, 2002.
- [77] P. Viot, J. Talbot, and G. Tarjus. *Fractals*, 11:185, 2003.
- [78] F. Krzakala. *Phys. Rev. Lett.*, 94:077204, 2005.
- [79] M. Depken and R. Stinchcombe. *Phys. Rev. E*, 71:065102, 2005.
- [80] S. Fielding and P. Sollich. *Phys. Rev. Lett.*, 88:050603, 2002.
- [81] L. F. Cugliandolo and J. Kurchan. *Phys. Rev. B*, 60:922, 1999.
- [82] D. S. Fisher and D. A. Huse. *Phys. Rev. Lett.*, 56:1601, 1986.
- [83] D. S. Fisher and D. A. Huse. *Phys. Rev. B*, 38:373, 1988.
- [84] D. S. Fisher and D. A. Huse. *Phys. Rev. B*, 38:386, 1988.
- [85] K. Jonason, E. Vincent, J. Hammann, J.P. Bouchaud, and P. Nordblad. *Phys. Rev. Lett.*, 81:3243, 1998.
- [86] V. Dupuis, E. Vincent, J.-P. Bouchaud, J. Hammann, and A. Ito. *Phys. Rev. B*, 64:174204, 2001.
- [87] P. E. Jönsson, H. Yoshino, and P. Nordblad. *Phys. Rev. Lett.*, 89:097201, 2002.
- [88] F. Bert, V. Dupuis, E. Vincent, J. Hammann, and J.-P. Bouchaud. *Phys. Rev. Lett.*, 92:167203, 2004.
- [89] L. Berthier and J.-P. Bouchaud. *Phys. Rev. B*, 66:054404, 2002.
- [90] L. Berthier and A. P. Young. *Phys. Rev. B*, 71:214429, 2005.
- [91] A. Barrat and L. Berthier. *Phys. Rev. Lett.*, 87:087204, 2001.
- [92] L. Berthier, P. C. W. Holdsworth, and M. Sellitto. *J. Phys. A*, 34:1805, 2001.
- [93] H. E. Castillo, C. Chamon, L. F. Cugliandolo, and M. P. Kennett. *Phys. Rev. Lett.*, 88:237201, 2002.
- [94] C. Chamon, M. P. Kennett, H. E. Castillo, and L. F. Cugliandolo. *Phys. Rev. Lett.*, 89:217201, 2002.
- [95] H. E. Castillo, C. Chamon, L. F. Cugliandolo, J. L. Iguain, and M. P. Kennett. *Phys. Rev. B*, 68:134442, 2003.
- [96] C. Chamon, P. Charbonneau, L. F. Cugliandolo, D. R. Reichman, and M. Sellitto. *J. Chem. Phys.*, 121:10120, 2004.
- [97] X. Xia and P. G. Wolynes. *Phys. Rev. Lett.*, 86:5526, 2001.
- [98] G. Tarjus, S. A. Kivelson, Z. Nussinov, and P. Viot. *J. Phys. Cond. Matt.*, 17:R1143, 2005.
- [99] G. Biroli and J.-P. Bouchaud. *Europhys. Lett.*, 67:21, 2004.
- [100] S. Franz. *J. Stat. Mech.*, page P04001, 2005.
- [101] M. Dzero, J. Schmalian, and P. G. Wolynes. *Phys. Rev. B*, 72:100201, 2005.
- [102] S. Franz. *Europhys. Lett.*, 73:492, 2006.
- [103] A. Montanari and G. Semerjian. *Phys. Rev. Lett.*, 94:247201, 2005.
- [104] A. Montanari and G. Semerjian. *J. Stat. Phys.*, 124:103, 2006.
- [105] W. Kob and H. C. Andersen. *Phys. Rev. E*, 48:4364, 1993.
- [106] J. Kurchan, L. Peliti, and M. Sellitto. *Europhys. Lett.*, 39:365, 1997.
- [107] M. Sellitto. *Eur. Phys. J. B*, 4:135, 1998.
- [108] A. Barrat, J. Kurchan, V. Loreto, and M. Sellitto. *Phys. Rev. Lett.*, 85:5034, 2000.
- [109] M. Sellitto. *Phys. Rev. E*, 63:060301, 2001.
- [110] M. Sellitto. *Phys. Rev. E*, 66:042101, 2002.
- [111] J. J. Arenzon and M. Sellitto. *European Physical Journal B*, 42:543, 2004.
- [112] A. Crisanti, F. Ritort, A. Rocco, and M. Sellitto. *J. Chem. Phys.*, 113:10615, 2000.
- [113] A. Crisanti, F. Ritort, A. Rocco, and M. Sellitto. *J. Phys. Cond. Matt.*, 14:1523, 2002.
- [114] A. Buhot and J. P. Garrahan. *Phys. Rev. Lett.*, 88:225702, 2002.
- [115] A. Buhot. *J. Phys. A*, 36:12367, 2003.
- [116] P. Sollich and M. R. Evans. *Phys. Rev. Lett.*, 83:3238, 1999.
- [117] P. Sollich and M. R. Evans. *Phys. Rev. E*, 68:031504, 2003.
- [118] J. P. Garrahan and M. E. J. Newman. *Phys. Rev. E*, 62:7670, 2000.
- [119] P. Sollich, S. Fielding, and P. Mayer. *J. Phys. Cond. Matt.*, 14:1683, 2002.
- [120] G. Diezemann. Preprint cond-mat/0609762.

- [121] L. Berthier. Preprint cond-mat/0701094.
- [122] C. Chatelain. *J. Phys. A*, 36:10739, 2003.
- [123] C. Chatelain. *J. Stat. Mech.*, page P06006, 2004.
- [124] F. Ricci-Tersenghi. *Phys. Rev. E*, 68:065104, 2003.
- [125] P. Mayer, S. Léonard, L. Berthier, J. P. Garrahan, and P. Sollich. *Phys. Rev. Lett.*, 96:030602, 2006.
- [126] R. L. Jack, L. Berthier, and J. P. Garrahan. *J. Stat. Mech.*, page P12005, 2006.
- [127] P. Mayer and P. Sollich. Preprint cond-mat/0702618.
- [128] I. S. Graham, L. Piché, and M. Grant. *J. Phys. Cond. Matt.*, 5:L349, 1993.
- [129] C Godrèche and J M Luck. *J. Phys. A*, 33(50):9141–9164, 2000.
- [130] R Stinchcombe. *Adv. Phys.*, 50:431, 2001.
- [131] K. Krebs, M. P. Pfannmüller, B. Wehefritz, and H. Hinrichsen. *J. Stat. Phys.*, 78:1429, 1995.
- [132] M. Henkel, E. Orlandini, and J. Santos. *Annals Phys.*, 259:163, 1997.
- [133] D. X. Zhong and D. Ben-Avraham. *J. Phys. A*, 28:33, 1995.
- [134] U. C. Täuber, M. Howard, and B. P. Vollmayr-Lee. *J. Phys. A*, 38:R79, 2005.
- [135] M. Henkel, E. Orlandini, and G. M. Schütz. *J. Phys. A*, 28:6335, 1995.
- [136] P. Mayer, L. Berthier, J. P. Garrahan, and P. Sollich. *Phys. Rev. E*, 68:016116, 2003.
- [137] P. Mayer, L. Berthier, J. P. Garrahan, and P. Sollich. *Phys. Rev. E*, 70:018102, 2004.
- [138] A. B. Bortz, M. H. Kalos, and J. L. Lebowitz. *J. Comp. Phys.*, 17:10, 1975.
- [139] M. Doi. *J. Phys. A*, 9:1479, 1976.
- [140] L. Peliti. *Journal de Physique*, 46:1469, 1985.
- [141] B. P. Lee. *J. Phys. A*, 27:2633, 1994.
- [142] U. C. Täuber, M. Howard, and B. P. Vollmayr-Lee. *J. Phys. A*, 38:R79, 2005.
- [143] D. Aldous and P. Diaconis. *J. Stat. Phys.*, 107:945, 2002.
- [144] B. Derrida, C. Godrèche, and I. Yekutieli. *Phys. Rev. A*, 44:6241, 1991.
- [145] S. Eisinger and J. Jäckle. 73:643, 1993.
- [146] L. S. Gradshteyn and I. M. Ryzhik. *Table of Integrals, Series, and Products*. Academic Press, New York, 2000.